Nonlinear Dynamics of Wave Propagation in Heterogeneous Excitable Media

by

S. Sridhar

A Thesis in Physics

submitted to

UNIVERSITY OF MADRAS

CHENNAI-600 005, INDIA

in partial fulfillment of the

degree of **Doctor of Philosophy (Ph.D.)**

THE INSTITUTE OF MATHEMATICAL SCIENCES

CHENNAI-600 113, INDIA

November 2010

DECLARATION

I declare that the thesis entitled *Nonlinear Dynamics of Wave Propagation in Heterogeneous Excitable Media* submitted by me for the degree of Doctor of Philosophy is the record of work carried out by me during the period *February 2007* to *November 2010* under the guidance of *Prof. Sitabhra Sinha* and has not formed the basis for the award of any degree, diploma, associateship, fellowship, titles in this or any other University or other similar institution of Higher Learning.

S. Sridhar

THE INSTITUTE OF MATHEMATICAL SCIENCES
C I T CAMPUS, TARAMANI, CHENNAI 600 113, INDIA

Prof. Sitabhra Sinha

Professor G, Physics Group

Phone: (044) 2254 3301
Fax: (044) 2254 1586
E-mail: sitabhra@imsc.res.in

November 27, 2010

CERTIFICATE

I certify that the thesis entitled *Nonlinear Dynamics of Wave Propagation in Heterogeneous Excitable Media* submitted for the degree of Doctor of Philosophy by Mr. S. Sridhar is the record of research work carried out by him during the period *February 2007* to *November 2010* under my guidance and supervision, and that this work has not formed the basis for the award of any degree, diploma, associateship, fellowship or other titles in this University or any other University or Institution of Higher Learning. I further certify that the new results presented in this thesis represent his independent work in a very substantial measure.

Sitabhra Sinha

ACKNOWLEDGEMENT

It is not work if no one is making you do it.

– from *Calvin & Hobbes*.

A doctoral thesis, like most things in the world, is not just the result of a single person's effort. As in the old Tamil adage, the whole town has to help pull the chariot. The story of my thesis is no different. I am indebted to lots of people who have readily and cheerfully spared time for me, and have shared ideas, thoughts, programs and jokes and made my Ph.D. years a pleasurable time.

At the top of the list of people I am deeply indebted to, will by my advisor Prof Sitabhra Sinha. He has been an amazing mentor and a constant source of inspiration, encouragement and guidance and introduced me to the field of Complex Systems Science. His liberal and friendly nature and readiness to spend time with students makes him a wonderful person to work with and learn from.

I am extremely grateful to the Director of IMSc, Prof R Balasubramanian, for kindly giving me an opportunity to pursue my PhD at the Institute. I would like to thank my funding agency, the Department of Atomic Energy and the IMSc Complex Systems project (X and XI Plan), for providing me financial support throughout the period of my doctoral research.

I have been a fortunate beneficiary of the very good infrastructure at IMSc. I am especially lucky to have reaped the benefits of various state-

of-the-art high-performance computer clusters and supercomputers at the institute. I am extremely thankful to IMSc for providing me these facilities.

I am grateful to my doctoral committee members, Prof Ramesh Anishetty of IMSc and Prof N Gautham of the Department of Biophysics, Madras University, for their advice and guidance. I would like to thank Prof Sudeshna Sinha and Dr Ronojoy Adhikari of IMSc who taught me as part of my PhD course requirements. I have been extremely fortunate to have been able to work and interact with Prof Alain Pumir of Ecole Normale Supérieure Lyon, France, and Prof Alexander Panfilov of the Utrecht University, The Netherlands. What I learnt from exchanges with them were an invaluable part of my education.

I would like to thank the IMSc Computer Systems Administrators, especially Dr G Subramoniam, Dr Ravindra Reddy, Mr Mangala Pandi and Mr G Srinivasan for their invaluable help in resolving various computer related issues. I would also like to thank my friends at IMSc, Dr Raj Kumar Pan, Vinu Lukose, Maruthi Pradeep and Rajeev Singh for useful advice and suggestions at all times, both technical and non-technical. I would like to thank Dr Ranga Suri of the Center for Artificial Intelligence and Robotics, for guiding me in my initial attempts at parallel programming. I would like to convey my heartfelt thanks to my friends Mr R. Chandrashekar, Mr Naina Mohammed, Ms Uma Maheshawari and Ms Nirupa of Madras University for their guidance and help in various matters. I would also like to thank my friend Mr Roopas Kiran at IIT Madras for helping me get access to many journals that were not available at IMSc. I would like to thank the entire administrative, library and non-technical staff of IMSc for their help in matters

both academic and non-academic.

On the personal front, first and foremost I would like to thank my mother Lalitha, for not only constantly supporting my endeavours, but also for being an immense source of motivation. I have often been inspired by her intellectual acumen and thirst for knowledge. I would also like to thank my sister Sumathi for her constant encouragement and support.

Though the first science books I read were the ones published from the erstwhile Soviet Union, I really got hooked on to science only after reading Isaac Asimov's *Inside the Atom* and Michael Crichton's *Lost World* which introduced me to the term "Chaos Theory". I owe a sizeable part of the joy I derive from doing science to these two authors. My thanks to the city of Chennai (formerly Madras) which has been my home for the last twenty years. Many have been the happy hours that I have spent in the various libraries that mark the city. I especially owe a lot to the library at the American Consulate, the British Council Library, the Connemara Public Library, the Elloor Library and the library at the Institute of Mathematical Sciences. A word of special thanks to Maestro Illayaraja, whose music has been a much cherished companion on many a long day and weary night.

Finally, I would like to thank Reva for being there, through the good and bad times. This thesis would not have been possible without her ever supportive and encouraging presence.

ABSTRACT

Excitable media is a generic term for a wide range of physical, chemical and biological systems that exhibit spontaneous formation of spatial patterns. Examples of such patterns include spiral waves in a two-dimensional medium and their generalization in a three-dimensional system, scroll waves. Under certain conditions, these waves may become unstable and break up, giving rise to spatiotemporal chaos. Controlling these patterns using low-amplitude external perturbations is of fundamental importance as these patterns are known to have critical functional consequences for vital biological systems, such as the heart. Specifically, spatial patterns of electrical excitation have been implicated in many life-threatening disturbances to the natural rhythm of the heart. Hence understanding the dynamics of these patterns is critical for developing safe and efficient clinical treatment for these disturbances. In this thesis we explore different aspects of the dynamics of spiral and scroll waves using both simple and realistic models of excitable media. Specifically, we study the dynamical evolution of these patterns upon their interaction with different kinds of heterogeneities in the medium. We also propose several low-amplitude control schemes to eliminate such patterns from an excitable medium.

We begin the thesis with a brief overview of various features of excitable systems in **Chapter 1**. In the first few sections, important concepts, terms and models that are used throughout the thesis are defined. This is followed by a brief discussion of the role of heterogeneities on spiral and scroll wave dynamics. Following this is a section with a detailed review of various low-amplitude chaos control schemes for spatially extended chaos in excitable

media. In **Chapter 2**, we study the drift dynamics of spiral waves in the presence of different gradients using simple models of excitable media. The model parameters for which the spiral drifts to regions of lower and higher excitability are determined. Drift of a spiral wave to a region where it rotates faster is of special relevance as it suggests a possible mechanism for the onset of "mother-rotor" fibrillation. We discuss the possible mechanism underlying such anomalous drift. In **Chapter 3**, we discuss the conditions under which a pinned spiral can be unpinned using a high frequency wave-train in a simple model of excitable media. We then derive a relation between pacing period and the size of the obstacle. We also show that unpinning the spiral from an inexcitable obstacle becomes easier with the decrease of medium excitability. In **Chapter 4** we study the breakup of an otherwise stable scroll wave in the presence of an inexcitable obstacle which does not extend throughout the medium. The scroll wave breaks up at the edge of the obstacle, where a transition from a quasi-two-dimensional propagation front to a fully three-dimensional spherical wave front occurs. In **Chapter 5** we propose a non-global spatially extended low-amplitude chaos control scheme, using an array of control points. A travelling wave of control is simulated as the spatially separated array points are excited in a sequence. We find that, depending on wave velocity and spacing of the control points, the chaotic activity can be eliminated completely. Moreover our scheme is robust in the presence of heterogeneities. In **Chapter 6** we apply sub-threshold stimuli, whose effect on a solitary wave propagating in an extended medium is negligible, on a system with spatiotemporally heterogeneous activity. Surprisingly, the signal which is not sufficient to excite a resting medium, fundamentally

alters the recovery dynamics and terminates all activity in the medium. We determine model-independent generic conditions under which this effect can be observed. Finally we conclude in **Chapter 7** with a summary of our results on the role of heterogeneities in the dynamics of excitable media, and how control of spatiotemporal patterns in these systems need to take into account the presence of such features.

List of Publications

- S. Sinha and S. Sridhar, **Controlling spatiotemporal chaos and spiral turbulence in excitable media** in *Handbook of Chaos Control* (Eds. E. Schöll and H-G. Schuster) Weinheim: Wiley-VCH Verlag, pp 703-718 (2007) [also at arxiv:0710.2265].

- S. Sridhar and S. Sinha, **Controlling spatiotemporal chaos in excitable media using an array of control points**, Europhysics Letters **81**, 50002 (2008) [also at arxiv:0711.1489].

- S. Sinha and S. Sridhar, **Controlling spiral turbulence in simulated cardiac tissue by low-amplitude traveling wave stimulation** in *Complex Dynamics in Physiological Systems: From Heart to Brain* (Eds. S. K. Dana, P. K. Roy and J. Kurths) Springer, pp 69-87 (2009).

- A. Pumir, S. Sinha, S. Sridhar, M. Argentina, M. Horning, S. Filippi, C. Cherubini, S. Luther and V. Krinsky, **Wave-train-induced termination of weakly anchored vortices in excitable media**, Physical Review E **81**, 010901(R) (2010) [also at arXiv:0902.3891].

- S. Sridhar, S. Sinha and A. V. Panfilov, **Anomalous drift of spiral waves in heterogeneous excitable media**, Physical Review E **82**, 051908 (2010) [also at arxiv:0909.4398].

- S. Sridhar and S. Sinha, **Response to sub-threshold stimulus is enhanced by spatially heterogeneous activity**, *communicated* [also at arxiv:1005.5032].

- S. Sridhar, A. Ghosh and S. Sinha, **Inexcitable obstacles can induce transition to scroll wave breakup in three-dimensional active media**, *in preparation.*

Contents

Chapter 1

Introducing excitable media

Living Nature, not dull Art
Shall plan my ways and rule my heart
– *Cardinal John Henry Newman*

1.1 Introduction

From the womb to the deathbed, our lives are determined by the properties of excitable systems. Excitable media denote a class of systems that share a set of features which make their dynamical behavior qualitatively similar. These features include (i) the existence of two characteristic dynamical states, comprising a stable *resting state* and a metastable *excited state*, (ii) a *threshold* value associated with one of the dynamical variables characterising the system, on exceeding which, the system switches from the resting state to the excited state, and (iii) a *recovery period* following an excitation, during which the response of the system to a supra-threshold stimulus is diminished,

if not completely absent [1]. Natural systems which exhibit such features include, in biology, cells such as neurons, cardiac myocytes and pancreatic beta cells, all of which are vital to the function of a complex living organism [2]. Other examples of dynamical phenomena associated with excitable media include cAMP waves observed during aggregation of slime mold [3], intracellular calcium waves observed in Xenopus oocytes [4], muscle contractions during childbirth in uterine tissue [5], intercellular calcium waves in brain slices [6, 7], chemical waves observed in the Belusov-Zhabotinsky reaction [8] and concentration patterns in CO-oxidation reaction on Pt(110) surface [9]. Excitation in such systems is observed as a characteristic *action potential*, where a variable associated with the system (e.g., membrane potential, in the case of biological cells) increases rapidly from its resting value to the peak value corresponding to the excited state, followed by a slower process during which it gradually returns to the resting state.

One of the simplest model systems capable of exhibiting all these features is the generic Fitzhugh-Nagumo system of two coupled differential equations [10, 11]:

$$\frac{\partial e}{\partial t} = e(1-e)(e-b) - g, \quad \frac{\partial g}{\partial t} = \epsilon(ke - g), \tag{1.1}$$

and its variants where the cubic nonlinear function is replaced by piecewise linear approximations [12, 13, 14]. Having only two variables, such a system is obviously incapable of exhibiting chaos. However, when several such excitable elements are coupled together to simulate a spatially extended medium, e.g., a piece of biological tissue made up of a large number of cells, the resulting high-dimensional dynamical system may display chaotic behav-

ior under certain conditions [1]. The genesis of this *spatiotemporal chaos* lies in the distinct property of interacting waves in excitable media, which mutually annihilate on colliding. This is a consequence of the region immediately behind the excitation wavefront exclusively consisting of cells that are all in the recovery phase. Thus, these cells in the waveback cannot be stimulated by another excitation wavefront when two such waves meet and attempt to cross each other [2]. As a result, the collision of two excitation fronts leads to mutual annihilation.

Interaction between such waves results in the creation of spatial patterns, referred to variously as *reentrant excitations* (in 1D), *vortices* or *spiral waves* (in 2D) and *scroll waves* (in 3D). These patterns form when an excitation wavefront is broken as the wave propagates across partially recovered tissue or encounters an inexcitable obstacle [15]. The free ends of the broken wavefront gradually curl around to form spiral waves. Once formed, these waves become self-sustained sources of high-frequency excitation in the medium, and, usually can only be terminated through external intervention. In general, spiral waves are associated with periodic or quasiperiodic patterns of temporal activity. Thus, the existence of nonlinear properties of wave propagation in several excitable media can lead to complex non-chaotic spatiotemporal rhythms.

Under certain conditions these spiral or scroll waves become unstable, eventually breaking up into multiple wavelets leading to a spatiotemporally

[1] Strictly speaking, it is the model systems with piecewise linear function approximating the cubic nonlinearity that are capable of exhibiting chaos when coupled together.

[2] Note that, unlike waves in ordinary diffusive media which dissipate as they propagate further, excitation waves are self-regenerating.

chaotic state. Various mechanisms of such breakup have been identified, including interaction of waves with inexcitable obstacles, meandering of the spiral, negative filament tension, etc [3]. For example, in a system where meandering is sufficiently high, part of the spiral wave can collide with another part of itself and break up spontaneously, resulting in the creation of multiple smaller spirals (Fig. 1.1). The process continues until the spatial extent of the system is spanned by several coexisting spiral waves that activate different regions without any degree of coherence. This state of *spiral turbulence* marks the onset of spatiotemporal chaos, as indicated by the Lyapunov spectrum and Kaplan-Yorke dimension [18].

1.2 Models of excitable media

Simple phenomenological models

The generic Fitzhugh-Nagumo model for excitable media (Eq. 1.1) exhibits a structure that is common to most models used in the papers discussed here. Typically, the dynamics is described by a fast or activation variable, $e(\mathbf{x}, t)$, and a slow or recovery variable, $g(\mathbf{x}, t)$, the ratio of the two timescales being denoted by ϵ. The resulting phase space behavior is shown in Fig. 1.2. For biological cells, the fast variable is often associated with the transmembrane potential, while the slow variable stands for an effective time-evolving membrane conductance that is a simplified representation of the actual complexity of several different types of ion channels. For the spatially extended

[3] For a detailed discussion of the multiple scenarios of spiral wave breakup, see Refs.[16, 17].

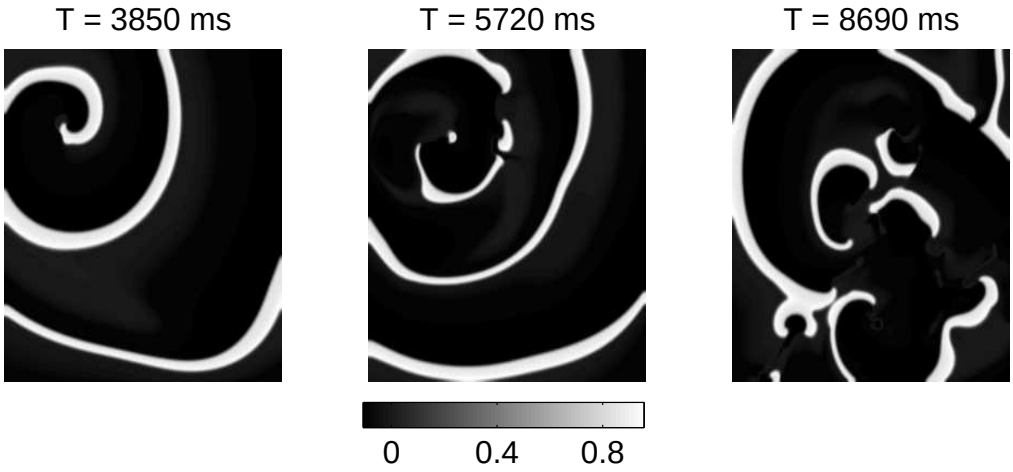

Figure 1.1: Onset of spatiotemporal chaos in the Panfilov model in a 2D simulation domain with linear dimension $L = 256$. The initial condition is a broken plane wave that is allowed to curl around into a spiral wave (left). Meandering of the spiral focus causes wavebreaks to occur (centre) that eventually results in spiral turbulence, with multiple independent sources of high-frequency excitation (right). The colorbar indicates the value of the activation variable e at each spatial point.

system, the fast variable of neighboring cells are coupled diffusively. There are several models belonging to this general class of excitable media that display breakup of spiral waves (in 2D) and scroll waves (in 3D), including the one proposed by Panfilov [13, 14]

$$\frac{\partial e}{\partial t} = \nabla^2 e - f(e) - g, \quad \frac{\partial g}{\partial t} = \epsilon(e,g)(ke - g). \tag{1.2}$$

The function $f(e)$, which specifies the fast activation processes is piecewise linear: $f(e) = C_1 e$, for $e < e_1$, $f(e) = C_2 e + a$, for $e_1 \leq e \leq e_2$ and $f(e) = C_3(e-1)$, for $e > e_2$. The parameters determining the shape of the function $f(e)$ are $e_1 = 0.0026$, $e_2 = 0.837$, $C_1 = 20$, $C_2 = 3$, $C_3 = 15$, $a = 0.06$. The recovery dynamics is determined by k $(= 3)$ and the time-scale $\epsilon(e,g)$, with $\epsilon(e,g) = \epsilon_1$ for $e < e_2$, $\epsilon(e,g) = \epsilon_2$ for $e > e_2$ and $\epsilon(e,g) = \epsilon_3$ for $e < e_1$ and $g < g_1$. The parameter ϵ_3^{-1} specifies the recovery time constant for small values of e and g. Similarly, ϵ_1^{-1} specifies the recovery time constant for relatively large values of g and intermediate values of e. We observe spatiotemporal chaos for a range of values, e.g., $g_1 = 1.8$, $\epsilon_2 = 1.0$, $\epsilon_3 = 0.3$. and $\epsilon_1 = 0.0133$.

Variants that also display spiral wave breakup in 2D include (i) the Barkley model [12]:

$$\frac{\partial e}{\partial t} = \nabla^2 e + \epsilon^{-1} e(1-e)(e - \frac{g+b}{a}), \quad \frac{\partial g}{\partial t} = e - g, \tag{1.3}$$

the appropriate parameter values being given in Ref. [19], and (ii) the Bär-Eiswirth model [20], which differs from (1.3) only in having $\partial g/\partial t = f(e) - g$, the functional form of $f(e)$ and parameter values being as in Ref. [21]. The Aliev-Panfilov model [22] is a modified form of the Panfilov model, that takes into account nonlinear effects such as the dependence of the action potential

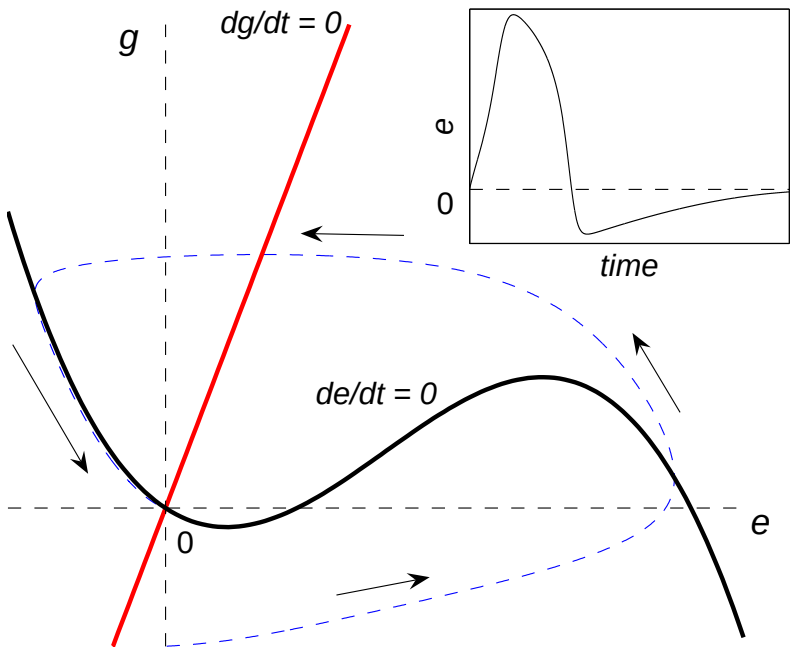

Figure 1.2: Dynamics in the phase-space of the Fitzhugh-Nagumo model, with the resulting time evolution of the action potential shown in the inset. The resting state corresponds to $e = 0, g = 0$.

duration on the distance of the wavefront to the preceding waveback. It has been used for demonstrating control of spiral turbulence in Refs. [23, 24].

Ionic models

The preceding simple models tend to disregard several complex features of actual biological cells, e.g., the existence of different types of ion channels. A class of models, inspired by the Hodgkin-Huxley formulation of a model describing action potential in the squid giant axon, explicitly takes such details into account. While the simple phenomenological models described above do reproduce generic features of several excitable media seen in nature, the more realistic models describe many properties of specific systems, e.g., ventricular tissue. The general form of such models are described by a partial differential equation for the transmembrane potential V,

$$\frac{\partial V}{\partial t} + \frac{I_{ion}}{C} = D\nabla^2 V, \tag{1.4}$$

where C is the membrane capacitance and D is the diffusion constant, which is a scalar if the medium is isotropic, and a tensor matrix if it is anisotropic. I_{ion} is the instantaneous total ionic-current density, and different realistic models essentially differ in its formulation. For example, in the Luo-Rudy I model [25] of guinea pig ventricular cells, I_{ion} is assumed to be composed of six different ionic current densities, *viz.* $I_{ion} = I_{Na} + I_K + I_{K1} + I_{Kp} + I_{Ca} + I_b$, where I_{Na} is the sodium ion current, I_{Ca} is the slow inward calcium current, I_K, I_{K1} and I_{Kp} are the different potassium currents and I_b is the background current. These currents are determined by several time-dependent ion-channel gating variables whose time-evolution is governed by ordinary

differential equations of the form:

$$\frac{d\xi}{dt} = \frac{\xi_\infty - \xi}{\tau_\xi}. \tag{1.5}$$

Here, $\xi_\infty = \frac{\alpha_\xi}{(\alpha_\xi+\beta_\xi)}$ is the steady state value of ξ and $\tau_\xi = \frac{1}{\alpha_\xi+\beta_\xi}$ is the corresponding time constant. The voltage-dependent rate constants, α_ξ and β_ξ, are complicated functions of V obtained by fitting experimental data.

1.3 Interaction of excitation waves with heterogeneities

Naturally occurring excitable systems are generally not homogeneous. Heterogeneities in these systems can be of many types, e.g., spatial gradients in the values of the system parameters, regions of varying conduction speed, occurrence of inexcitable obstacles, etc. These heterogeneities produce marked changes in the nature and dynamics of spatial patterns of activity. Studying the effect of these heterogeneities on the dynamics of excitable media is important as they are known to have critical consequences for the regular functioning of vital biological organs such as the heart. Various different kinds of heterogeneities that occur in the heart have often been implicated in several dangerous clinical conditions. Thus understanding the effect of such features on the dynamics of spiral/scroll waves is necessary to develop better treatment for heart disorders related to cardiac arrhythmias. We briefly review below the various known effects of such heterogeneities on activity in excitable systems.

Twisting of scrolls in heterogeneous medium

Three dimensional scroll waves in inhomogeneous media can exhibit twist. A twisted scroll can be pictured as several rotating spirals stacked on each other, with the rotation phase gradually changing along the *filament*, which is the line joining the singularities of the spiral wave on each plane. Twist may arise as a result of differences in rotation periods around the filament at different regions in the medium. However, a scroll does not keep getting twisted indefinitely but instead attains an equilibrium configuration which depends on the gradient of the varying rotation periods.

In a numerical study by Mikhailov *et al* [26] using a 3-dimensional system (described by FHN equations) that was divided into two regions having different rotation periods for the scroll wave, it was shown that the twisted vortices were stable. Further, the twisted scroll wave rotated faster than the untwisted ones, with the difference in rotation period increasing with ϵ, the ratio of time scales of the fast and slow variables. Using gradients in temperature, Pertsov *et al* later experimentally demonstrated the occurrence of twisted scrolls in the Belusov-Zhabotinsky reaction [27]. But unlike the numerical observations, the rotation period showed little dependence on twist. An interesting finding of the experiment was the occurrence of wavebreak on increasing the twist beyond a critical value. By using a heterogeneous medium with a step-like discontinuity comprising two regions of different rotation periods, as well as different recovery times, Panfilov *et al* showed that the twisted scroll breaks at the boundary between the regions to form two independently rotating vortices [28]. The breakup was seen to occur when the refractory period in one region was longer than the period of rotation of

the scroll in the other.

Inexcitable obstacles can have opposite dynamical effects

Inexcitable obstacles or defects in excitable media (such as scar tissue or pectinate muscle in the heart) may have both stabilising and destabilising influence on the dynamics of spatial patterns. It is well known that inexcitable obstacles in 2D or 3D medium can pin or anchor vortices that would have otherwise drifted through the system. In the heart, anchoring establishes a reentrant activity circuit, often termed as anatomical reentry. This is considered to be one of the primary mechanisms for occurrence of cardiac arrhythmias such as Ventricular Tachycardia(VT) [29]. The interaction of high-frequency wave trains with obstacles can also result in wave breaks leading to the occurrence of spiral waves [30], especially when the obstacle is sufficiently large and has sharp edges. On the other hand, it has been observed in both numerical and experimental studies that a sufficiently large obstacle can stabilize a rotating wave, preventing a transition to spatiotemporal chaos [31, 32]. Based on numerical studies, Garfinkel *et al* showed that for a given excitable system the size of the obstacle determines the stability of reentrant wave propagation [31]. For simulations carried out on an annular domain, it was shown that as the size of a central circular obstacle was gradually increased, spatiotemporal chaos was replaced by periodic activity of a pinned rotating wavefront. From the point of view of cardiology, this implies that an inexcitable region in the heart can, depending on its size, stabilize and convert a life-threatening arrhythmia like VF into a less dangerous one

like VT. This surprising consequence of the presence of inexcitable regions was experimentally confirmed by Valderrabano *et al* in experiments done in isolated pig ventricles [32]. More generally it has been shown that spiral wave dynamics is sensitively dependent on the location, size and type of inhomogeneity [33]. This sensitive dependence can be understood as a consequence of the complex, fractal-like structure of the boundary that separates the basins of attraction associated with the spiral wave and spatiotemporal chaos, respectively. Recently Jimenez *et al* [34] have experimentally observed the pinning of scroll rings to inexcitable heterogeneities which prevent the collapse of the rings.

Vinson *et al* have studied the role of both parameter gradients and tissue defects in the dynamics of scroll waves in a system described by FHN equations [35, 36]. They used an obstacle that did not extend along the entire length of the filament. This caused one end of the scroll wave to be anchored to the obstacle while the other end was free. The heterogeneity of the excitation threshold induces a drift along the gradient. The scroll wave twists because of differential rotation periods in different sections of the wave. However, depending on the size of the obstacle, the attachment of the wave to the obstacle may be only a transient phenomenon and the scroll wave could eventually detach.

To summarise, investigating the role of different types of heterogeneities in pattern formation through wave propagation dynamics in excitable media is extremely important for developing a deeper understanding of the processes that generate and maintain life-threatening cardiac arrhythmias. As, depending on the context, inhomogeneities can either promote or suppress

the transition to spatiotemporal chaos, it is vital to take them into account when devising control methods for terminating fibrillation.

1.4 Chaos control in excitable medium

Controlling spatiotemporal chaos in excitable media has certain special features. Unlike other chaotic systems, response to a control signal is not proportional to the signal strength because of the existence of a threshold and a characteristic action potential with a specific maximum amplitude. As a result, an excitable system shows discontinuous response to control as regions, which have not yet recovered from a previous excitation or where the applied signal is below the threshold, will not be affected by the control algorithm at all. Also, the focus of control in excitable media is to eliminate all activity rather than to stabilize unstable periodic behavior. This is because the problem of chaos termination has tremendous practical importance in the clinical context, as the spatiotemporally chaotic state has been associated with the cardiac problem of ventricular fibrillation (VF). VF involves incoherent activation of the heart that stops it from pumping blood to the rest of the body, and is fatal within minutes in the absence of external intervention. At present, the only effective treatment is electrical defibrillation, which involves applying very strong electrical shocks across the heart muscles, either externally using a defibrillator or internally through implanted devices. The principle of operation for such devices is to overwhelm the natural cardiac dynamics, so as to drive all the different regions of the heart to rest simultaneously, at which time the cardiac pacemaker can take over

once again. Although the exact mechanism by which this is achieved is still not completely understood, the danger of using such large amplitude control (involving $\sim$ 1 A cm^{-2} externally and $\sim$ 20 mA cm^{-2} internally [37]) is that, not only is it excruciatingly painful to the patient, but by causing damage to portions of cardiac tissue which subsequently result in scars, it can potentially increase the likelihood of future dynamical disorders of the heart. Therefore, devising a low-power control method for spatiotemporal chaos in excitable media promises a safer treatment for people at risk from potentially fatal cardiac arrhythmias.

1.5 Classifying chaos control schemes

In this section, we discuss most of the recent control methods that have been proposed for terminating spatiotemporal chaos in excitable media [4]. These methods are also often applicable to the related class of systems known as oscillatory media, described by complex Landau-Ginzburg equation [39], which also exhibit spiral waves and spatiotemporal chaos through spiral breakup. We have broadly classified all control schemes into three types, depending on the nature of application of the control signal. If every region of the media is subjected to the signal (which, in general, can differ from region to region) it is termed as *global control*; on the other hand, if the control signal is applied only at a small, localised region from which its effects spread throughout the media, this is referred to as *local control*.

Between these two extremes lie control schemes where perturbations are

[4] An earlier review, discussing methods proposed till 2002, can be found in Ref. [38].

applied simultaneously to a number of spatially distant regions. We have termed these methods as *non-global, spatially extended control*. While global control may be the easiest to understand, involving as it does the principle of synchronizing the activity of all regions, it is also the most difficult to implement in any practical situation. On the other hand, local control (as it can be implemented using a single control point) will be the easiest to implement but hardest to achieve.

1.5.1 Global control

The first attempt at controlling chaotic activity in excitable media dates back almost to the beginning of the field of chaos control itself, when proportional perturbation feedback (PPF) control was used to stabilize cardiac arrhythmias in a piece of tissue from rabbit heart [40]. In this method, small electrical stimuli were applied at intervals calculated using a feedback protocol, to stabilize an unstable periodic rhythm. Unlike in the original proposal for controlling chaos [41], where the location of the stable manifold of the desired unstable periodic orbit (UPO) was moved using small perturbations, in the PPF method it is the state of the system that is moved onto the stable manifold. However, it has been later pointed out that PPF does not necessarily require the existence of UPOs (and, by extension, deterministic chaos) and can be used even in systems with stochastic dynamics [42]. Later, PPF method was used to control atrial fibrillation in human heart [43]. However, the effectiveness of such control in suppressing spatiotemporal chaos, when applied only at a local region, has been questioned, especially as other experimental attempts in feedback control have not been able to terminate

fibrillation by applying control stimuli at a single spatial location [38].

More successful, at least in numerical simulations, have been schemes where control stimuli is applied throughout the system. Such global control schemes either apply small perturbations to the dynamical variables (e.g. the transmembrane potential) or one of the parameters (usually the excitation threshold). The general scheme involves introducing an external control signal A into the model equations, e.g., in the Panfilov model [Eq. (1.2)]: $\partial e/\partial t = \nabla^2 e - f(e) - g + A$, for a control duration τ. If A is a small, positive perturbation, added to the fast variable, the result is an effective reduction of the threshold (Fig. 1.3), thereby making simultaneous excitation of different regions more likely.

In general, A can be periodic, consisting of a sequence of pulses. Fig. 1.4 shows the results of applying a pulse of fixed amplitude but varying durations. While in general, increasing the amplitude, or the duration increases the likelihood of suppressing spatiotemporal chaos, it is not a simple, monotonic relationship. Depending on the initial state at which the control signal is applied, even a high amplitude (or long duration) control signal may not be able to uniformly excite all regions simultaneously. As a result, when the control signal is withdrawn, the inhomogeneous activation results in a few regions becoming active again and restarting the spatiotemporal chaotic behavior.

Most global control schemes are variations or modifications of the above scheme. Osipov and Collins [44] have shown that a low-amplitude signal used to change the value of the slow variable at the front and back of an excitation wave can result in different wavefront and waveback velocities which desta-

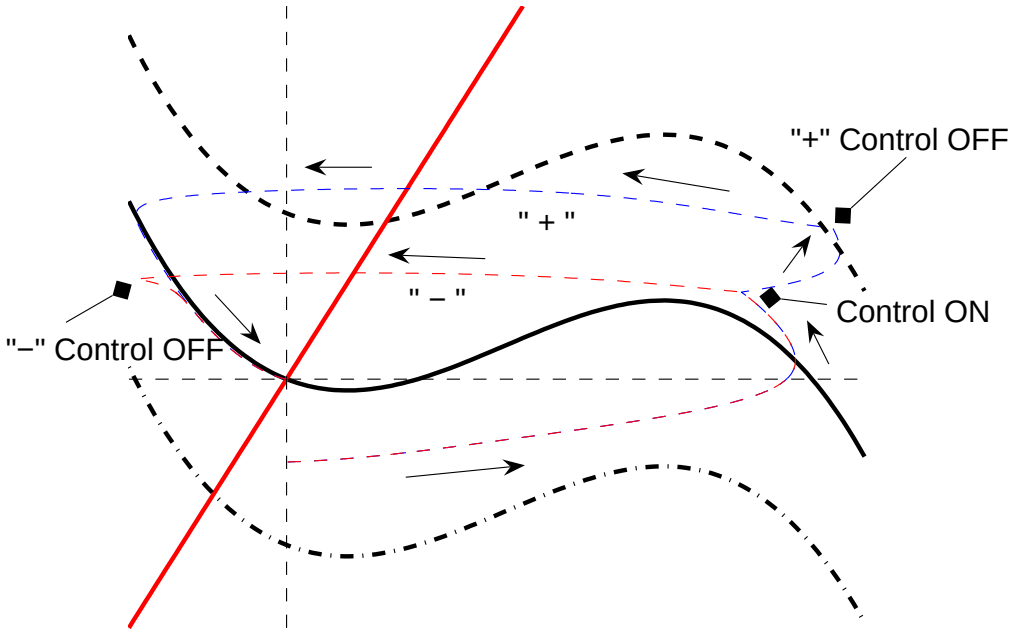

Figure 1.3: The result of applying a positive ("+") or negative ("−") additive perturbation of the same duration to the e variable in the Fitzhugh Nagumo model: "+" control decreases the threshold and makes excitation more likely, while "−" control decreases the duration of the action potential and allows the system to recover faster. For the duration of the control signal, the e-nullcline shifts upward (downward) for positive (negative) perturbation as indicated by the dashed (dash-dotted) curve.

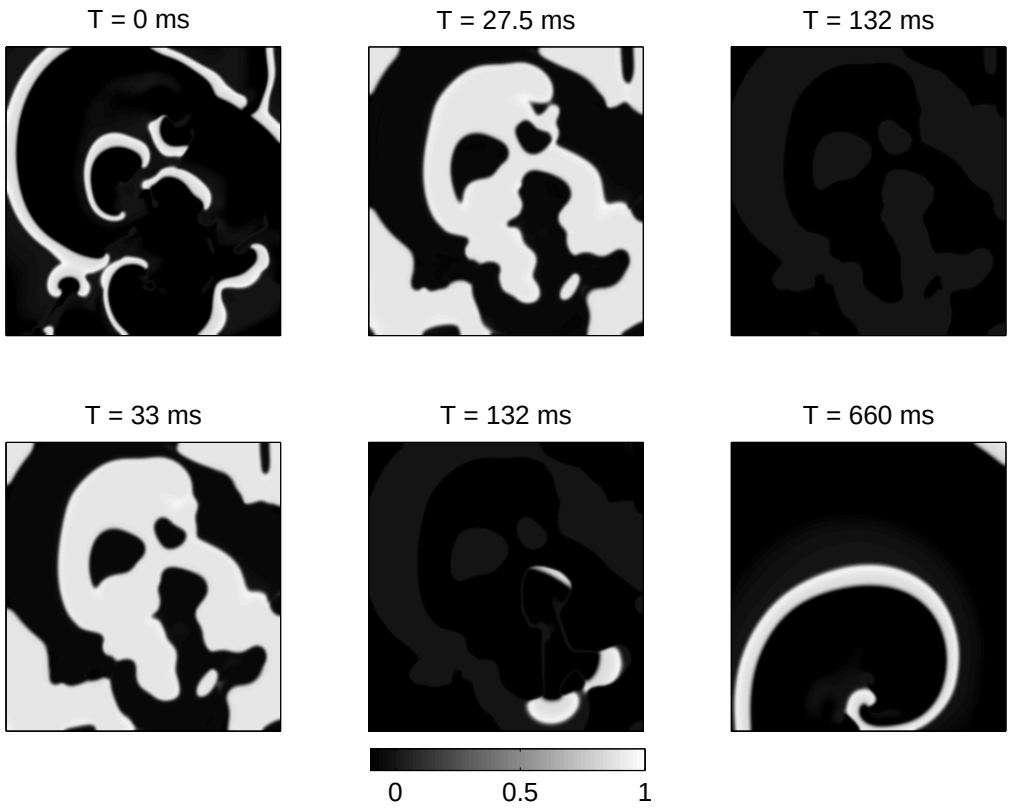

Figure 1.4: Global control of the 2-dimensional Panfilov model with $L = 256$ starting from a spatiotemporally chaotic state (top left). Pseudo-gray-scale plots of excitability e show the result of applying a pulse of amplitude $A = 0.833$ between $t = 11$ ms and 27.5 ms (top centre) that eventually leads to elimination of all activity (top right). Applying the pulse between $t = 11$ ms and 33 ms (bottom left) results in some regions becoming active again after the control pulse ends (bottom centre) eventually re-initiating spiral waves (bottom right).

bilizes the traveling wave, eventually terminating all activity, and, hence, spatiotemporal chaos. Gray [45] has investigated the termination of spiral wave breakup by using both short and long-duration pulses applied on the fast variable, in 2D and 3D systems. This study concluded that while short duration pulses affected only the fast variable, long duration pulses affected both fast and slow variables and that the latter is more efficient (using less power) in terminating spatiotemporal chaos. The external control signal can also be periodic [$A = Fsin(\omega t)$], in which case the critical amplitude F_c required for terminating activity has been found to be a function of the signal frequency ω [23].

Other schemes have proposed applying perturbations to the parameter controlling the excitation threshold, b, in Eq. (1.3). Applying a control pulse on this parameter ($b = b_f$, during duration of control pulse; $b = b_0$, otherwise) has been shown to cause an excitation wave to split into a pair of forward and backward moving waves [21]. Splitting of a spiral wave causes the two newly created spirals to annihilate each other on collision. For a spatiotemporally chaotic state, a sequence of such pulses may cause termination of all excitation, there being an optimal time interval between pulses that results in fastest control. Another control scheme that also applies perturbation to the threshold parameter is the uniform periodic forcing method suggested by Alonso *et al* [19, 46] for controlling scroll wave turbulence in three-dimensional excitable media. Such turbulence results from negative tension between scroll wave filaments, i.e., the line joining the phase singularities about which the scroll wave rotates. In this control method, the threshold is varied in a periodic manner [$b = b_0 + b_f cos(\omega t)$] and the result

depends on the relation between the control frequency ω and the spiral rotation frequency. If the former is higher than the latter, sufficiently strong forcing is seen to eliminate turbulence; otherwise, turbulence suppression is not achieved. The mechanism underlying termination has been suggested to be the effective increase of filament tension due to rapid forcing, such that, the originally negative tension between scroll wave filaments is changed to positive tension. This results in expanding scroll wave filaments to instead shrink and collapse, eliminating spatiotemporal chaotic activity. In a variant method, the threshold parameter has been perturbed by spatially uncorrelated Gaussian noise, rather than a periodic signal, which also results in suppression of scroll wave turbulence [47].

As already mentioned, global control, although easy to understand, is difficult to achieve in experimental systems. A few cases in which such control could be implemented include the case of eliminating spiral wave patterns in populations of the *Dictyostelium* amoebae by spraying a fine mist of cAMP onto the agar surface over which the amoebae cells grow [48]. Another experimental system where global control has been implemented is the photosensitive Belusov-Zhabotinsky reaction, where a light pulse shining over the entire system is used as a control signal [49]. Indeed, conventional defibrillation can be thought of as a kind of global control, where a large amplitude control signal is used to synchronize the phase of activity at all points by either exciting a previously unexcited region (advancing the phase) or slowing the recovery of an already excited region (delaying the phase) [50].

1.5.2 Non-global spatially extended control

The control methods discussed so far apply control signal to all points in the system. As the chaotic activity is spatially extended, one may naively expect that any control scheme also has to be global. However, we will now discuss some schemes that, while being spatially extended, does not require the application of control to all points of the system.

The control method of Sinha *et al* [51] involving suprathreshold stimulation along a grid of points, is based on the observation that spatiotemporal chaos in excitable media is a long-lived transient that lasts long enough to establish a non-equilibrium statistical steady state displaying spiral turbulence. The lifetime of this transient, τ_L, increases rapidly with linear size of the system, L, e.g., increasing from 850 ms to 3200 ms as L increases from 100 to 128 in the two-dimensional Panfilov model. This accords with the well-known observation that small mammals do not get life-threatening VF spontaneously whereas large mammals do [52] and has been experimentally verified by trying to initiate VF in swine ventricular tissue while gradually reducing its mass [53]. A related observation is that non-conducting boundaries tend to absorb spiral excitations, which results in spiral waves not lasting for appreciable periods in small systems.

The essential idea of the control scheme is that a domain can be divided into electrically disconnected regions by creating boundaries composed of recovering cells between them. These boundaries can be created by triggering excitation across a thin strip. For two-dimensional media, the simulation domain (of size $L \times L$) is divided into K^2 smaller blocks by a network of lines with the block size ($L/K \times L/K$) small enough so that spiral waves

cannot form. For control in a 3D system, the mesh is used only on one of the faces of the simulation box. Control is achieved by applying a suprathreshold stimulation via the mesh for a duration τ. A network of excited and subsequently recovering cells then divides the simulation domain into square blocks whose length in each direction is fixed at a constant value L/K for the duration of control. The network effectively simulates non-conducting boundary conditions (for the block bounded by the mesh) for the duration of its recovery period, in so far as it absorbs spirals formed inside this block. Note that τ need not be large at all because the individual blocks into which the mesh divides the system (of linear size L/K) are so small that they do not sustain long spatiotemporally chaotic transients. Nor does K, which is related to the mesh density, have to be very large since the transient lifetime, τ_L, decreases rapidly with decreasing L. The method has been applied to multiple excitable models, including the Panfilov and Luo-Rudy models (Fig. 1.5).

An alternative method [24] for controlling spiral turbulence that also uses a grid of control points has been demonstrated for the Aliev-Panfilov model. Two layers of excitable media are considered, where the first layer represents the two-dimensional excitable media exhibiting spatiotemporal chaos that is to be controlled, and the second layer is a grid structure also made up of excitable media. The two layers are coupled using the fast variable but with asymmetric coupling constants, with excitation pulses travelling $\sqrt{D}$ times faster in the second layer compared to the first. As the second layer consists only of grid lines, it is incapable of exhibiting chaotic behavior in the uncoupled state. If the coupling from the second layer to the first layer

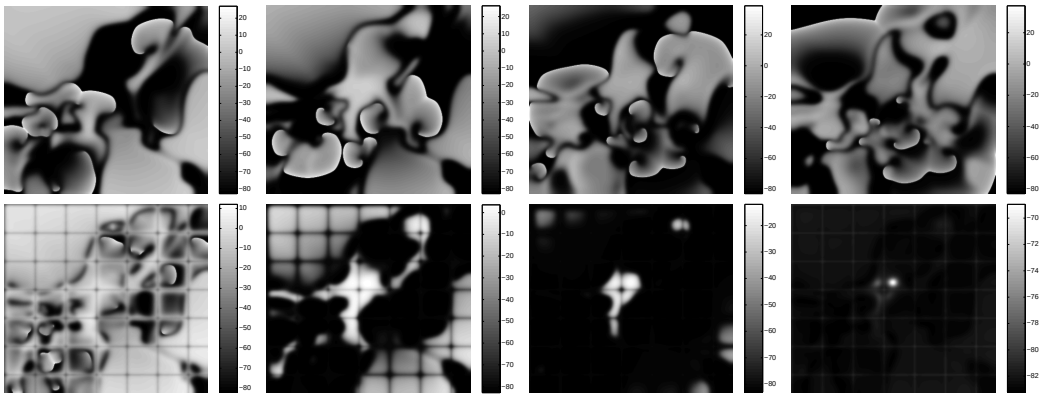

Figure 1.5: Spatiotemporal chaos (top row) and its control (bottom row) in the 2-dimensional Luo-Rudy I model with $L = 90$ mm. Pseudo-gray-scale plots of the transmembrane potential V show the evolution of spiral turbulence at times $T = 30$ ms, 90 ms, 150 ms and 210 ms. Control is achieved by applying an external current density $I = 150\mu A/cm^2$ for $\tau = 2.5$ ms over a square mesh with each block of linear dimension $L/K = 1.35$ cm. Within 210 ms of applying control, most of the simulation domain has reached a transmembrane potential close to the resting state value; moreover, the entire domain is much below the excitation threshold. The corresponding uncontrolled case shows spatiotemporal chaos across the entire domain.

is sufficiently stronger than the other way round, the stable dynamics of the second layer (manifested as a single rotating spiral) overcomes the spiral chaos in the first layer, and drives it to an ordered state characterized by mutually synchronized spiral waves.

Another method of spatially extended control is to apply perturbations at a series of points arranged in a regular array. Rappel *et al* [54] had proposed using such an arrangement for applying a time-delayed feedback control scheme. However, their scheme only prevented a spiral wave from breaking up and did not suppress pre-existing spatiotemporal chaos.

1.5.3 Local control of spatiotemporal chaos

We now turn to the possibility of controlling spatiotemporal chaos by applying control at only a small localized region of the spatially extended system. Virtually all the proposed local control methods use *overdrive pacing*, generating a series of waves with frequency higher than any of the existing excitations in the spiral turbulent state. As low-frequency activity is progressively invaded by faster excitation, the waves generated by the control stimulation gradually sweep the chaotic activity to the system boundary where they are absorbed. Although we cannot speak of a single frequency source in the case of chaos, the relevant timescale is that of spiral waves which is limited by the recovery period of the medium. Control is manifested as a gradually growing region in which the waves generated by the control signal dominate, until the region expands to encompass the entire system. The time required to achieve termination depends on the frequency difference between the control stimulation and that of the chaotic activity, with control being achieved faster,

the greater the difference.

Stamp *et al* [55] have looked at the possibility of using low-amplitude, high-frequency pacing using a series of pulses to terminate spiral turbulence. However, using a train of pulses (having various waveform shapes) has met with only limited success in suppressing spatiotemporal chaos. By contrast, a periodic stimulation protocol [56] has successfully controlled chaos in the 2D Panfilov model, as well as in other models [5]. The key mechanism underlying such control is the periodic alternation between positive and negative stimulation. A more general control scheme proposed in Ref. [58] uses *biphasic pacing*, i.e., applying a series of positive and negative pulses, that shortens the recovery period around the region of control stimulation, and thus allows the generation of higher frequency waves than would have been possible using positive stimulation alone. A simple argument shows why a negative rectangular pulse decreases the recovery period for an excitable system. The stimulation vertically displaces the e-nullcline and therefore, the maximum value of g that can be attained is reduced. Consequently, the system will recover faster (Fig. 1.3).

To understand how negative stimulation affects the response behavior of the spatially extended system, one can use *pacing response diagrams* indicating the relation between the control stimulation frequency f and the effective frequency f_{eff} , measured by applying a series of pulses at one site and then recording the number of pulses that reach another site located at a distance without being blocked by a region in the recovery period. Depending on

[5] A related case of this control scheme is that proposed in Ref. [57], where the high-frequency periodic signal is applied from the boundaries.

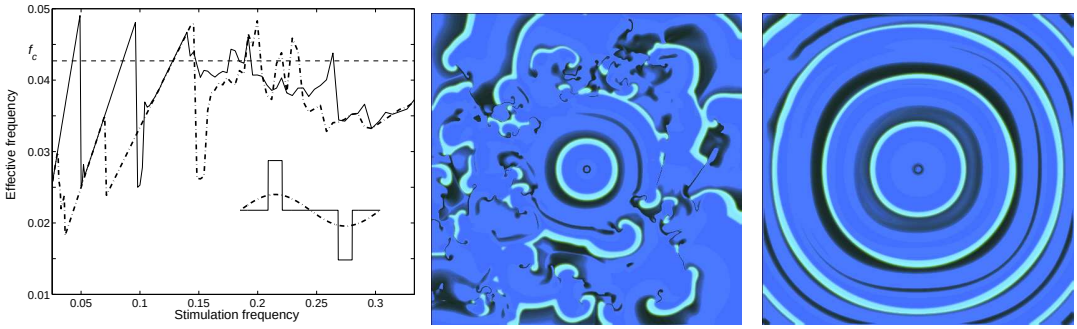

Figure 1.6: (left) Pacing response diagram for 2D Panfilov model ($L = 26$) showing relative performance of different waveforms. The dash-dotted line represents a sinus wave and the solid curve represents a wave of biphasic rectangular pulses, such that they have the same total energy. Successful control occurs if the effective frequency lies above the broken line representing the effective frequency of chaos (f_c), as seen for a larger system ($L = 500$) at times $T = 1000$ (center) and $T = 3800$ (right) time units, where the control signal is applied only at the center of the simulation domain. The excitation wavefronts are shown in white, black marks the recovered regions ready to be excited, while the shaded regions indicate different stages of recovery.

the relative value of f^{-1} and the recovery period, we observe instances of $n : m$ response, i.e., m responses evoked by n stimuli. If, for any range of f, the corresponding f_{eff} is significantly higher than the effective frequency of spatiotemporal chaos, then termination of spiral turbulence is possible. As shown in Ref. [58], there are indeed ranges of stimulation frequencies that give rise to effective frequencies that dominate chaotic activity. As a result, the periodic waves emerging from the stimulation region gradually impose control over the regions exhibiting chaos. Note that there is a tradeoff involved here. If f_{eff} is only slightly higher than the chaos frequency, control takes too long; if it is too high the waves suffer conduction block at inhomogeneities produced by chaotic activity that reduces the effective frequency, and control fails.

Recently, another local control scheme has been proposed [59] that periodically perturbs the model parameter governing the threshold. In fact, it is the local control analog of the global control scheme proposed by Alonso *et al* [19] discussed earlier. As in the other methods discussed here, the local stimulation generates high-frequency waves that propagate into the medium and suppress spiral or scroll waves. Unlike in the global control scheme, $b_f >> b_0$, so that the threshold can be negative for a part of the time. This means that the regions in resting state can become spontaneously excited, which allow very high-frequency waves to be generated.

1.5.4 Comparing chaos control schemes

Most of the methods proposed for controlling spatiotemporal chaos in excitable media involve applying perturbations either globally or over a spa-

tially extended system of control points covering a significant proportion of the entire system. However, in most practical situations this may not be a feasible option, either because of issues concerned with their implementation, or because of the large values of power involved. Moreover, if one is using such methods in the clinical context, e.g., terminating fibrillation, a local control scheme has the advantage that it can be readily implemented with existing hardware of the Implantable Cardioverter Defibrillator (ICD). This is a device implanted into patients at high risk from fibrillation that monitors the heart rhythm and applies electrical treatment when necessary through electrodes placed on the heart wall. A low-energy control method involving ICDs should therefore aim towards achieving control of spatiotemporal chaos by applying small perturbations from a few local sources.

However, the problem with most local control schemes proposed so far is that they use very high-frequency waves to overdrive chaos. Such waves are themselves unstable and may breakup during propagation, resulting in re-initiation of spiral waves after the original chaotic activity has been terminated. The problem is compounded by the existence of inhomogeneities in real excitable media. Recently, Shajahan *et al* [33] have found complicated dependence of spatiotemporal chaos on the presence of non-conducting regions and other types of inhomogeneities in an excitable system. Such inhomogeneities make the proposed local control schemes more vulnerable to failure, as it is known that high-frequency pacing interacting with, e.g., non-conducting obstacles, results in wave breaks and subsequent genesis of spatiotemporal chaos [30].

The search is still on for a control algorithm for terminating spatiotem-

poral chaos in excitable media that can be implemented using low power, or, that need be applied in only a small, local region of the system, and which will yet be robust, capable of terminating spiral turbulence without the control stimulation itself breaking up subsequently. The payoffs for coming up with such a method are enormous, as the potential benefits include an efficient device for cardiac defibrillation.

1.6 Overview of the thesis

The aim of the present thesis is to explore several aspects of the dynamics of spatial patterns in excitable media, in particular, their evolution upon interaction with structural and functional heterogeneities in the medium. We also propose multiple low-amplitude control schemes to eliminate spatiotemporally chaotic patterns from an excitable medium.

In **Chapter 2**, we study the drift dynamics of stable spirals in the presence of a heterogeneity gradient. Specifically, we consider a linear gradient in either the expression of ionic channels or in the strength of inter-cellular coupling. It has been observed both in experiments and in numerical simulations that spirals typically drift towards regions of longer rotation period. Till date there has been no satisfactory theoretical understanding of this phenomenon. For the first time, we demonstrate spiral drift towards regions of *shorter* rotation period or stronger coupling in a simple model of excitable media. This corresponds to an *anomalous drift* of the spiral core (i.e., the phase singularity point at the tip of the spiral) towards regions of higher excitability. This is because increasing either ion-channel density or cellular coupling can be

qualitatively regarded as increasing the excitability. We observe that such anomalous drift occurs over a wide range of model parameters for gradients in both ion-channel expression and inter-cellular coupling. Anomalous drift may have clinical significance as it moves the spiral core to a section where it rotates faster. This increases the likelihood of new wave-breaks in regions away from the core where the wave has a relatively slower period of rotation. Thus, it is a plausible generation mechanism for "mother rotor" fibrillation which is characterised by a persistent source of high-frequency excitations giving rise to turbulent activity in the heart. Further, we show that drift of spiral waves to regions of stronger coupling in the presence of gradients in the diffusion coefficient implies that the anomalous drift direction is a result of long wavelength instabilities. These instabilities are also known to determine the drift of scroll wave filaments. It suggests that the occurrence of scroll expansion in a 3-dimensional medium implies the existence of anomalous drift due to diffusion gradient in the corresponding 2-dimensional medium. Conversely, observation of anomalous drift might suggest parameter regions where scroll wave expansion is possible.

Conduction inhomogeneities or inexcitable obstacles commonly occur in biological tissue. When these obstacles are sufficiently large, they anchor freely rotating spiral waves. As mentioned earlier, spirals are often observed to drift towards regions of longer rotation period. Thus in a medium without significant inexcitable obstacles the spirals drift towards the boundaries and eventually are removed from the system. This has consequences for clinical treatment of certain types of arrhythmias such as tachycardia that have been associated with existence of spiral waves. Such freely rotating vortices can

be terminated by generating high frequency waves through external periodic stimulation or "pacing". However, spiral waves that are anchored to inexcitable obstacles cannot be unpinned and removed easily. In fact, earlier work based on cellular automata models had made the claim that it may not be possible to unpin such vortices at all [60]. In **Chapter 3** we use a simple model of excitable media to show that under certain conditions unpinning of a spiral wave is indeed possible by using a high frequency source of excitation. This happens when the radius of the obstacle R_{obst} is smaller than the radius of the free spiral core R_{core}, which is the trajectory traced by the tip of an unpinned spiral wave. As the excitability is decreased, we observe that spirals can unpin from larger obstacles as a result of increasing R_{core}. The maximum period of pacing which is successful in dislodging a pinned spiral decreases with the increasing size of obstacle. Thus, unpinning fails when the obstacle is larger than a specific size which is related to R_{core}. While prior work had shown that pinned waves can be removed in special cases, such as in the presence of slow conduction regions [61] or by exploiting "alternans" effects [62], this is the first time that such unpinning is shown to be possible even in the absence of such special conditions. We have verified that our results are model independent and apply to more realistic descriptions. Our work is a positive step towards understanding why the existing clinical treatment of cardiac arrhythmias involving rapid stimulation of cardiac tissue is often successful, in spite of the presence of a large number of conduction inhomogeneities in the heart.

In **Chapter 4**, we study the transition from a stable 3-dimensional scroll wave to a spatiotemporally chaotic state in the presence of an inexcitable

obstacle. The important point to note is that the parameter regime considered in this work is such that, in the absence of the inexcitable obstacle, the scroll wave is stable. Hence, the observed scroll wave breakup resulting in spatiotemporal chaos is purely obstacle induced and not dependent on other dynamical parameters. The initial wave break typically occurs at the boundary of the obstacle where the wave propagation exhibits a transition from properties characteristic of a pinned wave to that of a freely rotating wave. The key to the underlying mechanism is the difference in rotation periods between the free and pinned regions of the scroll wave. The portion of the scroll wave attached to a large obstacle has a longer rotation period than the rest of the wave. This difference in rotation periods leads to a helical winding of the wave around the obstacle, that causes the wave to slow down as it approaches a bounding edge of the obstacle because of changes in the curvature of the front. In certain circumstances, the resulting interaction between the waveback and a following wavefront can cause conduction block of the latter along the obstacle surface. As a result, there is a detachment of the following wave from the obstacle, the free end curling up and forming a new phase singularity. Unlike previously reported mechanisms for scroll breakup, this scenario does not involve the dynamics of the existing filament and the tearing of the scroll wave which characterizes the breakup occurs far from the line of phase singularities. Successive creation of multiple scroll filaments and their interactions rapidly result in a spiral turbulent state. Our observation has potential significance for the explanation of the origin of spatiotemporally chaotic states observed during lethal disturbances to cardiac rhythm such as fibrillation. Inexcitable obstacles are known to occur in normal hearts and

increase in number with age. For example, scars resulting from after-effects of myocardial infarction can create obstacles that often occur deep inside the cardiac tissue. Although they may not be easily observed by epicardial imaging, they can have a significant role in the evolution of reentrant waves, as seen from our work. Our results, which are model independent, suggest a new 3-dimensional mechanism for the transition from rapid but stable periodic activity (corresponding to tachycardia) to spatiotemporal chaos (corresponding to fibrillation) in the presence of inexcitable obstacles.

As mentioned above, the breaking up of spirals or scroll waves in excitable media is associated with the onset of spatiotemporal chaos. Typically such states can be eliminated or controlled using external perturbations. Terminating spatiotemporally chaotic states using low amplitude external stimulation assumes added importance in light of their connection to life-threatening disturbances in the cardiac rhythm. Hence there is a pressing need for developing low-amplitude control schemes that do not involve very large perturbations to the system. In **Chapter 5** we propose a spatially extended but non-global scheme using an array of control points for terminating spatiotemporally chaotic excitations. A low-amplitude control signal applied sequentially at each point on the array results in a travelling wave of excitation in the underlying medium which drives away the turbulent activity. Our method is robust even in the presence of significant heterogeneities in the medium, which have often been an impediment to the success of other control schemes. Energy required to eliminate all chaotic activity depends on the number of points used to bring about control. As we use an array of spatially separated control points and because all of them are not activated

simultaneously, the energy applied to the medium at any instant of time is much lower than the case where the current is applied globally. In addition, as our scheme does not involve high frequency excitations, we avoid the potential problem of destabilising such waves in the presence of conduction inhomogeneities, which could have resulted in further breakup of the existing spiral waves.

The control method we have just described uses small-amplitude stimuli which are nevertheless supra-threshold, i.e., stimulation that will excite a homogeneous resting tissue. In **Chapter 6** we investigate the effect of sub-threshold stimulus on regular and chaotic patterns in detailed ionic models of excitable media. A sub-threshold stimulus will not elicit an excitation from a quiescent medium, but we find that when applied on a medium with spatially heterogeneous activity, it can significantly alter the dynamics of the recovering front of the wave. Such a stimulus typically slows down the waveback velocity while the speed of the excitation front is unchanged. The reduction of waveback velocity induced by globally applied sub-threshold stimulation leads to spatial coherence that can terminate all activity in the medium, including spatiotemporal chaos. We analytically derive a relation between the stimulation parameters for which such behavior can be observed. This result is not just significant as a low-amplitude chaos control scheme but could be a possible explanation for why electrical signals that are strongly attenuated while passing through biological tissue can still significantly affect excitation dynamics.

We conclude with a general discussion of the role of heterogeneities in the dynamics of excitable media, and how control of spatiotemporal patterns in

these systems need to take into account the presence of such features.

Chapter 2

Anomalous drift of spiral waves

> Had I been present at the Creation, I would have given some useful hints for the better ordering of the universe.
>
> – *Alfonso the Wise*

> Nature does not proceed by leaps.
>
> – *Carolus Linnaeus*

Spiral waves, as mentioned in Chapter 1, are high frequency sources of excitation observed in a broad class of physical, biological and chemical excitable systems [2]. The dynamics of spiral waves is primarily characterised by the motion of its core (i.e., the trajectory of the spiral wave tip, defined to be a phase singularity). These waves can display a range of dynamics including steady stationary rotation, and non-stationary meander and drift [63].

Studying the phenomenon of spiral drift in biological excitable medium is important because of their possible connection with various life-threatening disturbances to the heart. In a heterogeneous excitable medium such as the heart, spiral waves of excitation can have significant drift. In fact spiral drift

is believed to be a possible underlying mechanism for arrhythmias like polymorphic ventricular tachycardia [64, 63]. This arrhythmia is characterised by an aperiodic electrocardiogram, and can be a precursor to fully disordered activity that characterizes potentially fatal ventricular fibrillation [65]. Therefore, understanding the mechanisms leading to spiral wave drift is not only a problem of central interest for physics of excitable media, but also has potential clinical significance [17].

In this chapter we study the drift dynamics of spiral waves in the presence of gradients in a simple model of heterogeneous excitable medium. Drift motion is characterised by significant linear translational component. In our study we consider linear gradients in the (a) distribution of ion-channel expression and (b) inter-cellular coupling. Spirals which generally have stationary non-meandering rotation, tend to drift in the presence of such linear gradients. This drift motion has both longitudinal (along or against the direction of the gradient) and transverse (perpendicular to the gradient) components. We classify the drift as either *normal* or *anomalous* depending on longitudinal direction of the drift. For the type of gradient considered here, normal drift would take the spiral towards region of either longer period or smaller inter-cellular coupling, while anomalous drift would move the spiral to a region of faster period or stronger inter-cellular coupling. Here we report for the first time the anomalous drift of spiral waves towards regions having shorter period or stronger coupling, in reaction-diffusion models of excitable media.

In section 2.1 we introduce briefly a few previously known results on the problem of drift in excitable media. In section 2.2 we give details of the model

of excitable media that is used in this study as well as the type of gradients that are applied. In section 2.3 we discuss the results of our study detailing the parameter ranges over which anomalous drift is observed. In section 2.4 we explain the physical mechanism of anomalous drift. We conclude with a brief discussion on the potential relevance of our study and its limitations.

2.1 The drift so far

One of the most important causes of spiral drift is the heterogeneous nature of the excitable medium. This was first predicted in cellular automata models with step-like or discontinuous inhomogeneity [66], which was later confirmed by experiments [27, 67]. Subsequently, drift has been shown to be induced by a smooth gradient of excitability in both simple and biologically realistic ionic models of cardiac tissue [68, 69, 70]. Theoretical arguments indicate that the direction of the transverse component of the spiral drift (i.e., orthogonal to the gradient) depends on model parameters [71]. On the other hand, the longitudinal component is always directed towards the region with longer spiral rotation period [70]. This phenomenon has been seen in a variety of excitable media models of different complexity [68, 70]. However, till date there is no satisfactory understanding of the reasons behind the spiral wave drift towards regions with longer rotation period. Although earlier kinematic studies suggested the possibility of drift towards region with shorter period [72], it has never actually been observed in a model of excitable tissue. The occurrence of drift in the direction of shorter period may have clinical significance, as it moves the spiral core to a section where it rotates faster.

This increases the likelihood of additional wavebreaks in regions where the wave has a relatively slower period of rotation. Thus, it is a possible generation mechanism for "mother rotor" fibrillation [73, 74, 75], characterised by a stationary persistent source of high-frequency excitations giving rise to turbulent activity in the heart.

Electro-physiological heterogeneities in cardiac tissue may arise, in general, through spatial variation in the distribution of ion-channel expression in excitable tissue [76]. There can also be gradients in the inter-cellular coupling as a result of the inhomogeneous distribution of the conductances of gap junctions connecting neighboring cells [77]. In this chapter, we use a simple model of cardiac tissue to investigate the role of both these types of heterogeneities in governing the direction of the spiral wave drift. We report the existence of a regime where the spiral wave core moves towards the region having (a) shorter period (due to higher expression of ionic channels), and/or (b) higher inter-cellular coupling. As reduction in either the ion-channel density or the inter-cellular coupling can impede wave propagation, it can be qualitatively regarded as decreasing the excitability of the medium. Thus, both the cases mentioned above may be considered as a drift towards region of higher excitability, a result that may increase our understanding of how heterogeneities affect spiral wave dynamics in the heart.

2.2 Model and methods

A generic model of excitable media that describes the dynamics of transmembrane potential V in cardiac tissue has the form

$$\partial V/\partial t = \nabla\gamma D\nabla V + \alpha I_{ion}(V, g_i), \tag{2.1}$$

$$\partial g_i/\partial t = F(V, g_i). \tag{2.2}$$

Here, I_{ion} is the total ionic current traveling through the channels on the cellular membrane, D accounts for the inter-cellular coupling and g_i describes the dynamics of gating variables for the various ion-channels. In this chapter, we study the effects of a heterogeneous distribution of ion-channel expression and intercellular coupling. For this purpose, we introduce the parameters α and γ, which represent the spatial variation in ion-channel expression and conduction properties (respectively) for an inhomogeneous medium. Parameter α directly scales the value of ion-channel expression in Eq. 2.1, while γ scales the diffusion coefficient as $D = D_0 + \gamma(x)$ ($D_0 = 1$ for the rest of the chapter). In this study, we have used the Barkley model [12], where the several gating variables are aggregated into a single variable g that controls the slow recovery dynamics of the medium with $F(V, g) = V - g$. The nonlinear dependence of the ionic current on the fast variable V is represented by the cubic function $I_{ion} = [V(1-V)(V-((g+b)/a)]/\epsilon$, where a and b are parameters governing the local kinetics and ϵ is the relative time scale between the local dynamics of V and g. The spatial heterogeneity of ion-channel expression and cellular coupling are assumed to have linear functional form, viz., $\alpha(x) = \alpha_0 + \Delta\alpha\ x$ and $\gamma(x) = \gamma_0 + \Delta\gamma\ x$. The variable x $(= -d/2, \ldots, d/2)$ represents the spatial position along the principal direction of the inhomo-

geneity gradient, where d is the length of the domain measured along this direction and the origin (i.e., $x = 0$) is at the midpoint of the simulation domain. At this point, $\alpha = \alpha_0$, $\gamma = \gamma_0$, and $\Delta\alpha, \Delta\gamma$ measure their rate of change along the gradient. For all the figures in this chapter, we have used $\alpha_0 = 1.15$, $\gamma_0 = 1.3$ and $\epsilon = 0.02$.

The two dimensional system is discretized on a square spatial grid of size $L \times L$ ($L = 200$ for the figures shown here). The values of space step Δx and time step Δt used are 0.5 and 0.005 respectively (in dimensionless units). A sample of simulations have been repeated for $\Delta x = 0.25$ to verify numerical accuracy. The model equations are solved using forward Euler scheme with a standard 5-point stencil for the spatial second derivatives and central differences for the spatial first derivatives. No-flux boundary conditions are implemented at the edges of the simulation domain. The initial condition for all simulations is a stable spiral wave generated in a homogeneous medium with $\alpha = \alpha_0$ and $\gamma = \gamma_0$.

2.3 Results

To investigate the role of heterogeneity in spiral drift, we have considered spatial gradients in α or γ individually (keeping the other parameter constant). After extensive numerical simulations that scan over the (a, b) parameter space of the Barkley model, we have found that it is indeed possible to observe *anomalous drift* of the spiral, i.e., a drift towards regions with shorter period or higher inter-cellular coupling. Examples of such anomalous drift are shown in Fig. 2.1 (A,C). In both of these cases, *anomalous drift* is towards

the region of higher excitability (in the qualitative sense) because increase in either α or γ enhances wave propagation. For comparison, in Fig. 2.1 (B,D) we show the normal drift of the spiral, i.e., towards regions of lower excitability. This is seen for a set of (a, b) values which is farther from the boundary with the sub-excitable region of the Barkley model [78] than the (a, b) parameter set for which anomalous drift is observed in Fig. 2.1 (A,C).

To analyse the genesis of anomalous drift, we first look at how the parameters γ and α affect the spiral wave in an *homogeneous* medium. As γ is only a scaling factor for the diffusion coefficient, the period of the spiral wave does not depend on it. Thus, neither normal nor anomalous drift is associated with a significant change in the period. However, due to the discrete nature of wave propagation in real systems such as cardiac tissue, there is a small decrease in the period when the spiral wave moves towards regions having higher cellular coupling during anomalous drift. Fig. 2.2 (A) shows the variation of the spiral period as a function of the parameter α, which decreases as α increases [1]. Thus, for normal drift in the presence of α gradient, the period of the spiral increases as the core moves towards lower α regions. On the other hand, we see a decrease in the period in the case of anomalous drift towards regions having higher values of α. In contrast, the wavelength does not appear to be a determinant of the drift. For anomalous drift in presence of a gradient in γ, the wavelength increases (as $\sqrt{\gamma}$), while it decreases for an α gradient, as it moves towards regions of higher α

[1]For a, b parameters where anomalous drift is observed, the period and wavelength of spiral wave exhibits a more rapid divergence with decreasing α compared to the parameter regime showing normal drift.

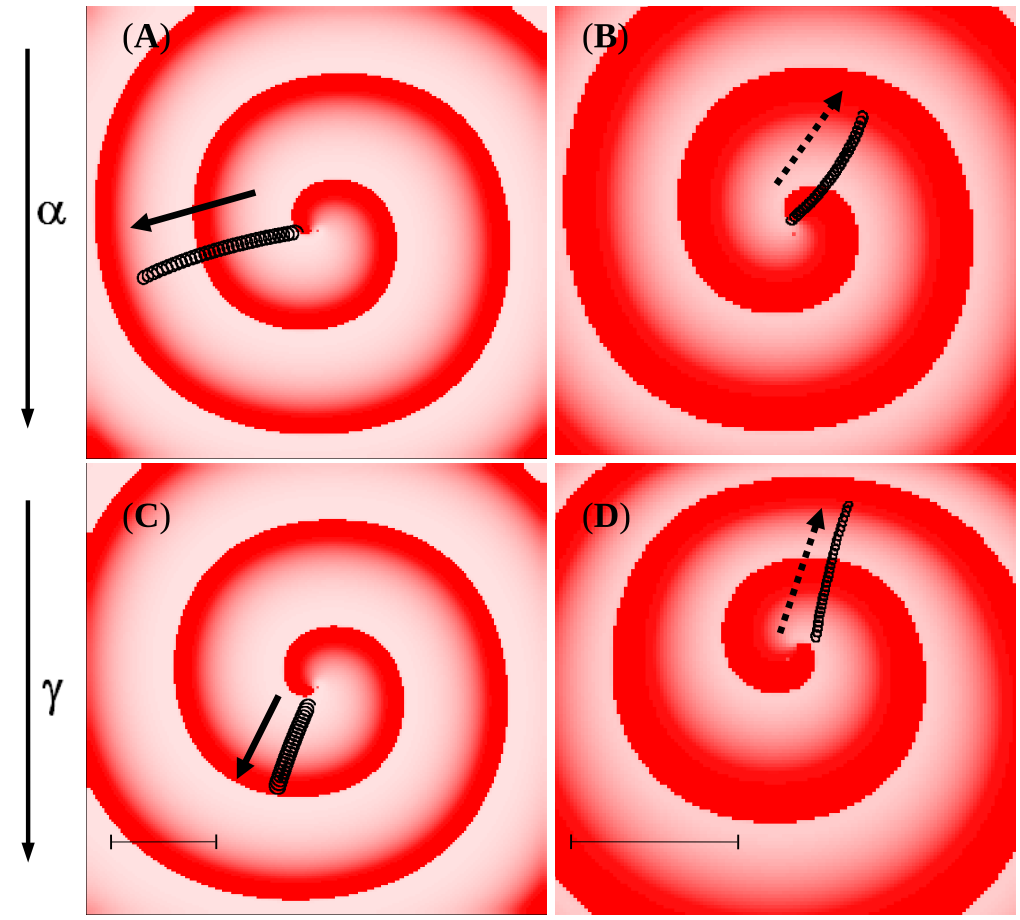

Figure 2.1: Pseudocolor images of spiral wave at the instant when the gradient in ion-channel expression α (top row) and cellular coupling (bottom row) is applied. (A, C) Anomalous drift towards increasing values of α (A) or γ (C), the direction being shown by solid arrows. (B, D) Normal drift in α (B) or γ (D) gradient. Parameter values are $a = 0.82$, $b = 0.13$ (for A, C) and $a = 1.02$, $b = 0.15$ (for B, D). The gradients applied are (A, B) $\Delta\alpha = 0.005$, $\Delta\gamma = 0$, and (C, D) $\Delta\alpha = 0$, $\Delta\gamma = 0.040$. In all cases, the gradient is along the vertical direction, with α or γ increasing from top to bottom. In (B,D) the region around the core is magnified to make the wavelength of the spiral comparable to that in (A,C). The trajectories shown correspond to 100 time units and are obtained using the algorithm given in Ref. [79]. The bar indicates a scale of 25 space units.

[Fig. 2.2 (B)].

Next, we study the effect of the magnitude of spatial gradient in α or γ on the velocity of spiral drift. Fig. 2.3 shows the longitudinal component of the drift velocity, v_L, i.e., along the gradient, as a function of the spatial variation in α or γ. Note that, positive v_L corresponds to anomalous, while, negative v_L corresponds to normal drift of the spiral wave. Fig. 2.3 shows that, for normal drift, increasing either of the gradients results in a monotonic increase of v_L (broken lines). However, in the case of anomalous drift as a result of α gradient, we see a *non-monotonic* behavior in v_L, which first increases but then decreases and becomes negative [Fig. 2.3 (A)]. Thus, the anomalous drift of the spiral towards shorter period in α gradient is seen only for small $\Delta\alpha$. For higher $\Delta\alpha$, there is a reversal of direction and the spiral exhibits normal drift. On the other hand, Fig. 2.3 (B) shows that for a gradient in γ, the anomalous drift is observed for the entire range of $\Delta\gamma$ that is investigated.

We have also studied the effect of the local kinetics on anomalous drift by varying the Barkley model parameter a [Fig. 2.4 (A)]. Increasing a (keeping b fixed) decreases the activation threshold of the medium, and thus makes the system more excitable. We observe that for both α and γ gradients, the variation of v_L as a function of a is non-monotonic. For the cellular coupling (γ) gradient, the presence of anomalous regime clearly correlates with excitability. The drift is anomalous at lower excitability, but becomes normal at higher excitability. However, for the gradient in α, the anomalous drift occurs only over an intermediate range of a. For lower and higher excitability, the drift becomes normal. Note that, arguments put forth in Ref. [80] suggest that in the *large core limit* (corresponding to very low excitability), the

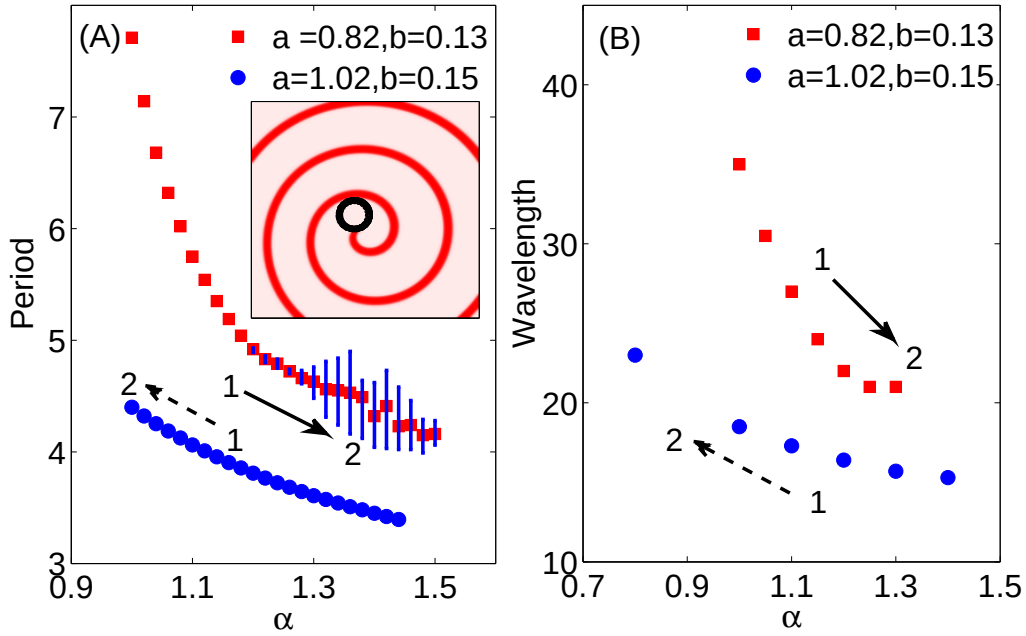

Figure 2.2: The variation of spiral period (A) and wavelength (B) as a function of the parameter α. The symbols "1" and "2" correspond to the values of α in the region around the initial and final positions (respectively) of the spiral waves in Fig. 2.1, with the same sets of Barkley model parameters being used. The solid and broken arrows represent the directions of anomalous and normal drift, respectively, in presence of a gradient in α. Results shown are obtained by averaging over multiple values recorded from symmetrically placed points in the simulation domain to smooth variations arising from spiral wave meandering at high values of α. Error bars are indicated when the standard deviation is larger than the symbol size used. The inset in (A) is a pseudocolor image of a spiral wave showing its trajectory in a *homogeneous* medium with parameters $a = 0.82$, $b = 0.13$ and $\alpha = 1.275$.

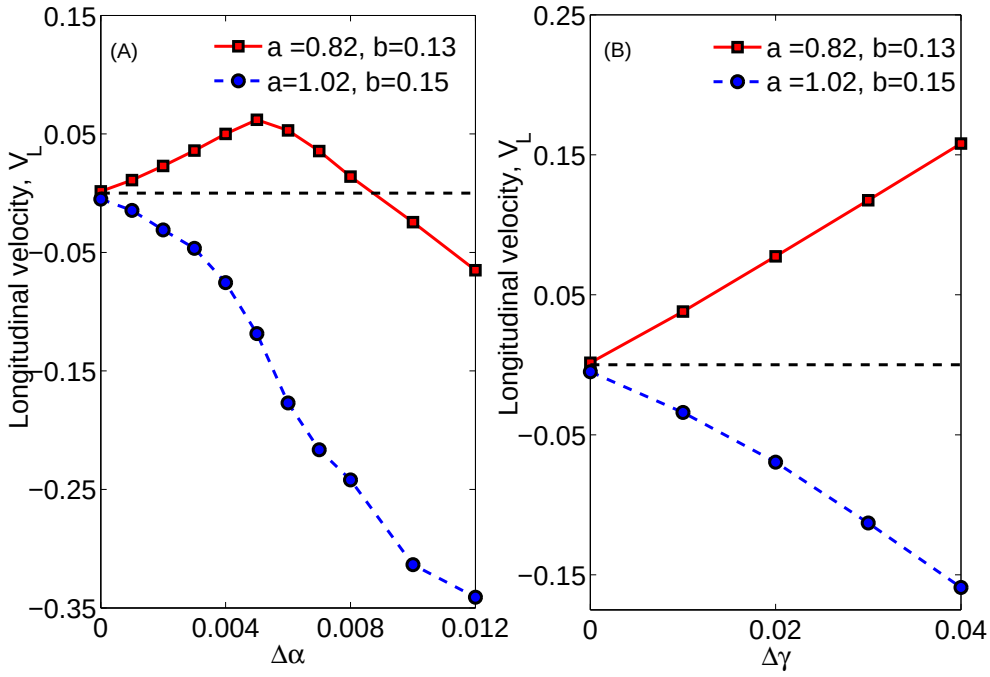

Figure 2.3: Drift velocity depends on the gradient in parameters α and γ. (A) Non-monotonic variation (solid curve) of the longitudinal component of spiral wave drift velocity v_L as a function of the gradient in ion-channel expression, $\Delta\alpha$, for a model system with parameters $a = 0.82, b = 0.13$. Positive values of v_L indicate anomalous drift. For a different set of parameters ($a = 1.02, b = 0.15$), normal drift is seen for the entire range of gradients used (broken curve). (B) Variation of v_L with the gradient in cellular coupling, $\Delta\gamma$. Solid and broken curves represent the anomalous and normal drift seen for the two parameter sets mentioned earlier (respectively), and are observed throughout the range of gradients used.

longitudinal component of drift velocity resulting from a parameter gradient in α should disappear.

2.4 Mechanism

The mechanism of anomalous drift in α gradient remains unclear. However, we can understand the anomalous drift for the cellular coupling (γ) gradient, by relating it to other drift phenomena in excitable media. Note that the Laplacian term in Eq. (2.1) can be expanded as,

$$\nabla\gamma(x)D\nabla V = (D_0 + \gamma(x))\nabla^2 V + \partial\gamma/\partial x\ \partial V/\partial x. \tag{2.3}$$

Therefore, the heterogeneous cellular coupling $\gamma(x)$ contributes to both the gradient ($\partial\gamma/\partial x\ \partial V/\partial x$), as well as, second order ($\gamma(x)\nabla^2 V$) terms. The relative contributions of these terms to the longitudinal component of drift velocity is shown in Fig. 2.4 (B). We observe that the principal effect on v_L is due to the $\partial\gamma/\partial x\ \partial V/\partial x$ term, while $\gamma(x)\nabla^2 V$ accounts only for about 10% of the observed drift. This allows us to propose the following explanation for anomalous drift in the presence of a gradient in γ. If we do not consider the $\gamma(x)\nabla^2 V$ term in the Laplacian, the spatial operators in Eq. (2.3) are seen to be identical to those in equations describing drift of a spiral wave in the presence of an electric field [81]. This latter, in turn, is similar to the Laplacian describing the drift of radially symmetric filaments of a scroll ring in three-dimensional excitable media [82, 83]. As shown in Refs. [84, 85], the drifts observed in these two kinds of systems are induced by the same instabilities. We see from Fig. 2.4 (B) that the gradient $\partial\gamma/\partial x\ \partial V/\partial x$, which determines the drift in an electric field and that of scroll wave filaments, also

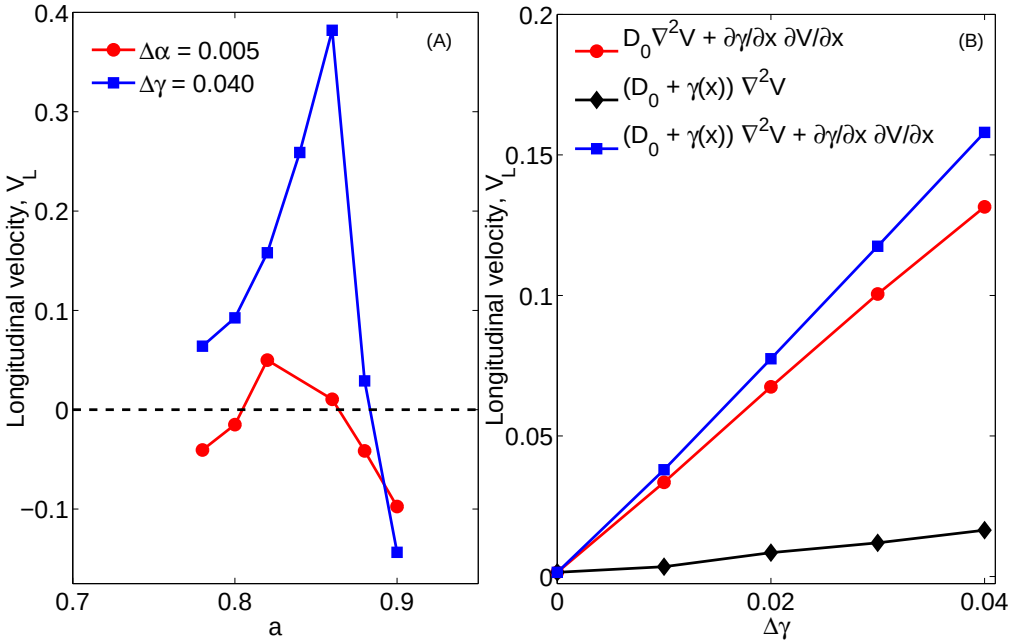

Figure 2.4: (A) Non-monotonic variation of the longitudinal component of drift velocity, v_L, as a function of the model parameter a ($b = 0.13$). The two curves correspond to media having a constant gradient in excitability (circles: $\Delta\alpha = 0.005$, $\Delta\gamma = 0$) and cellular coupling (squares: $\Delta\alpha = 0$, $\Delta\gamma = 0.040$). (B) The contribution to v_L from the different components in the diffusion term as a function of the gradient in cellular coupling, $\Delta\gamma$. The circles and diamonds correspond to the linear and second-order contributions, and, squares correspond to the complete Laplacian term, respectively. All data points shown are for $a = 0.82$, $b = 0.13$.

determines the drift as a result of γ gradient. Therefore, we infer that the anomalous drift direction (towards stronger cellular coupling) observed by us is also a result of the same long wavelength instabilities determining the drift of scroll wave filaments. This suggests that the occurrence of scroll expansion in 3-D implies the existence of anomalous drift in γ gradient in 2-D. Conversely, observation of anomalous drift might suggest parameter regions where scroll wave expansion is possible.

2.5 Discussion

In this chapter, we have explicitly demonstrated in a simple model of smoothly varying heterogeneous excitable medium that spiral waves can drift towards regions with shorter rotation period (corresponding to larger expression of ion-channels) and/or stronger cellular coupling. Both can be broadly considered to be drift towards a more excitable region.

Our analysis can be easily extended to biologically realistic models, such as Luo-Rudy I or TNNP [25, 86], which have the same form as Eq. (2.1), and to types of heterogeneity inferred from direct experimental measurements [87], although gradients in ion channel expression may not affect all ion channels and do not always affect excitability. It might be possible to infer the parameter range in realistic models where anomalous drift may occur by using the relation between the cellular coupling gradient induced drift and scroll ring expansion. Note that the latter phenomenon has recently been seen in the Luo-Rudy I model [83].

Spiral waves are not only relevant for cardiac tissue, but are also ob-

served in many different excitable media. Thus, it may be possible to relate our observation with results of kinematic studies [72] and models of cyclic catalysis in replicating entities [88], which predict drift towards region with shorter periods. From a clinical perspective, anomalous drift is important as it may result in fibrillation by promoting wavebreaks away from the spiral core. Spiral drift in the presence of a cellular-coupling gradient maybe a key factor giving rise to abnormal wave activity in regions of the heart where conductivity changes, e.g., at Purkinje-muscle cell junctions or in an infarct border zone [89]. It can also be studied experimentally and numerically in many model systems, such as, heterogeneous mono-layers of neonatal rat cardiomyocytes [90].

To conclude, we have observed that spiral waves in heterogeneous excitable media, having linear gradient in ion-channel expression or cellular coupling, can drift towards regions having shorter spiral rotation period or stronger cellular coupling. It appears to be related to regimes where expansion of 3-dimensional scroll wave filaments is observed. Such anomalous drift of spiral waves may increase the likelihood of complex spatio-temporal patterns in excitable medium, e.g., turbulent electrical activity in the heart.

Chapter 3

Wave-train induced termination of weakly anchored vortices

The only cure for grief is action.

— *George Henry Lewes*

Though you drive away Nature with
a pitchfork, She always returns.

— *Horace*

Spatial patterns of electrical excitation often take the form of rotating spirals. When these spirals occur in biological excitable medium like the heart, they are associated with the breakdown of its normal rhythmic pumping action. Controlling these spiral waves using low-amplitude external perturbation is not only a problem of fundamental interest in the study of dynamics of excitations in active media [51, 91, 92, 93, 94, 95, 96], but also has significant implications for the clinical treatment of cardiac arrhythmias [97].

Periodic high frequency stimulation (pacing) from a localised region in the excitable medium can generate wave-trains that interact with the spiral wave [98]. If the frequency of external stimulation is higher than the rotation frequency of the spiral wave, the wave-train induces the vortex to drift. In a finite medium, the vortex is eventually driven to the boundary and thereby eliminated from the system [99, 100, 101]. However while the above argument can account for the removal of spirals in a homogeneous medium, it may not apply to the case of spirals in a medium with inexcitable obstacles. Spiral waves tend to anchor or pin themselves to heterogeneities. The anchoring can be considered as analogous to the pinning of vortices in disordered superconductors [102, 103]. Attachment of the spiral to an obstacle prevents its removal by the use of a rapid external wave-train [104, 35, 34, 105]. In the heart, obstacles such as blood vessels or scar tissue, can play the role of pinning centres [106], leading to anatomical reentry, the sustained periodic excitation of the region around the obstacle.

In this chapter we use a simple model of excitable media to detail the conditions for which unpinning of an anchored spiral wave by pacing can happen. We also derive a relation between the size of the obstacle and the pacing period which can successfully detach the pinned vortex. In section 3.1 we describe in brief the argument based on a classical result of Wiener and Rosenblueth that a pinned spiral cannot be detached using a wave-train. In section 3.2 we describe the model and the method used in our study. Section 3.3 reports the results of our simulations, while in section 3.4 we discuss the relation between the size of the obstacle and the pacing period required for unpinning a spiral wave attached to it. We conclude with suggestions about

possible experiments that can be done to validate our predictions

3.1 Classical theory and its failure

In the immediate neighborhood of an inexcitable obstacle, pinned vortices are qualitatively equivalent to waves circulating in a one-dimensional ring. They can be removed by external stimulation provided the electrode is located on the reentrant circuit, i.e., the closed path along which the vortex propagates around the obstacle, and the stimulus is delivered within a narrow time interval [107]. However, for the more general situation of pacing waves generated far away from the reentrant circuit, a classical result due to Wiener and Rosenblueth (WR) states that, all waves circulating around such obstacles are created or annihilated in pairs (see Ref. [60], in particular, pp.216-224). This implies that it is impossible to unpin the spiral wave by a stimulated wave train.

However, as we demonstrate later in this chapter, the WR mechanism for the failure of pacing in unpinning spiral waves is valid only when the radius of the *free* spiral core (i.e., the closed trajectory of the spiral tip defined as a phase singularity [52]) is small compared to the size of the obstacle. We elucidate below the transition between the case of a free vortex and one attached to a large obstacle as a result of systematic reduction of the core radius of the free spiral, R_{FS}, relative to the obstacle size, R_{obst}, by increasing the excitability of the medium. Our main result is that an anchored rotating wave can be removed by a stimulated wave train provided $R_{FS} > R_{obst}$.

3.2 Models and methods

To illustrate our arguments, we use the Barkley model of excitable media [12], described by an excitatory (u) and a recovery (v) variable:

$$\begin{aligned} \partial_t u &= \frac{1}{\epsilon} u(1-u)[u-(v+\frac{b}{a})] + \nabla^2 u, \\ \partial_t v &= (u-v), \end{aligned} \tag{3.1}$$

where, a and b are parameters describing the kinetics. The relative time-scale ϵ between the local dynamics of u and v is set to 0.02. We discretize the system on a square spatial grid of size $L \times L$, with a lattice spacing of $\Delta x = 0.25$ and time step of $\Delta t = 0.01$ in dimensionless units. For our simulations reported here we have chosen $L = 200$. We solve Eq. 3.1 using forward Euler scheme with a standard nine-point stencil for the Laplacian. No-flux boundary conditions are implemented at the edges of the simulation domain. An obstacle is implemented by introducing a circular region of radius R_{obst} in the center of simulation domain, inside which diffusion is absent. Pacing is delivered by setting the value of u to $u_p = 0.9$ in a region of 6×3 points at the center of the upper boundary of the simulation domain. We have explicitly verified that minor variations in the pacing scheme does not qualitatively alter the results. The maximum pacing frequency is limited by the *refractory period*, T_{ref}, the duration for which the stimulation of an excited region does not induce a response.

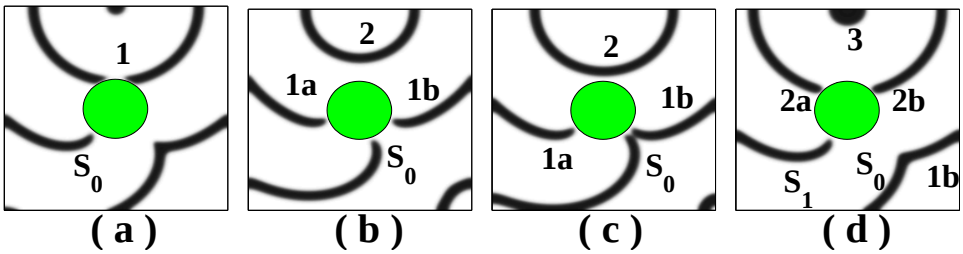

Figure 3.1: (a) Wave S_0, pinned to an obstacle (shaded), rotates counterclockwise; wave 1 is the first pacing wave. (b) Wave 1 hits the obstacle, and separates into a wave rotating counterclockwise ($1a$) and a wave rotating clockwise ($1b$). (c) Waves S_0 and $1b$ collide and merge leaving only one rotating wave $1a$ denoted S_1 hereafter. (d) The wave resulting from the merging of S_0 and $1b$ leaves the system. The interaction between the following pacing wave, 2 and S_1, is similar to that shown in (a-c). Thus, the pinned vortex persists. Numerical simulation of the Barkley model with parameters: $a = 0.9$, $b = 0.17$; the pacing period is $T_p = 6.7$ and the radius of the obstacle is $R = 6.5$.

3.3 Results

When the obstacle size is large relative to the core radius of the free spiral, R_{FS}, the failure of a wave train in unpinning the vortex is illustrated in Fig. 3.1. Initially, the spiral wave S_0 rotates counterclockwise around the obstacle. During the interaction with pacing waves, the number of waves attached to the obstacle can change due to two possible processes (see Ref. [60], p.216 and 220). First, when the pacing wave reaches the obstacle, it splits into two oppositely rotating waves: one clockwise and the other counterclockwise. Second, collision between two rotating waves, as seen in Fig. 3.1(c), results in the annihilation of a pair of counterclockwise and clockwise waves. In both cases, the number of waves rotating counterclockwise is always larger than the number rotating clockwise by 1. Thus, in addition to conservation of total topological charge (i.e., sum of the individual chiralities, $+1$ or -1) for *all* spiral waves in a medium [108, 52], topological charge *around* the obstacle also appears to be conserved. However, in the limiting case of infinitesimally small obstacle corresponding to a free vortex, a stimulated wave-train with frequency higher than that of the spiral wave will always succeed in displacing the latter, eventually removing it from a finite medium. Thus, there is a transition from failure to successful pacing as R_{obst} is reduced relative to R_{FS}.

The primary fact responsible for this transition is that the spiral wave is no longer in physical contact with an obstacle of size smaller than R_{FS} [106], contrary to the fundamental assumption of Ref. [60]. Fig. 3.2 shows an explicit example of successful detachment of a pinned wave from the obstacle boundary, where the core radius of a free spiral in the medium is made larger

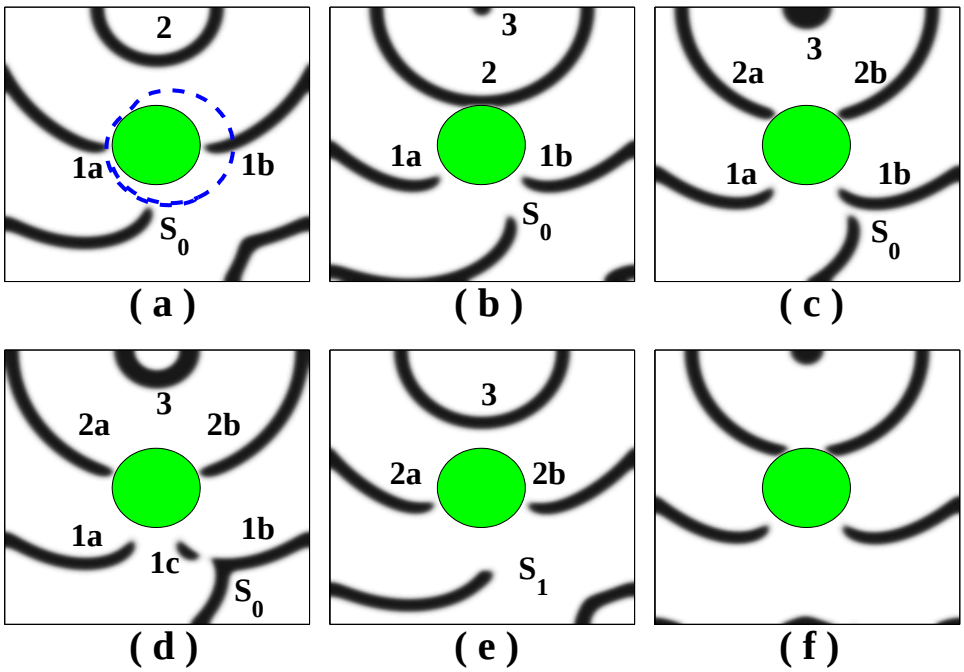

Figure 3.2: Lowering excitability results in successful detachment of pinned vortex by pacing. S_0 is a rotating wave whose core (dashed line) is larger than the pinning center (shaded). (a-c) are topologically as in Fig. 3.1. (d) A wavelet $1c$ is produced after collision of waves S_0 and $1b$, in contrast with Fig. 3.1(d). (e) The wavelet $1c$ collides with $1a$ and the resulting wave S_1 is displaced away from the obstacle. (f) Subsequent pacing induces drift of the spiral wave S_1 to the boundary, eventually removing it from the medium. The parameters are as in Fig. 3.1, except for $a = 0.895$ and $b = 0.1725$, resulting in increasing the vortex core size.

than R_{obst} by diminishing the excitability of the system.

The possibility of unpinning the wave in Fig. 3.2 can be traced to the following fact: the collision between S_0 and the pacing wave-branch $1b$ occurs *a small distance away* from the obstacle boundary and does not result in complete annihilation of both waves. A small fragment $1c$ survives in the spatial interval between the collision point and the obstacle [Fig. 3.2(d)]. If the tip of S_0 is close to the obstacle, the fragment $1c$ is small, and rapidly shrinks and disappears. However, if the gap between the reentrant wave tip and the obstacle is large at the collision point, such that the size of $1c$ is larger than a critical value l_n, the fragment can survive. As $1c$ propagates further away, it collides with the pacing wave $1a$ and forms a new broken wave S_1 that is completely detached from the obstacle. Interaction with successive pacing waves progressively pushes the vortex further away from the obstacle, and eventually from a finite medium. The difference between the number of spirals rotating counterclockwise and clockwise *around the obstacle* changes from 1 initially (Fig. 3.2, a), to 0 in Fig. 3.2(e), contrary to what happens for a larger obstacle (Fig. 3.1). The absence of topological charge conservation for waves rotating *around* a smaller obstacle underlines the breakdown of the fundamental assumption behind the WR argument for why pacing cannot detach pinned waves. The unpinned wave is subsequently driven outside the system boundaries by pacing (Fig. 3.2, f), thus eventually also reducing the total topological charge of the *finite* medium to 0.

The relative size of the obstacle, compared to the free spiral core, is the key parameter that decides whether a pinned reentrant wave can be removed or not. Indeed, the radius of the free spiral core in the successful case,

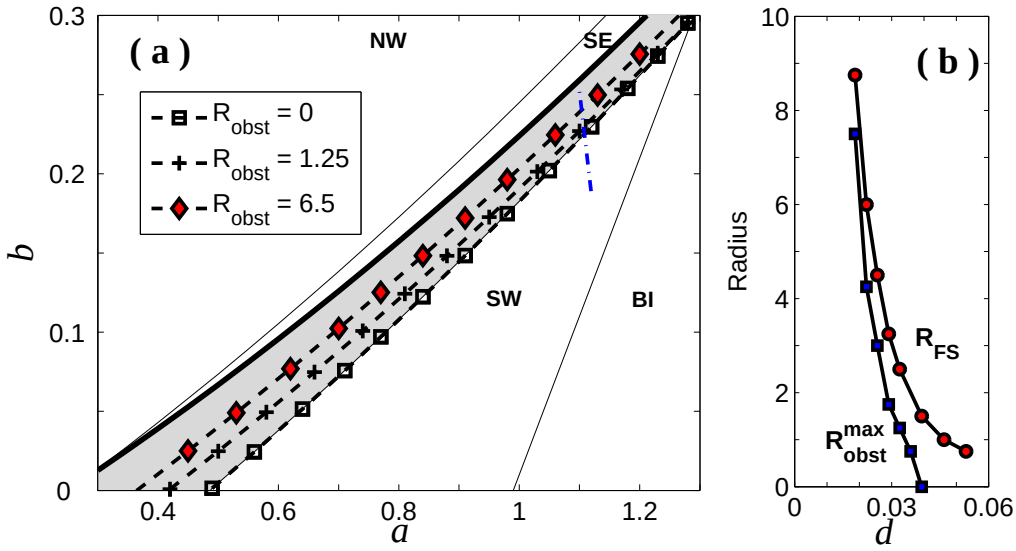

Figure 3.3: (a) Parameter space of the Barkley model. Unpinning is possible in the shaded portion of the *SW* region, which exhibits persistent spiral waves. The thick line indicates the boundary with the SE region, where spirals cannot form. The domain where unpinning is possible shrinks with increasing size of the pinning center, the three dashed lines corresponding to $R_{obst} = 0$, i.e., no obstacle (square), $R_{obst} = 1.25$ (plus) and $R_{obst} = 6.5$ (diamond). (b) Radius R_{FS} of the free spiral and the maximum obstacle radius R_{obst}^{max} from which wave trains can unpin vortices, as a function of the distance d from the SE-SW boundary, along the dot-dashed line indicated in (a). Note that $R_{FS} > R_{obst}^{max}$, and both increase with decreasing d. [In (a), NW (BI) indicates the parameters for which steady waves are absent (the medium is bistable).]

$R_{FS} = 9.05$ (Fig. 3.2) is significantly larger than in the unsuccessful one, $R_{FS} = 5.80$ (Fig. 3.1). It is further confirmed by a detailed numerical study of the interaction between a pacing wave train and a pinned spiral over the (a, b) parameter space of the Barkley model. As shown in Fig. 3.3(a), the rotating wave anchored to the obstacle can be removed by pacing only in the neighborhood of the sub-excitable (SE) region (using the terminology of Ref. [19]), where R_{FS} diverges [Fig. 3.3(b)]. This is explained by noting that in the SE regime, the tangential velocity of a broken wavefront is negative, thus causing the front to shrink and not form a spiral. As we approach the regime where spiral waves are persistent (SW), the tangential velocity of the wavebreak gradually increases to zero and becomes positive on crossing the SE-SW boundary, so that the broken wave front can now evolve into a spiral. As R_{FS} increases with decreasing tangential velocity of the wave front, the spiral core becomes large close to the SE region resulting in successful pacing-induced termination of pinned reentry.

We observe that there is a maximum radius of the obstacle (R_{obst}^{max}) close to R_{FS} above which pacing is unsuccessful in detaching the anchored spiral wave [Fig. 3.3(b)]. Fig. 3.4(a) shows that the pacing period for successful unpinning from the obstacle is bounded by the refractory period (T_{ref}) and a maximum value T_p^{max} that is independent of R_{obst} for small obstacles. As we approach R_{obst}^{max}, the upper bound sharply decreases, becoming equal to the refractory time at R_{obst}^{max}, which indicates that pacing will be unsuccessful in unpinning waves attached to obstacles of radii larger than R_{obst}^{max}. Thus, the results shown in Figs. 3.3(b) and 3.4(a) demonstrate our earlier assertion that pacing induced removal of anchored waves will be possible only when

the obstacle is smaller than the core radius of the free spiral wave in the medium.

Relation between spiral period and obstacle size

Our numerical results indicate that the maximum pacing period necessary for detaching a pinned spiral wave is a decreasing function of the obstacle size [Fig. 3.4(a)]. This can be explained semi-quantitatively by the following geometric argument, valid when the size of the obstacle is small compared to the core size of the spiral, and supported by the simulations shown in Fig. 3.4(c-f). The tip of the spiral S moves along its circular trajectory, shown by the broken line in Fig. 3.4(b), and interacts with the pacing wave coming from the top, represented by a solid line. The part $1b$ of the pacing wave collides with S at the point C characterized by an angle θ that the spiral tip makes with the symmetry axis (i.e., the line joining the centers of the obstacle and spiral core); the resulting wave eventually leaves the system [Fig. 3.4(d)]. The remaining section of the pacing wave splits into two waves, $1a$ and $1c$, propagating along either side of the obstacle. The wave tip moves approximately in a straight line from C, so that the length of the wave $1c$ at the symmetry axis is $l = R_{FS}(1 + \cos\theta) - 2R_{obst}$. When the fragment $1c$ is larger than the nucleation size l_n, it expands into a wavefront that reconnects with wave $1a$. This results in a displacement of the wave $1a$ away from the obstacle, leading to unpinning (as in Fig. 3.2). For $l < l_n$, $1c$ shrinks and eventually disappears, resulting in unsuccessful pacing.

Thus, the condition for detachment is $l \geq l_n$. The length l is a decreasing function of the angle θ, which in turn, is a decreasing function of the

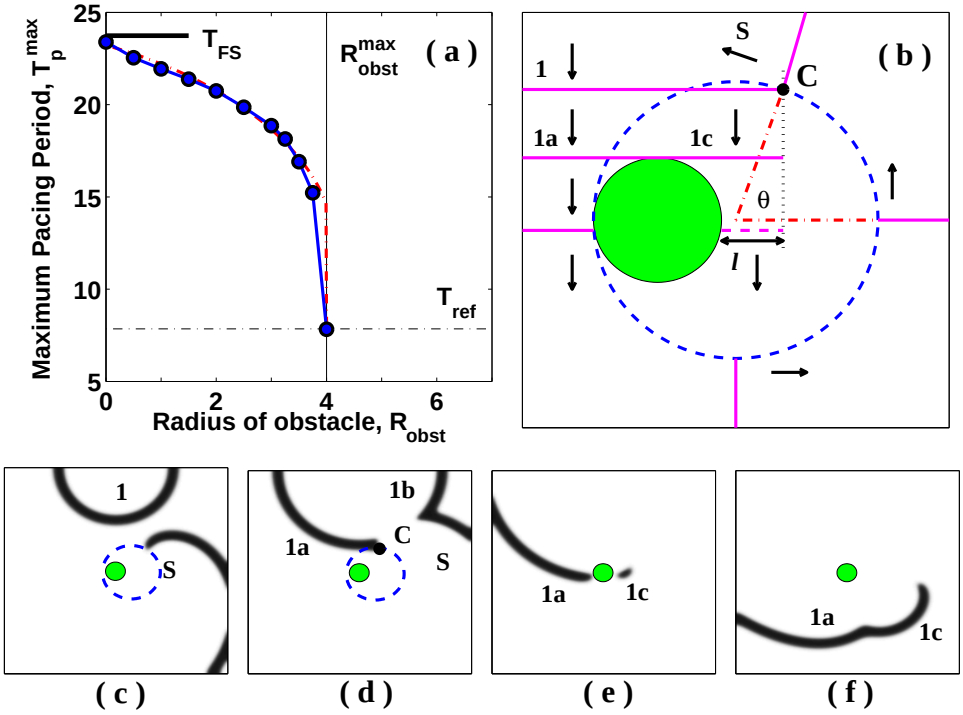

Figure 3.4: (a) The maximum pacing period T_p^{max} at which unpinning is possible as a function of the obstacle radius R_{obst}. For the parameters $a = 1.1323, b = 0.2459$ that we have used, the maximum radius of obstacle from which unpinning can occur is $R_{obst}^{max} = 4$. T_{FS} is period of a free spiral wave and T_{ref} is the refractory period. The dashed line indicates the prediction from Eq. 3.2. (b) The wavelet formation mechanism leading to the detachment of the pinned vortex (schematic). (c-f) Numerical simulation of the Barkley model. S collides with wave 1 at point C at an angle θ. The part $1b$ of the pacing wave merges with S, moving out of the system. The remaining part of the pacing wave collides with the obstacle (shaded) separating into $1a$ and a small wavelet $1c$. When the length l of wavelet $1c$ is larger than the critical nucleation length, $1c$ survives and collides with S. This results in unpinning of S.

pacing period, T_p, as explained below. The relation between T_p and θ can be established by estimating the time interval for two successive collisions of the spiral with the pacing waves. From the point of collision C, the pacing wave reaches the obstacle after time $T_1 = (R_{FS} \sin\ \theta - R_{obst})/v$, and the symmetry axis after time $T_2 = T_1 + (R_{obst} T_{FS}/4R_{FS})$. From the symmetry axis, the new reentrant wave S moves by an angle $(\theta + \pi)$ to arrive at C at time $T_3 = T_2 + [T_{FS}(\theta + \pi)/2\pi]$, where it collides with the next pacing wave. Noting that $T_3 = T_p$ allows us to implicitly express T_p as a function of θ, and thereby, l. The maximum pacing period leading to detachment is obtained when $l = l_n$, as:

$$T_p^{max} = \frac{R_{FS}}{v}(\sin\theta_c - f_R) + \frac{f_R T_{FS}}{4} + \frac{T_{FS}(\theta_c + \pi)}{2\pi}, \tag{3.2}$$

where, $\theta_c = \arccos(2f_R - 1 + [l_n/R_{FS}])$ and $f_R = R_{obst}/R_{FS}$. When $R_{obst} > R_{obst}^{max} = R_{FS} - (l_n/2)$, T_p^{max} has complex values, indicating that for larger obstacles the fragment is too small to survive. The nucleation length l_n can thus be estimated from R_{obst}^{max}, which allows us, in turn, to determine the dependence of T_p^{max} as a function of R_{obst} from Eq. 3.2. Fig. 3.4(a) shows this to be in fair agreement with our numerical simulations.

3.4 Discussion

We stress that the arguments used here are model independent, and are based only on the property that waves in excitable media annihilate on collision. We verified numerically [109] that wave-train induced unpinning is also observed in a more detailed and realistic description of cardiac tissue, the Luo-Rudy I model [25], under conditions of reduced excitability. Meandering, which

occurs in the Barkley model at low a, b values (Fig. 3.3, a), does not affect the physical effect discussed here. Note that the proposed unpinning mechanism is for the case of an obstacle smaller than the vortex core. It is possible under certain circumstances to unpin waves from obstacles larger than the core because of other effects such as the presence of slow conduction regions [110, 61] and nonlinear wave propagation (alternans) [62].

Our results thus predict that in cardiac tissue, the removal of spiral waves pinned to a small obstacle by high-frequency wave trains is facilitated by decreasing the excitability of the medium. This is consistent with previous experimental results on cardiac preparations using Na^+-channel blockers [106] and our prediction could be directly tested in a similar experimental setup [106, 100].

In conclusion, we have shown that for a pinned vortex interacting with a pacing wave train, unpinning is possible when the size of the obstacle is smaller than that of the spiral core. The minimum wave train frequency necessary for unpinning in the presence of an inexcitable obstacle is higher than that for inducing drift in a free vortex towards the boundaries of a finite domain, and it increases with the size of the pinning center. Our results suggest that lowering the excitability of the medium makes it easier to unpin vortices by pacing.

Chapter 4

Obstacle induced transition from scroll waves to chaos

For the wise man looks into space
and he knows there is no limited dimensions.
— *Lao Tzu*

In Chapters 2 and 3 we have primarily focused on reentrant wave patterns in two-dimensional media that are manifested as spiral waves. However, most excitable systems that we encounter in reality are three-dimensional and we have to consider the generalization of a spiral wave for such systems, namely, the scroll wave [52]. The additional dimension opens up the possibility of encountering new dynamical phenomena, a specific aspect of which we will explore in this chapter. In particular, we shall focus on the transition to spatiotemporal chaos from a scroll wave through a mechanism that is not encountered in two-dimensional media.

Scroll waves have been experimentally observed in a broad range of nat-

ural systems, including, chemical waves in the Belusov-Zhabotinsky reaction [111, 112, 27], aggregation patterns observed during *Dictyostelium* morphogenesis [113, 114] and electrical waves of excitation in cardiac muscles [2]. Scroll waves in the heart have been implicated in several types of arrhythmia that are potentially fatal disturbances to the natural rhythm of the heart. Under certain conditions, these three-dimensional reentrant waves can also develop various instabilities resulting in their breakup into multiple scroll wavelets. The ensuing spatiotemporally chaotic state of electrical activity is associated, in the context of the heart, with life-threatening arrhythmias such as ventricular fibrillation. Thus, apart from being a problem of theoretical interest in nonlinear dynamics, a deeper understanding of the various mechanisms that lead to chaos through breakup of scroll waves is of great practical significance.

In this chapter, we have considered an isotropic three-dimensional medium with an inexcitable obstacle that does not span the entire thickness of the system. A scroll wave adjacent to such an obstacle would have a part of the wave attached and moving around it with a time period that increases with the circumference of the obstacle boundary. The part that is away from the obstacle rotates freely with a period that is governed by refractory properties of the medium. The differential rotation period in various sections of the wave results in a helical structure wound around the obstacle that (in most cases) attains a steady state after some initial transients. However, under certain circumstances, the wave can breakup far from the scroll wave filament (the line joining the phase singularities in the scroll) close to an edge of the obstacle. This transition to spatiotemporal chaos from a scroll is obstacle

induced as the wave is stable in the absence of the object. The breakup phenomenon can only be observed in three dimensions, as the obstacle should not span the entire thickness of the medium for the transition to chaos to occur.

In section 4.1 we briefly describe the background and physiological motivation for our study. In section 4.2 we describe the models and methods used in the work reported here. Section 4.3 reports the results of our simulations, while in section 4.4 we outline the possible physical mechanism for the generation of additional phase singularities that eventually lead to spatiotemporal chaos. We conclude with a discussion of the potential relevance of our results for the heart, where scar tissue that are embedded inside the bulk of the myocardium (and hence unobservable by epicardial imaging) can nevertheless critically affect the evolution of arrhythmia.

4.1 Inexcitable obstacles: Adding a new dimension

The interaction between conduction inhomogeneities and wave propagation in excitable media is increasingly becoming an active area of research, partly as a result of the improved understanding of the role played by inexcitable obstacles and partially excitable regions in promoting arrhythmias in the heart [30, 31, 110, 61]. Most such studies have focused on two-dimensional systems, which in a few cases can be reduced to an one-dimensional problem by considering only the reentrant circuit surrounding the obstacle. While even this simplified situation can show unexpected complexity, such as fractal

basins of attraction for different dynamical states corresponding to pinned spiral, spatiotemporal chaos and complete termination of activity [115, 33, 116], these models are nevertheless only an approximation to real systems which are three-dimensional. Adding an extra dimension is equivalent to considering the thickness of biological tissue, so that one can in principle distinguish between phenomena on the surface and in the bulk.

It is against this background that we choose to focus on the interaction between rotating waves and inexcitable obstacles in a three-dimensional medium. For simplicity we consider an obstacle with uniform cross-section. However, the obstacle does not span the entire thickness of the medium, as in that case each 2D section of the system would appear identical thereby reducing the problem to an effectively two-dimensional one. Our model is also motivated by physiological situations observed in the heart [117, 118]. The general setting is shown schematically in Fig. 4.1, where an inexcitable obstacle is located deep in the bulk of the heart and cannot be detected by imaging the outer surface (epicardium). Thus, observing from the top, one may not be able to distinguish a freely rotating spiral from one that is actually anchored deep inside the bulk to an obstacle. However, it is obvious that the dynamics of such a partially attached scroll wave can be distinct from both a pinned spiral wave (similar to the two-dimensional situation that we analyzed in Chapter 3) and a freely rotating scroll wave. In particular, one can ask whether in such a situation novel dynamical transitions can occur that will appear neither in the absence of the obstacle nor in the effectively 2D situation where the obstacle fully spans the medium.

The question of whether a three-dimensional obstacle can induce an other-

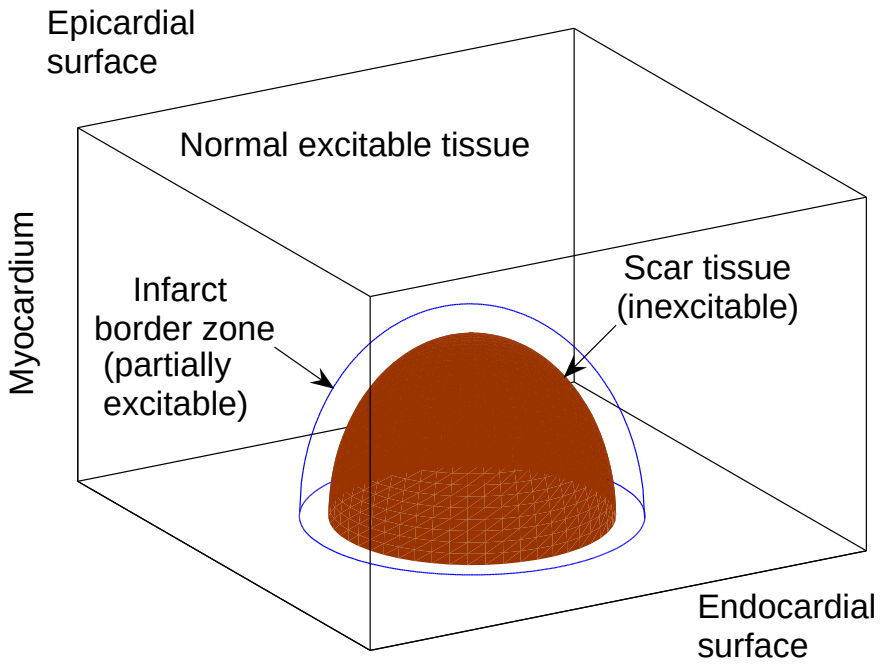

Figure 4.1: Schematic diagram of an inexcitable obstacle surrounded by a border zone comprising partially excitable cells embedded in tissue composed of fully excitable cells. The obstacle extends only partly through the thickness of the medium, and cannot be seen by observing the top surface alone. In the context of the heart, such situations can arise after myocardial infarction, when a region of scar tissue is formed inside the bulk of the myocardium and cannot be detected by imaging the epicardial surface.

wise stable rotating wave to break up into spatiotemporal chaos is extremely pertinent from the point of view of the heart, which gradually accumulates a number of inexcitable obstacles through increased instances of local tissue necrosis with age [98]. While obstacles in three-dimensional media that do not extend through the entire thickness of the system have been considered earlier, these studies typically focused on whether scroll waves pinned by such heterogeneities can be detached as a result of a parameter gradient that induces a tendency to drift [35, 36]. However, even in the absence of drift, complex dynamics can arise from the wave winding around the obstacle as a result of the difference in rotation periods in different sections of the wave.

For example, while the rotation period of the free spiral wave is essentially limited only by the refractory period of the medium, that of the pinned wave is related to the circumference of the obstacle. Thus, by increasing the cross-sectional area of the obstacle it is possible to enhance the difference in the rotation periods between the pinned and freely rotating sections of the scroll wave. As a result, when the wave winds around the obstacle, in addition to the velocity components along the plane perpendicular to the scroll wave filament, there will be propagation along the axis parallel to it. In this chapter we show that at the interface where the additional velocity components appear, the wave may suddenly slow down. Under appropriate conditions, the succeeding wave may interact with the refractory tail of the preceding wave resulting in a conduction block close to the edge of the obstacle. This causes a "tearing" of the front of the succeeding wave which evolves into a new scroll filament. This process can occur repeatedly, creating multiple filaments that can interact with each other leading to fully developed

spatiotemporal chaos.

4.2 Models and methods

To simulate spatiotemporal activity in three-dimensional excitable tissue we use two models with the same basic form,

$$\partial V/\partial t = \nabla D \nabla V + I_{ion}(V, g_i), \tag{4.1}$$

$$\partial g_i/\partial t = F(V, g_i), \tag{4.2}$$

but incorporating different degree of detail in describing I_{ion}. Here, V represents the activation variable (typically, the transmembrane potential), I_{ion} is the total ionic current crossing the membrane, D is the diffusion constant (a scalar parameter, as we assume isotropic coupling between cells), and g_i describes the dynamics of gating variables for the various ion channels that control each component comprising the total ionic current.

For the simple, phenomenological two-variable Panfilov model (PV), I_{ion} is described by a piecewise linear function of the transmembrane potential $f(V)$ [14]. The single recovery variable g of this model, which represents an effective membrane conductance, is governed by three rate constants, ϵ_1, ϵ_2 and ϵ_3. In our study, we fix the values of ϵ_2 $(= 1)$ and ϵ_3 $(= 0.3)$ and consider a range of different values for ϵ_1 for which the scroll wave is stable in the absence of an obstacle. Specifically, we choose $\epsilon_1^{-1} < 53$, as above this value, a scroll wave generated in the medium spontaneously breaks up to form a spatiotemporally chaotic state even in a homogeneous system. The values of other parameters are taken to be same as given in Ref. [14].

To verify the model independence of our results, we also use the biologically realistic Luo-Rudy I (LRI) model for a cardiac myocyte [25]. In this model where the ion channel details are incorporated, I_{ion} is described as being composed of six distinct types of ionic currents (for further details see Chapter 1). For all our simulations reported in this chapter, the maximum K^+ channel conductance G_K has been increased to 0.705 mS cm^{-2} in order to reduce the duration of the action potential to make it comparable to that in the human ventricle [70]. To avoid spontaneous scroll breakup in the absence of any obstacle, the value of the channel conductance for the slow inward Calcium current G_{si} is chosen to be ≤ 0.04 mS cm^{-2}.

Both models are solved using a forward-Euler scheme, the system being discretized on a spatial grid with spacing δx (= 0.0225 cm for LR, = 0.05 cm for PV). The three-dimensional simulation domain has $L \times L \times L$ points with $L = 400$ for the LR1 simulations and $L = 128$ for the PV model. To ensure system size independence, we have repeated our simulation with $L = 160$ and $L = 200$ for the PV model and have observed qualitatively similar results. The Laplacian is calculated using the standard seven-point difference stencil. The time step for integration is chosen to be $\delta t = 0.01$ ms (for LRI) and = 0.11 ms (for PV). No-flux boundary conditions are applied on the boundary planes of the simulation domain as well as along the walls of the inexcitable obstacle.

We have considered both cylinder and rectangular parallelepiped shaped obstacles in our study. The diffusion constant is set to $D = 0$ in the region corresponding to the interior of the inexcitable obstacle. The cylindrical obstacle has radius R with a cross-sectional area = πR^2 and height L_z, while

the rectangular parallelepiped obstacle is of size $L' \times L' \times L_z$, with L_z being the height of the obstacle and $L' \times L'$, the cross-sectional area. For the PV model, we have used obstacles with heights ranging from $L_z = 1$ cm to $L_z = 5.5$ cm and cross-sectional area 12.5 cm^2 to 28.3 cm^2 . For the LRI model, we have used obstacles of height $L_z = 2.7$ cm to $L_z = 5.4$ cm and cross-sectional area of 35.8 cm^2.

Setting up the initial scroll

The initial scroll wave is obtained by breaking a 3-dimensional plane wavefront when it arrives at the center of the simulation domain starting from one of the boundary planes at $T = 0$. This is achieved by dividing the wavefront into two parts along a line parallel to the L_z axis of the obstacle. We then set one of the parts to the resting state values, resulting in a broken plane front which then dynamically evolves into a rotating scroll wave whose filament is parallel to the L_z axis. In the LR1 model simulations, an initial plane wave is first allowed to travel through the medium to reduce the recovery period. The next wave is then used to create the broken plane wavefront, so as to generate a scroll with one full turn inside the simulation domain. The location of the obstacle at the center of the domain, with its base touching the boundary of the simulation domain, ensures that the generated scroll wave is attached to it. We have also carried out simulations with the initial scroll wave being generated by a broken cylindrical front (the axis of the cylinder being perpendicular to the L_z axis of the obstacle). While the resulting scroll filament is curved compared to that seen in the previous method (broken plane wavefront), the subsequent breakup into multiple scroll waves is

qualitatively similar in both cases.

4.3 Results

While an extremely small inexcitable obstacle does not affect the dynamics of the scroll significantly, we observe that a sufficiently large one can promote wavebreaks in an otherwise stably rotating wave. For a medium with LRI dynamics, Fig. 4.2 shows how a cylindrical obstacle can induce breaks giving rise to new filaments whose interactions lead finally to spatiotemporal chaos. After the creation of the scroll wave, we observe that the section of wave adjacent to the obstacle is pinned by it. The large circumference of the obstacle implies a long rotation period for the portion of the wave attached to it. As the freely rotating part of the wave has a much shorter rotation period, this leads to the wave winding around the obstacle. Note that, the scroll wave filament which stretches from the top surface of the obstacle to the upper boundary of the simulation domain is unchanged by the presence of the obstacle. The wavefront traveling along the top or horizontal surface of the obstacle has a quasi 2D nature (i.e., the two-dimensional cross sections perpendicular to the filament appear almost identical). However, when the wave crosses the boundary of the top surface of the obstacle, it develops a fully three-dimensional nature as it not only has velocity components in the plane perpendicular to the filament but it also travels down the vertical surface of the obstacle (i.e., parallel to the filament). As seen from Fig. 4.2 (b), one of the wavefronts eventually detaches partially from the surface of the obstacle as it crosses the edge of the top surface and breaks, with the gen-

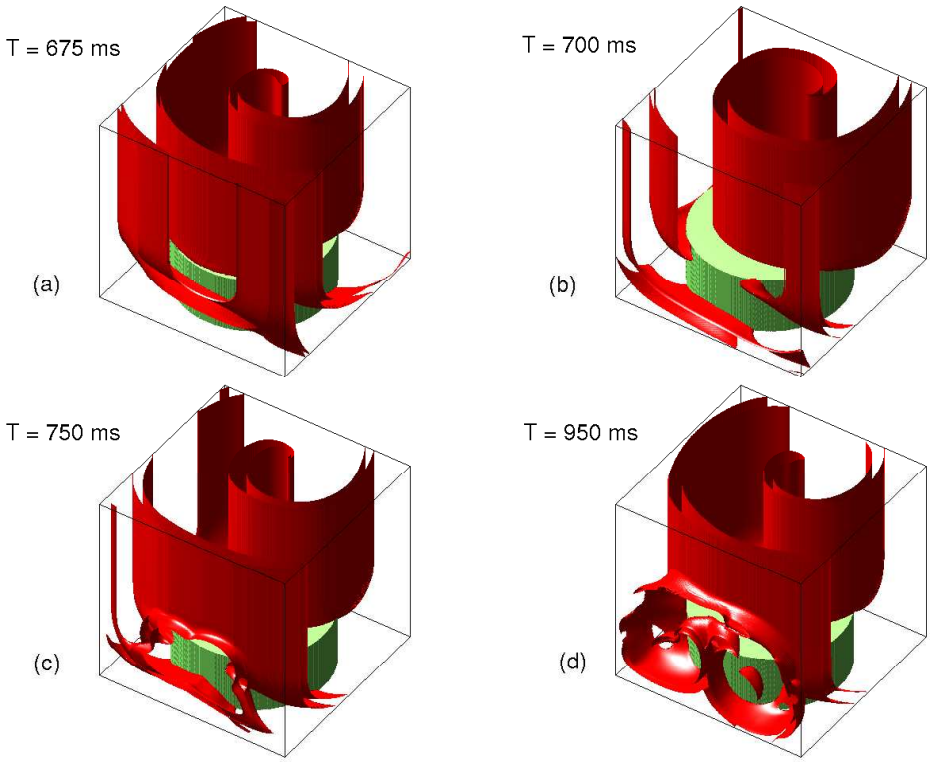

Figure 4.2: Breakup of a scroll wave induced by a cylindrical obstacle of radius $R = 3.375$ cm and height $H = 2.7$ cm where the activation dynamics is described by the LRI model. The scroll wave is generated by creating a broken wavefront at $T = 400$ ms. (a) By $T = 675$ ms, the scroll wave has wound around the obstacle. We observe a quasi two-dimensional propagation of the wave along the top surface of the obstacle that becomes fully three-dimensional when the wave moves past the boundary of the top surface and travels down the vertical surface of the obstacle. (b) By $T = 700$ ms, we observe a broken wavefront that has detached from the edge of the obstacle giving rise to two free ends, which eventually evolve into new scroll wave filaments (c-d). Interaction between these waves produce multiple excitation wave fragments that will eventually give rise to chaos.

eration of two free ends. These ends propagate and grow in size, colliding with the next wave (Fig. 4.2 c) to create new scroll wave filaments. Further evolution of the system produces more complex wave fragments (Fig. 4.2 d) that eventually results in spatiotemporal chaos.

To understand the mechanism behind the breakup of scroll waves partially pinned by an obstacle, we have to look at the cross-section of the system parallel to the filament (shown in Fig. 4.3). The bold arrows in Fig. 4.3 (a) indicate the direction of wave propagation as it moves first along the top surface and then along the vertical surface of the obstacle (shaded dark in the figures). The wave W_1 slows down as it travels past the boundary of the top surface of the obstacle. This results from the change in the nature of its wavefront, from plane to one with a convex curvature (Fig. 4.3 b). The increased curvature of a wave results in a decrease in its conduction speed [72]. The wave W_2 which is closely following W_1 therefore encounters an incompletely recovered region at the edge of the obstacle and cannot propagate into this section. This results in the dislodging of the wave from the surface of the obstacle, generating the free end seen as a wavebreak in Fig. 4.3 (d). This detached or free end subsequently interacts with later waves to give rise to a spatiotemporally chaotic state.

To ensure that our results are not sensitively model dependent, we have reproduced qualitatively identical scenarios in a medium whose dynamics is described by the PV model (Fig. 4.4). As is the case for the LRI model, we observe the initial wavebreak as the wave crosses the boundary of the top surface of the cylindrical obstacle, eventually giving rise to multiple scroll wave filaments. We also observe a similar evolution from a single scroll

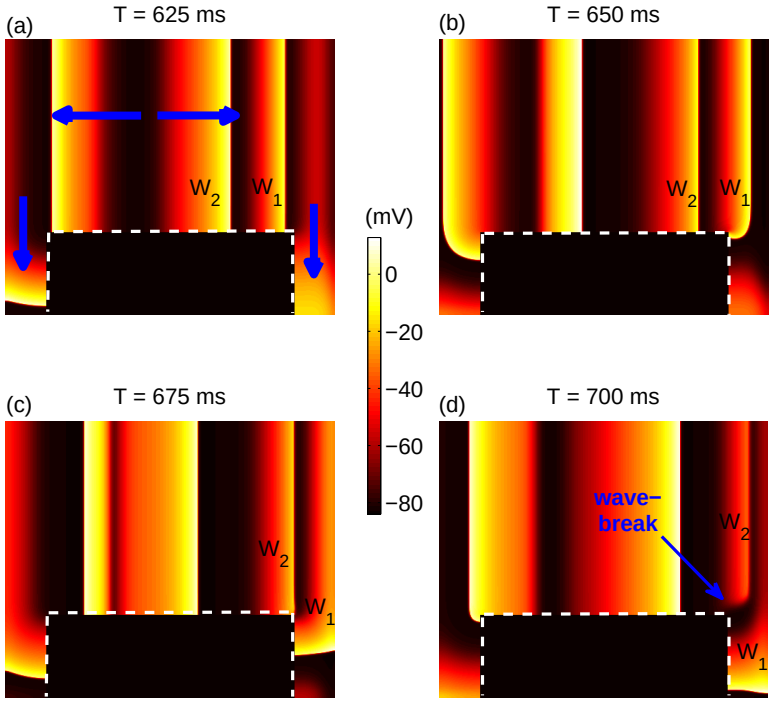

Figure 4.3: Cross-section parallel to the scroll wave filament (along the L_z axis of the obstacle) for the system shown in Fig. 4.2. The boundary of the obstacle (shaded dark) is marked by the broken lines. The solid arrows in (a) indicate the direction of propagation for waves W_1 and W_2. (b) W_1 slows down at the boundary of the top surface of the obstacle as a result of change in the nature of the front from a plane wave to one having convex curvature. (c) Wave W_2, that closely follows W_1, encounters a region that has not fully recovered from its prior excitation by W_1, leading to the detachment of W_2 from the surface of the obstacle (d).

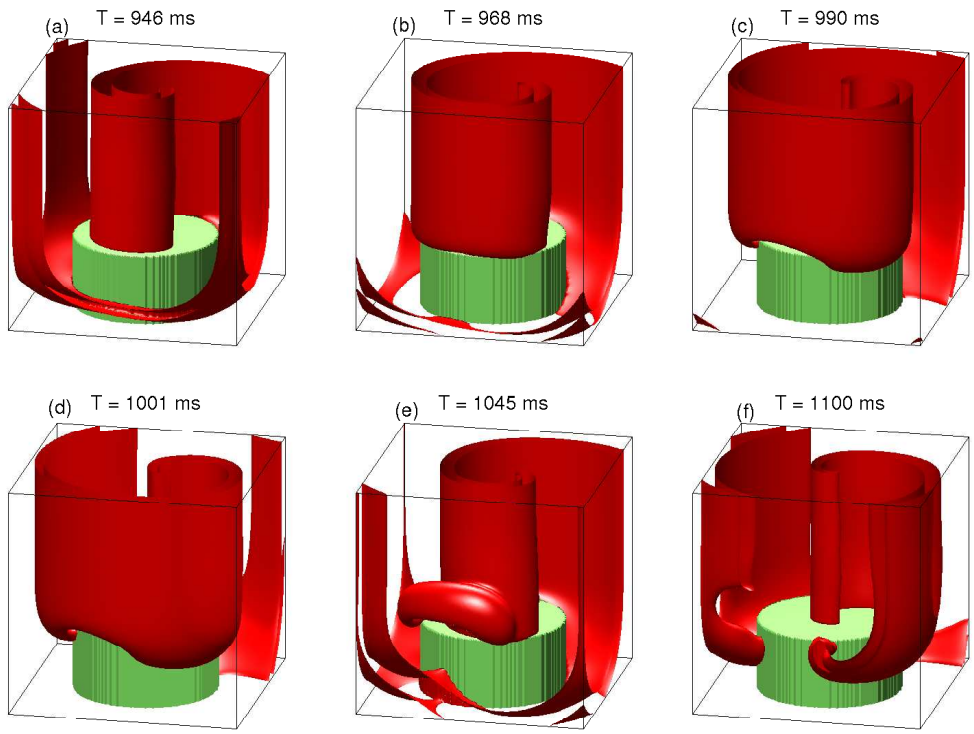

Figure 4.4: Breakup of scroll wave induced by a cylindrical obstacle of radius $R = 2$ cm and height $H = 2$ cm in an excitable medium described by the Panfilov model. The simulation domain is 6.4 cm $\times$6.4 cm $\times$6.4 cm. The scroll wave is generated from a plane wavefront that is broken at $T = 77$ ms. (a)-(b) The scroll wave has attached to and winds around the obstacle forming a helical structure. (c)-(e) A wave is seen to detach at the boundary of the top surface of the obstacle, generating a new scroll wave filament. (f) By $T = 1100$ ms, we observe multiple scroll waves that have been generated through successive wavebreaks at the obstacle top surface boundary.

wave to spatiotemporal chaos for obstacles having the shape of a rectangular parallelepiped, indicating that the mechanism does not depend critically on the exact shape of the inexcitable obstacle.

4.4 Discussion

The route to breakup of scroll waves into spatiotemporal chaos reported here is distinct from established physical mechanisms of transition to broken scroll states, most of which are associated with dynamics of the filament. The two principal mechanisms of scroll wave breakup that have been reported in the literature involve either (i) negative filament tension in a low excitability regime, or, (ii) cardiac fiber rotation with filament twist instability [17]. In addition, (iii) decreased cell coupling and discrete effects can also result in breakup of scroll waves, as they do in two-dimensional media [17]. However, the situation reported here does not correspond to any of these above scenarios. As mentioned earlier, the wavebreak occurs far from the filament (the line of phase singularities) in a medium which, apart from the existence of an inexcitable obstacle, is isotropic and homogeneous. To ensure that the breakup occurs exclusively in the presence of the obstacle, we have carried out simulations of the scroll wave in the absence of the obstacle for extremely long durations (e.g., up to $T = 10^4$ ms for LRI model and $T = 2.2 \times 10^4$ ms for PV model) without observing any wavebreaks in the scroll.

The primary role of the obstacle is to make the existing scroll wave wind around it by creating differential rotation periods. This results in the wave propagation having different directional components in different regions of

the medium. In particular at the boundary of the top surface of the obstacle, the nature of the front suddenly changes from being effectively quasi-2D to fully 3D with convex curvature. As increased curvature implies decreased propagation speed, there is an initial reduction in velocity of the wave component that starts flowing down the vertical surface of the obstacle. If the succeeding wavefront encounters a partially recovered region at the boundary of the top surface of the obstacle, it can detach due to conduction block, resulting in a wavebreak. However, this requires the interval between successive waves to be extremely small so that a small change in the propagation speed of the preceding wave can block the following wavefront because of restitution and dispersion effects of the medium. By periodically stimulating a line-electrode, in the place of the filament, we have observed that the highest possible frequency of the stimulated waves thus generated is still smaller than that of the scroll (for identical system parameters). Even with adaptive pacing (where the pacing frequency is gradually increased by progressively decreasing the time period between two successive stimulations), periodic stimulation from the line electrode at the frequency of the scroll wave results in conduction block of every other stimuli. This suggests that the scroll wave is exploiting the nonlinear adaptive property of the medium to generate waves at intervals very close to the minimum possible allowed by the system parameters. Therefore, even a small change in the propagation speed of a wave may result in the conduction block for the following wave as seen in our simulations. This phenomenon can be further enhanced by Doppler effect induced changes in the frequency of successive waves which are a consequence of the meandering of the filament. Thus, a relatively long time

interval between successive waves W_0 and W_1 traveling along the obstacle surface may be followed by a short duration between W_1 and W_2. This may cause interaction between waveback of W_1 and the W_2 wavefront, resulting in conduction block for the latter along the surface of the obstacle. This will lead to detachment of the wave from the obstacle surface giving rise to a new phase singularity.

In conclusion, we have shown that the presence of an inexcitable obstacle in three-dimensional excitable media can result in wavebreak leading to spatiotemporal chaos involving a novel physical mechanism. Unlike previously proposed mechanisms for scroll breakup, in our simulations the transition occurs far from the filament, the line connecting phase singularities. We suggest that the detachment of the wave from the obstacle that generates new singularities (eventually resulting in spatiotemporal chaos) arises from a mechanism involving the interaction of the wavebacks and fronts of successive waves generated by the scroll, at an edge of the obstacle. Our results imply that obstacles embedded deep inside the bulk of a medium, e.g., inexcitable scar tissue regions in the heart, may play a critical role in the genesis of arrhythmia such as fibrillation, even when they cannot be observed from the surface.

Chapter 5

Spatiotemporal chaos control using an array of control points

Stranger, you too are my kin
You stopped my heart's flutterin.
– *Kannadasan*

Dynamical spatial patterns in excitable media like spiral waves and scroll waves may become unstable under certain conditions, giving rise to turbulent states which correspond to spatiotemporal chaos. As mentioned in Chapter 1, such spatiotemporally chaotic states have been implicated in clinically significant disturbances of the natural rhythm of the heart [119, 120], e.g., fibrillation. Ventricular fibrillation in particular is lethal as it results in complete loss of coordination of activity between different regions in the heart [52]. The resulting cessation of the mechanical pumping action necessary for blood circulation, leads to a drastic fall in blood pressure. If not treated immediately death follows within a few minutes. However the conventional methods of

defibrillation require the application of large electrical shocks that are undesirable for a variety of reasons. Developing low-amplitude control schemes involving as few control electrodes as possible is an exciting challenge and has potential clinical relevance [121, 38, 122]. As detailed in Chapter 1, devising such control using low voltages or current, has to take into account the special features of excitable medium like the existence of a refractory period and excitation threshold. The amplitude and timing of the control signal needs to be appropriately chosen so that it results in the desired response from the medium. Note that the excited state is meta-stable, and the cell eventually recovers to the *resting* state associated in different biological systems with a characteristic resting transmembrane potential ($\simeq -84$ mV for cardiac myocytes). Thus, the control of spatiotemporal chaos in excitable media may be viewed as essentially a problem of synchronizing the excitation phase of every cell, so that the entire system returns to the resting state, resulting in the termination of all activity.

In this chapter we describe a novel method of controlling spatiotemporal chaos in excitable media, using an array of control points. The points are stimulated in a sequence so as to generate a travelling wave of activity across the medium, which interacts with the chaotic excitations and eliminates them. The proposed method is robust even in the presence of significant conduction heterogeneities in the medium which have often been an impediment to the success of other control schemes. In section 5.1 we give a brief introduction to the necessity of using spatially extended but non-global control scheme. In section 5.2 we describe the two models of excitable media that are used in our work. Section 5.3 contains details of the algorithm

used in our control scheme. In section 5.4 we discuss the results of applying this control scheme on 2-dimensional and 3-dimensional excitable media. We conclude the chapter with a brief discussion of the merits and advantages of the proposed scheme.

5.1 Low-amplitude chaos control

Chaos control schemes for excitable media may be broadly classified into [93]: (i) *global*, where the control signal is applied to all points of the system, (ii) *local*, where only a small localized region of the system is subject to control, and (iii) *spatially extended but non-global* schemes. Non-global methods use less power and also are relatively easier to implement practically, needing fewer control points. However, strictly local control methods almost always involve very high-frequency stimulation [59], that can by itself lead to reentrant waves in the presence of inhomogeneities [30, 33]. Moreover, the effect of local stimulation at a point can affect the rest of the system only through diffusion. As wavefronts annihilate on collision, control-induced waves are restricted to the local neighborhood of the stimulation point during spiral turbulence, with the existing excited fragments closer to the control point shielding chaotic activity further away. By using a spatially extended but non-global scheme [51] one can potentially avoid these drawbacks. In this chapter, we terminate chaos in excitable media by applying spatiotemporally varying stimulation along an array of control points. The control signal appears to propagate along the array, triggering an excitation wavefront in the underlying medium, that is regenerated after each collision with chaotic frag-

ments and in the process eliminating all existing activity. Stimulating each point once (or at most, twice) is seen to successfully control chaos in almost all instances. Although an array of control points have been used earlier to prevent the breakup of a single spiral [54], to the best of our knowledge this is the first instance showing control of fully developed spatiotemporal chaos in excitable media using only a finite number of control points without repeated stimulations at high frequency.

5.2 Models and methods

The spatiotemporal dynamics of excitation in several biological systems can be described by partial differential equations of the form:

$$\partial V/\partial t = \frac{-I_{ion} + I_{ext}(x, y, t)}{C_m} + D\nabla^2 V, \tag{5.1}$$

where V (mV) is the transmembrane potential, $C_m = 1\ \mu\text{F cm}^{-2}$ is the transmembrane capacitance, D (cm^2s^{-1}) is the diffusion constant, I_{ion} ($\mu\text{A cm}^{-2}$) is the transmembrane ionic current density and $I_{ext}(x, y, t)$ is the space- and time-dependent external stimulus current density that is applied for the purpose of control on a 2-dimensional surface. For the specific functional form of I_{ion}, we used the Luo-Rudy I (LR1) action potential model [25], where, the total ionic current is considered to be composed of six distinct currents, each of them being determined by several time-dependent ion-channel gating variables ξ whose time-evolution is described by differential equations $\frac{d\xi}{dt} = \frac{\xi_\infty - \xi}{\tau_\xi}$. The parameters in these equations are the steady-state values of ξ, $\xi_\infty = \alpha_\xi/(\alpha_\xi + \beta_\xi)$, and the time constants, $\tau_\xi = 1/(\alpha_\xi + \beta_\xi)$, which are governed by the voltage-dependent rate constants for the opening and

closing of the channels, α_ξ and β_ξ, themselves complicated functions of V. In order to verify the model independence of our results and to carry out three-dimensional simulations, we have also used a simpler description of the action potential, as given by Panfilov (PV) [13, 14]: $I_{ion} = f(V) - g$, where f is a piecewise linear approximation of a cubic function and g is an effective membrane conductance evolving with time as

$$\frac{dg}{dt} = \epsilon(V, g)(kV - g).$$

The time-constant ϵ is a function of both V and g and the parameters used are same as that in Ref. [51]. The models are solved using a forward-Euler scheme, the system being discretized on a spatial grid with spacing δx (=0.0225 cm for LR1, = 0.05 cm for PV). The simulation domain is a square lattice of $L \times L$ points in two dimensions or a cuboid with $L \times L \times L_z$ points in three dimensions. For the LR1 simulations, $L = 400$, while for PV, $L = 256$ (for 2-D) and $L = 128, L_z = 8$ (for 3-D). The standard five-point and seven-point difference stencils are used for the Laplacian in two and three dimensions, respectively. The time step for integration is chosen to be $\delta t =$ 0.01 ms (for LR1) and = 0.11 ms (for PV). No-flux boundary conditions are implemented at the edges of the simulation domain. The initial spatiotemporally chaotic state is obtained by creating a broken wavefront which evolves into a spiral wave and is then allowed to become unstable, eventually breaking up into multiple wavelets. For LR1 model, the broken wavefront is preceded by an earlier intact wavefront in order to reduce the recovery period (through the restitution property of the medium, by which recovery is a function of the time interval between two successive propagating waves) so as to enable a spiral wave with at least one complete turn to exist within

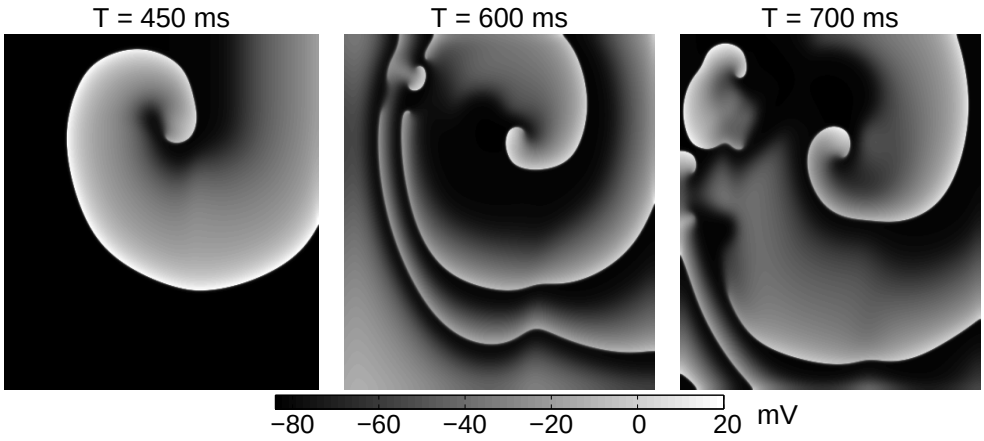

Figure 5.1: Pseudo-gray-scale plot of the transmembrane potential V for the two-dimensional LR1 model showing the time-evolution from single spiral (left) through breakup (center) to fully developed chaos (right).

the simulation domain. For the model parameters used here, this spiral is itself unstable, and after 200 ms (on average) breaks up, resulting in a state displaying fully developed spatiotemporal chaos (Fig. 5.1).

5.3 Algorithm for the array control

We now focus on the control term $I_{ext}(x, y, t)$. For a 2-D domain of size $L \times L$ we consider

$$I_{ext} = I(x, y, t)\delta_{x,md}\ \delta_{y,nd}\ , \tag{5.2}$$

where, the Kronecker delta function is defined as $\delta_{i,j} = 1$ if $i = j$, and $= 0$, otherwise, d is the spatial interval between points in an array where the control signal is applied and m, n are integers in the interval $[0, L/d]$. The current density $I(x, y, t) = I_0$ for $t \in [\sqrt{x^2 + y^2}/v, (\sqrt{x^2 + y^2}/v) + \tau]$, and

$= 0$ otherwise, corresponds to a rectangular control pulse of amplitude I_0 of duration τ that is travelling with velocity v. At the onset of control ($t = 0$), the point at $(0, 0)$ is stimulated, followed a short duration later by the points at $(0, d)$ and $(d, 0)$, and this process continues as the control pulse proceeds like a traveling wave across the array. At each control point, the stimulation may excite the underlying region depending on its recovery phase. An excited region can in turn spread the effect of the stimulation to the surrounding regions through diffusion. Fig. 5.2 shows this process of secondary wave generation at the stimulated control points, creating a sustained excitation wavefront. Note that, any portion of this stimulated wavefront in the medium that is broken through collision with chaotic fragments, can be regenerated by subsequent control points. Hence, there is effectively an unbroken wavefront that travels through the medium, sweeping away the spatiotemporal chaos and leaving the system in a recovering state. As each control point needs to impose order over a region of size $\sim d^2$ to eliminate spatiotemporal chaos, this highlights the critical role of d. Indeed, for large v, the method approaches global control as $d \to 0$, while for $d \sim L$ the activity resulting from the control stimulation is confined to a single, localized region. This implies that as d increases, terminating chaos becomes increasingly difficult. For example, in LR1 model, we observe that chaos control fails for $d \geq 13$.

5.4 Results

Before reporting the simulation results, we consider the role played by the traveling wave nature of the control pulse. The success of the proposed

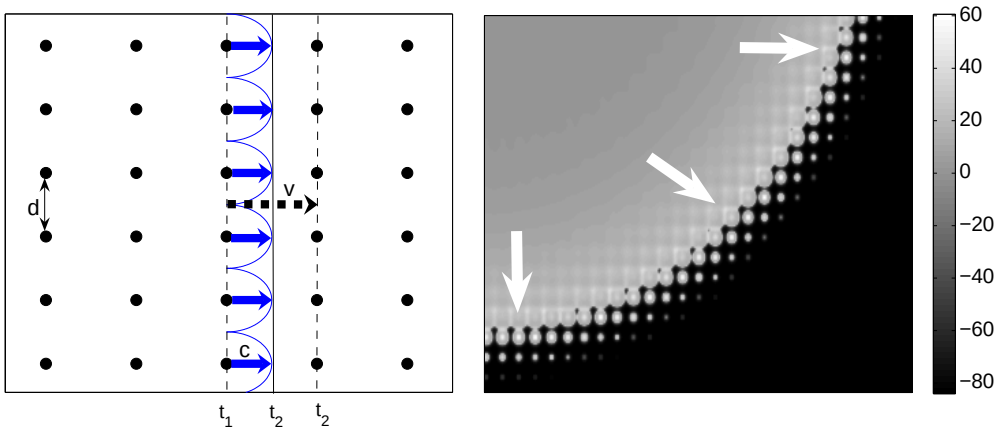

Figure 5.2: (left) Schematic diagram and (right) pseudo-gray-scale plot of the transmembrane potential V for the two-dimensional LR1 model, showing the propagation of the control-induced excitation wavefront. The control signal traveling with velocity v stimulates at time t_1 a column of points (spaced d apart) from which secondary excitations traveling with velocity c are generated. At time t_2 the control signal stimulates the next column of points, which the induced excitation wave may or may not have reached depending on the relative values of v and c [$v/c = 4$ in (right)].

method depends on the control signal velocity, v, relative to the velocity of the excitation wavefront propagating via diffusion, c (= 60.75 cm s^{-1} for LR-1, = 50.9 cm s^{-1} for PV, for the parameters used here). When $v \to 0$, the control method reduces to a local scheme regardless of d, as the effect of the external stimulation can only propagate in the system via diffusion. On the other hand, when v is very large, all the control points are stimulated almost simultaneously. While the traveling wave nature of the control pulse allows propagation of stimulation independent of diffusion through the excitable medium, for $v \simeq c$ the excitation propagating by diffusion reinforces the external stimulation at each control point. Further, for a control signal propagating with a finite velocity (thus engaging only a few points at any given time), the energy applied per unit time to the medium is much lower than that for simultaneous stimulation of all the control points (i.e., $v \to \infty$).

For a system undergoing chaotic activity, the medium will at any time be at an extremely heterogeneous state, with certain regions excited and other regions partially or fully recovered. The vital condition for successful termination of chaos is that after the passage of the control-stimulated wave there should not remain any unexcited region which is partially recovered and which can be subsequently activated by diffusion from a decaying excitation front. This places a lower bound on the control signal parameters, i.e., the signal amplitude I_0 and its duration τ. If either is decreased below this bound, the external stimulation is unable to excite certain partially recovered regions. If these regions have neighboring chaotic fragments, whose activity is slowly decaying after collision with the control-induced wave, then, there will be a diffusion current from the latter. Depending on the phase of recovery,

this may be sufficient to stimulate activity in the partially recovered regions, thereby re-initiating spatiotemporal chaos after the control signal has passed through.

To understand in detail the lower bound on the external stimulation parameters I_0 and τ, we first look at the condition for exciting a completely homogeneous medium in the resting state. The stimulation at each point must exceed the local threshold in order to generate an action potential. This could be achieved either directly through an external current I_{ext} or indirectly through diffusion from a neighboring excited region. Fig. 5.3 (left) shows the result of applying control signals with different I_0 and τ at points which are spaced a distance d apart. The resulting *strength-duration curve* [123, 124] indicates that the response of the system is not sensitively dependent on the propagation velocity v of the control signal along the grid. As d decreases, excitation is possible at lower values of I_0 and τ, the minimum being for the case when all points are subject to direct external stimulation ($d \to 0$). This is because the entire applied current I_0 at any point is used to raise its state above the threshold, no part being lost to neighboring regions through diffusion.

For systems with existing activity, such as self-sustaining spiral waves or spatiotemporal chaos, the regions in the relative recovery period can be excited by stimuli larger than that needed for a fully recovered medium. Hence, the strength-duration curve for control of such a system will shift towards higher values of I_0 and τ (Fig. 5.3, right). We observe that the minimum external stimulus required for control does not vary significantly if the medium is undergoing fully developed spatiotemporal chaos as opposed

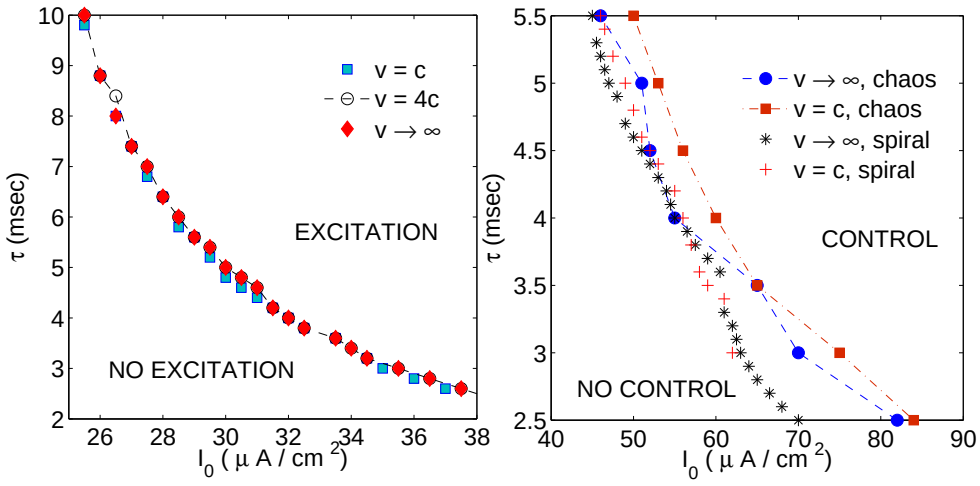

Figure 5.3: Strength-duration curves for LR1 model (in a two-dimensional domain with $L = 400$) when control stimulation is applied on (left) quiescent homogeneous medium and (right) medium with existing excitation activity, either a single spiral or spatiotemporal chaos. In both figures, control is applied over a grid of points which are spaced apart by $d = 10$. Different curves correspond to different control signal velocities v, relative to c, the excitation wavefront velocity in the medium. For values of I_0 and τ above the curves, the external stimulation results in (left) excitation of the domain or (right) control of existing activity.

to having a single spiral wave. Further, the velocity of the control signal along the array is not critical to the success in eliminating existing activity, provided v is not significantly smaller than c. Note that, if v is sufficiently small or d increases beyond a critical value, the control fails, as the effect of the control signal is confined to the region immediately surrounding the stimulated point.

Fig. 5.4 shows the successful termination of spatiotemporal chaos in the LR1 model using a control signal that travels across the 2-dimensional domain while exciting points in the medium that are spaced apart by $d = 10$. We verified that the control scheme is not model dependent by using it to eliminate spatiotemporal chaotic activity in the PV model. As most systems in reality have thickness, it is crucial to verify that the method is successful in controlling chaos in a 3-dimensional domain, even when the external stimulus is applied *only on one surface*. This latter restriction follows from the fact that, in most practical situations it may not be possible (or desirable) to penetrate the medium physically in order to apply control signals inside the bulk. We confirmed that our method works in thin slices of excitable media of size $L \times L \times L_z$ ($L_z \ll L$), when the array of control points is placed on one of the $L \times L$ surfaces (Fig. 5.5). Even in cases where a single control-stimulated wave across the medium is unable to terminate all activity, we notice that it results in driving the chaotic activity further towards the boundaries and away from the origin of control stimulation. Thus, using multiple waves through application of control signals at intervals which are larger than the recovery period of the medium, the chaos in the bulk of 3-dimensional systems is successfully terminated.

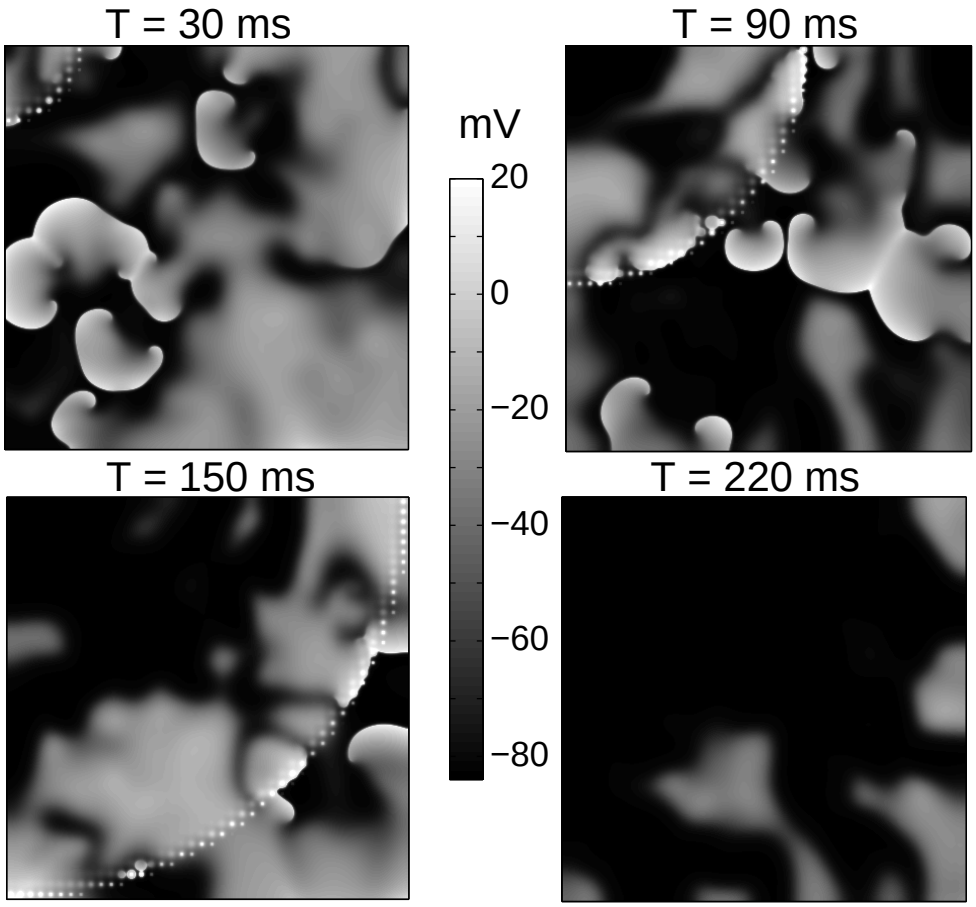

Figure 5.4: Pseudo-gray-scale plots of the transmembrane potential V for the two-dimensional LR1 model ($L = 400$) showing the elimination of all chaotic activity within 300 ms after initiation of control. A single wave of control stimulus ($I_0 = 75$ μA/cm^2, $\tau = 3$ ms) begins at the top left corner ($T = 0$) and travels across the domain with velocity $v = c$. This results in stimulating the region around the control points (spaced apart by $d = 10$) in a sequential manner, creating a stimulated wavefront seen as an arc consisting of excited points in the panels above.

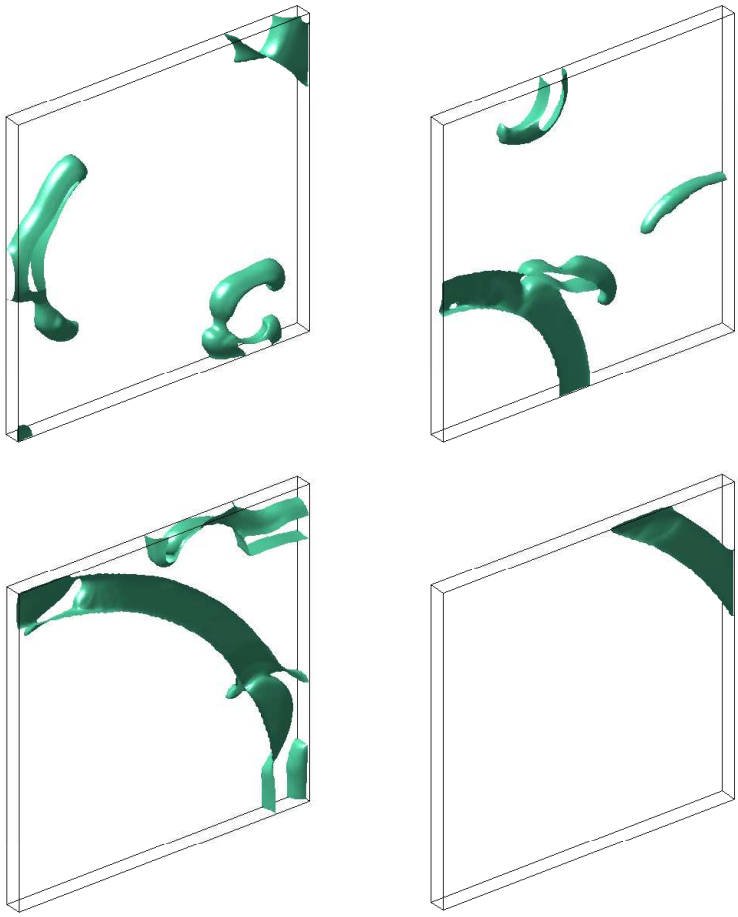

Figure 5.5: The effect of applying control on a single surface of a 3-dimensional domain using the PV model ($L = 128$ and $L_z = 8$). Two waves of control signal ($I_0 = 10$, $\tau = 16.5$ ms, $v = c$) are applied 165 ms apart resulting in termination of spatiotemporal chaos. The interval between control points, $d \to 0$. The panels show isosurface plots at T=178 ms (top left), 242 ms (top right), 308 ms (bottom left) and 341 ms (bottom right).

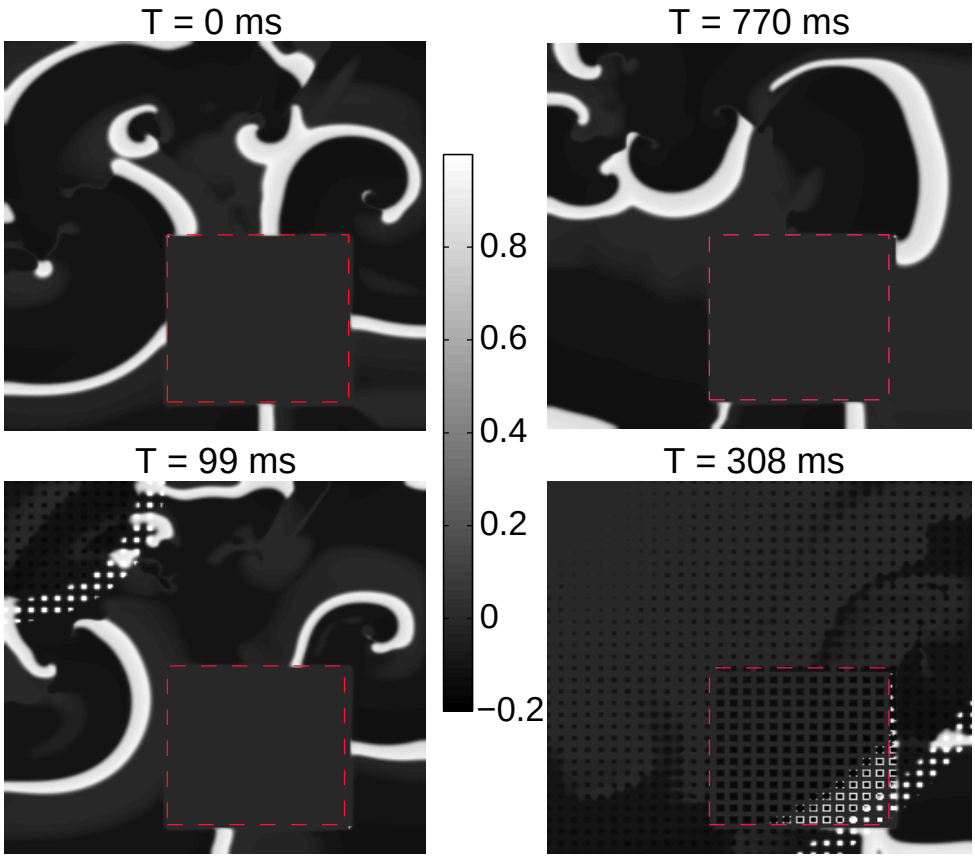

Figure 5.6: Pseudo-gray-scale plots of the transmembrane potential V for the two-dimensional PV model ($L = 256$) with a conduction inhomogeneity (of size 110×110, indicated by the broken lines), showing the time evolution of the system from a chaotic state at $T = 0$ ms in the absence (top) and presence (bottom) of control. Inside this region, $D_{inhomogen} = 0.01D$, D being the diffusion constant of the rest of the medium. A single pulse of control stimulus ($I_0 = 8$, $\tau = 17$ ms, $v = c$) is applied at $T = 0$ ms over an array of control points spaced apart by $d = 8$, resulting in termination of all activity by $T = 350$ ms.

We have checked that small distortions in the regular array of control points does not result in the failure of our method. Similarly, starting the control signal at different points of origin (and indeed, using a planar wave rather than a curved wave) does not affect the efficacy of the scheme. Further, our method is robust in the presence of conduction inhomogeneities (such as inexcitable obstacles) that tend to destabilise local control schemes. Fig. 5.6 shows the occurrence of spatiotemporal chaos in a medium containing a large region of slow conduction, i.e., an extremely small value of D compared to the rest of the medium, which is successfully controlled by the proposed scheme.

5.5 Discussion

In this chapter, we have presented a novel control scheme involving external stimulation applied over an array of points, that is successful in terminating spatiotemporal chaos in both simplified as well as realistic models of biological excitable media. The control signal amplitude is varied both spatially and temporally, such that it appears as a propagating wave along the array of control points. This results in a stimulated wavefront in the excitable medium, that, depending on the propagation velocity of the control signal and the space interval between control points, eliminates all existing activity. Our method requires very low-amplitude control currents applied for short durations at a finite number of points, each point being stimulated once (or at most, twice) in most situations. Further, it is successful in terminating chaos in the bulk of a three-dimensional medium even when applied only on one surface. The use of significantly lower number of control points than

that necessary for global control methods, makes the proposed scheme more suitable for practical implementation.

Chapter 6

Activity enhanced response to sub-threshold stimulus

What's big or small
About the blazing fire
That burns all.
– *Subramania Bharathi*

The excitation threshold is the key parameter governing the dynamics of spatial patterns in excitable systems. A stimulus that drives the system above this excitation threshold leads to a transition from quiescent to an active state, thereby generating an action potential (AP). Such a signal is called a supra-threshold signal. On the other hand, if an external signal is not able to initiate an action potential in a medium or cell at rest then the external signal is called sub-threshold. The demonstration of stochastic resonance (SR) [125] and coherence resonance (CR) [126] in excitable media suggest that weak sub-threshold signals could have a significant effect on the dynamics of these

media [127, 128]. Further, SR-like response resulting from chaotic dynamics in simple systems [129, 130] raises the intriguing possibility that spatially heterogeneous activity may enhance the response of an excitable medium to sub-threshold signals.

In this chapter we show that these sub-threshold perturbations produce surprising changes in the dynamics of spatiotemporally heterogeneous activity in the medium. Stimuli that cannot initiate action potentials in a resting medium can significantly alter the time-evolution of spatially heterogeneous activity by modifying the recovery dynamics of the medium. The application of a sub-threshold stimulus leads to a significant increase of the action potential duration and reduction in waveback velocity. This in turn causes a differential slowing down of recovery of the cells in the medium, leading to the development of spatial coherence, terminating all activity in the medium including spatiotemporal chaos. The results described here not only suggest alternate low-amplitude mechanism of chaos control in excitable medium, but can also potentially explain how signals that are extremely attenuated during passage through intervening biological medium, can still affect the excitation dynamics of organs such as the heart.

In section 6.1 we describe the nature of sub-threshold stimuli and briefly discuss their key effects on the dynamics of an excitable medium. In section 6.2 we give details of the models and the methods used in our study, while section 6.3 describes the results of applying sub-threshold stimulus on spatially heterogeneous activity. We also outline here the theoretical background of the control method and analytically derive model-independent conditions for successful elimination of all activity using a sub-threshold stimulus. We

conclude with a brief discussion on the generality of our results and their biological relevance.

6.1 Introducing sub-threshold stimulation

Prevailing methods of spatiotemporal chaos control in excitable systems are almost exclusively dependent on using supra-threshold signals, either through a local high-frequency source [59, 78] or using a spatially extended array [51, 94, 116]. Controlling spatial patterns with sub-threshold stimulation would not only utilize new physical principles, but also avoid many of the drawbacks in previously proposed schemes. Throughout this chapter *sub-threshold* refers to stimuli that are insufficient to drive the resting tissue above the excitation threshold. In the context of cardiac control, occasionally threshold may also be used to refer to the minimum stimulus amplitude required for successful defibrillation. However, if such a stimulus causes an AP in resting tissue (i.e., the medium crosses the excitation threshold), we refer to it as supra-threshold in this chapter.

We show here that sub-threshold stimulation, while having no significant effect on a quiescent medium, can induce a remarkable degree of coherence when applied on a system with spatially heterogeneous activity. Synchronizing the state of activation of all excited regions ensures that they return to rest almost simultaneously, in the process completely terminating activity in the medium. Thus, control of spatially extended chaos is achieved efficiently using a very low-amplitude signal. We explain the mechanism of this enhanced coherence in terms of the role played by sub-threshold stimulus in

increasing the recovery period of the medium. It significantly reduces the propagation velocity of the *recovery* front, thereby increasing the extent of the inexcitable region in the medium. We present a semi-analytical derivation of the relation between strength and duration of the globally applied sub-threshold signal necessary for complete elimination of spatially heterogeneous activity in excitable media.

6.2 Models and methods

A generic model for describing the spatiotemporal dynamics of several biological excitable systems has the form:

$$\frac{\partial V}{\partial t} = \frac{-I_{ion}(V, g_i) + I(t)}{C_m} + D\nabla^2 V, \tag{6.1}$$

where V (mV) is the potential difference across a cellular membrane, $C_m (= 1\mu\text{Fcm}^{-2})$ is the transmembrane capacitance, D is the diffusion constant ($= 0.001\text{cm}^2 s^{-1}$ for the results reported in the chapter), $I_{ion}(\mu\text{Acm}^{-2})$ is the total current density through ion channels on the cellular membrane, and g_i describes the dynamics of gating variables of different ion channels. The spatially uniform external signal, applied at all points of the simulation domain, is represented by the time-dependent current density, $I(\mu\text{Acm}^{-2})$. The specific functional form for I_{ion} varies for different biological systems. For the results reported here, we have used the Luo-Rudy I (LR1) model that describes the ionic currents in a ventricular cell [25]. For all our simulations, the maximum K^+ channel conductance G_K has been increased to 0.705 mS cm^{-2} to reduce the duration of the action potential (APD) [70].

To study the effect of sub-threshold stimulus on a stable spiral and on spatiotemporal chaos, we have used the maximum Ca^{2+} channel conductance $G_{si} = 0.04$ and 0.05 mS cm^{-2}, respectively. We have explicitly verified the model-independence of our results by observing similar effects in other realistic channel-based descriptions of the ionic current, such as the TNNP model [86, 131].

We consider in turn the response of a single cell, a 1-dimensional cable and a 2-dimensional sheet of excitable units to a sub-threshold current I. The spatially extended systems are discretized on a grid of size L (for 1-D) and $L \times L$ (for 2-D). For most results reported here $L = 400$, although we have used L up to 1200. The space step used for all simulations is $\delta x = 0.0225$ cm, while the time-step $\delta t = 0.05$ ms (for 1-D) or 0.01 ms (for 2-D). The equations are solved using a forward Euler scheme with a standard 3-point (for 1-D) or 5-point (for 2-D) stencil for the Laplacian describing the spatial coupling between the units. No-flux boundary conditions are implemented at the edges. The external current is applied globally, i.e., $I(t) = I$ in Eq. (6.1) at all points in the system for the duration of stimulation, τ. A stimulus $\{I, \tau\}$ is sub-threshold if it does not generate an action potential when applied on a quiescent medium. The initial spiral wave state is obtained by generating a broken wavefront which then dynamically evolves into a curved rotating wavefront. In the LR1 model simulations, an intact wavefront is allowed to travel through the medium before creating the broken wavefront in order to reduce the recovery period [1] so as to enable a spiral wave with at

[1]This is because of the restitution property of the medium, by which recovery is a function of the time interval between two successive propagating waves

least one complete turn to exist within the simulation domain. Over a large range of parameter values, this spiral wave is a persistent dynamical state of the excitable medium. Under certain conditions (e.g., for some parameter values or external perturbations), the spiral wave can become unstable, eventually breaking up into multiple wavelets leading to a spatiotemporally chaotic state. An alternative method for obtaining the spatiotemporally chaotic state is to randomly apply supra-threshold stimuli at different points in the medium over a small duration. In biological systems, spiral waves and chaos often appear spontaneously as a result of existing heterogeneities or stochastic fluctuations. In the cardiac medium, such dynamical phenomena can be initiated experimentally by applying cross-field stimulation [15]. The spatially extended chaotic state is a long-lived transient whose lifetime increases exponentially with the system size [51]. For biologically realistic simulation domain sizes, such as those used in this chapter, the chaotic state persists longer than any reasonable duration of simulation.

6.3 Results

Fig. 6.1 shows that when sub-threshold stimulation is applied to an excitable medium with spatially heterogeneous activity, viz., either a single spiral wave (a-c) or spatiotemporal chaos (d-f), there is a striking change in the subsequent dynamics of the system. Within a short duration (comparable to the APD) there is complete suppression of all activity in the medium, although in absence of this intervention, the existing dynamical state would continue to persist for an extremely long time. This result is surprising as the weak

sub-threshold signal appears to be incapable of significantly altering the dynamics of an excitable system. For example, if we had applied sub-threshold stimulation on a large domain with a *single* wave propagating across it, there would have been no significant change in the time-evolution of the system with the wave continuing to move across the medium. This differentiates sub-threshold from other weak (i.e., low-amplitude) but supra-threshold stimuli which, on being applied globally to the above system, would have excited almost the entire medium resulting in eventual cessation of all activity.

To understand this apparent paradox, we first note that the sub-threshold stimulation rapidly decreases the number of cells that can be excited by existing activity in the medium (Fig. 6.2,a). Indeed, global suppression of activity results when, by the end of the stimulation, the number of cells susceptible to excitation is insufficient to sustain the activity. This decrease in their number is because cells tend to remain in the recovering state for a longer period in the presence of a sub-threshold stimulus. We can see this clearly in the response of a single *excited* cell to a subsequent sub-threshold current I applied for a fixed duration τ (Fig. 6.2,b).

Increasing I significantly alters the recovery period resulting in a change in the APD. The time t' (measured from the initiation of the AP) at which the sub-threshold stimulation begins, also affects the response of the cell to the signal. These results clearly indicate that the dominant effect of a sub-threshold stimulus is to increase the time period that a cell spends in recovering from prior excitation.

In a spatially extended system, this enhanced recovery period of the cells results in altering the propagation characteristics of the traveling waves.

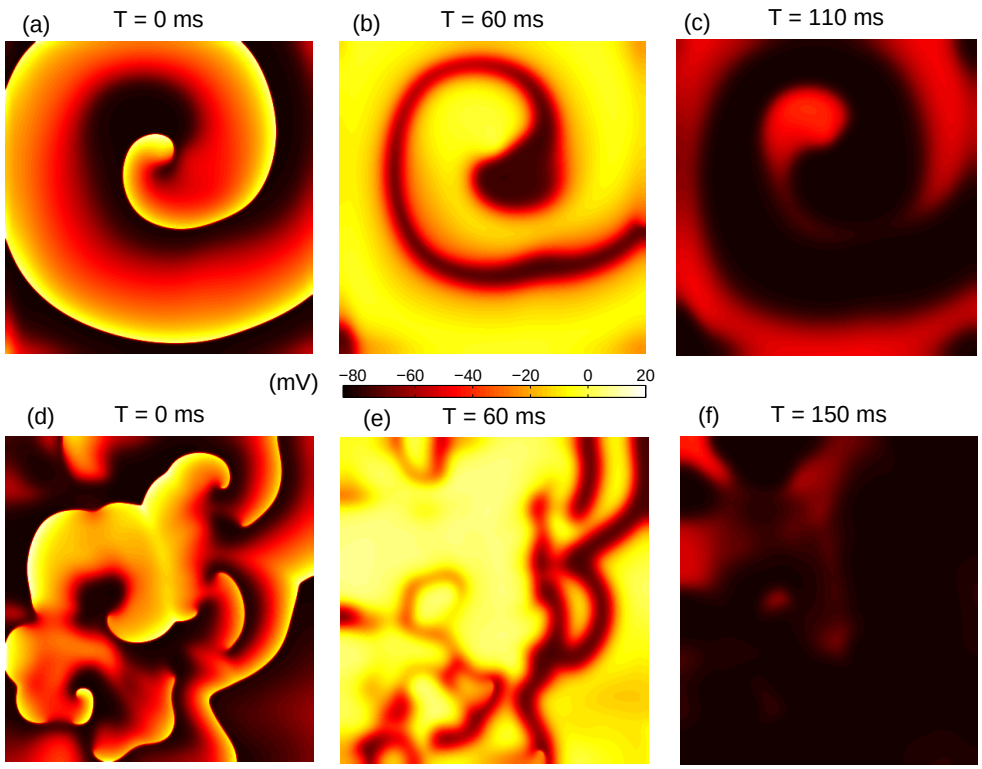

Figure 6.1: Pseudocolor plots of transmembrane potential V for the two-dimensional LR1 model ($L = 400$) showing the elimination of all activity on applying a sub-threshold current. The current I is switched on at $T = 0$ for a duration $\tau = 60$ ms on (a-c) a single spiral, with I =1.6μA cm^{-2}, and (d-f) a spatiotemporally chaotic state, with I =1.8μA cm^{-2}. By $T = 150$ ms, excitation has been effectively terminated throughout the simulation domain.

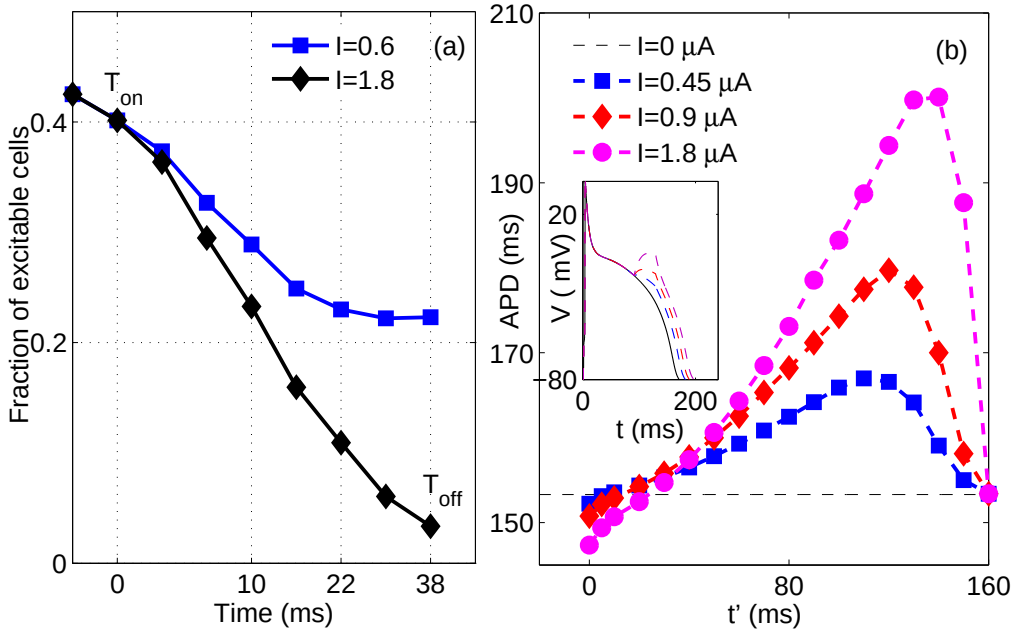

Figure 6.2: (a) The fraction of cells that can be potentially excited (i.e., with $V \leq -60mV$) decreases with time during stimulation by sub-threshold current I in a two-dimensional system with spatiotemporal chaos. The total duration of the external signal is $\tau = T_{on} - T_{off} = 38$ ms. Results shown correspond to failed (squares) and successful termination (diamonds) of activity in the medium. (b) Effect of sub-threshold current on APD of a single cell. The current I is varied keeping the duration τ fixed (= 38 ms). In all cases, the APD is shown as a function of the time interval t' between the initiation of AP and T_{on}. The inset shows the corresponding effect on the AP profile.

Fig. 6.3 (a) shows a spiral wave propagating in a two-dimensional medium, where each turn of the wave is a region of excited cells, with the successive turns separated by recovering regions. As the state of the cells evolve with time, it is manifested in space as movement of excitation and recovery fronts. Their propagation speeds are referred to as wavefront (c_f) and waveback (c_b) velocities, respectively. In the absence of any external stimulation, $c_f \simeq c_b$, ensuring that the width of the excited region remains approximately constant as the waves travel through the medium. However, on applying a sub-threshold stimulus, the waveback velocity becomes significantly lower than that of the wavefront which is almost unchanged. Fig. 6.3 (b) shows that, once stimulation begins, c_b quickly decreases to a minimum value dependent on I. It then gradually rises to eventually become equal to c_f again. For a large sub-threshold stimulus I, the waveback velocity rapidly falls to its lowest value and changes very slowly thereafter. Under these conditions, we can ignore the time-variation of c_b for small τ and use the time-averaged value $\tilde{c_b}(I)$. Increasing I leads to an increased difference in the velocities of the excitation and recovery fronts, $c_f - \tilde{c_b}(I)$ (Fig. 6.3, c). For short stimulus durations, this difference is almost independent of τ. A significantly lower waveback velocity results in the inexcitable region between the excitation and recovery fronts of a wave becoming extended through the course of the stimulation (compare the profiles of APs in a 1-D cable shown in Fig. 6.4). This increases the overall area of the medium that cannot be excited, thereby making it progressively unlikely for the system to sustain recurrent activity.

This is explicitly shown for a 1-dimensional cable in Fig. 6.4. When

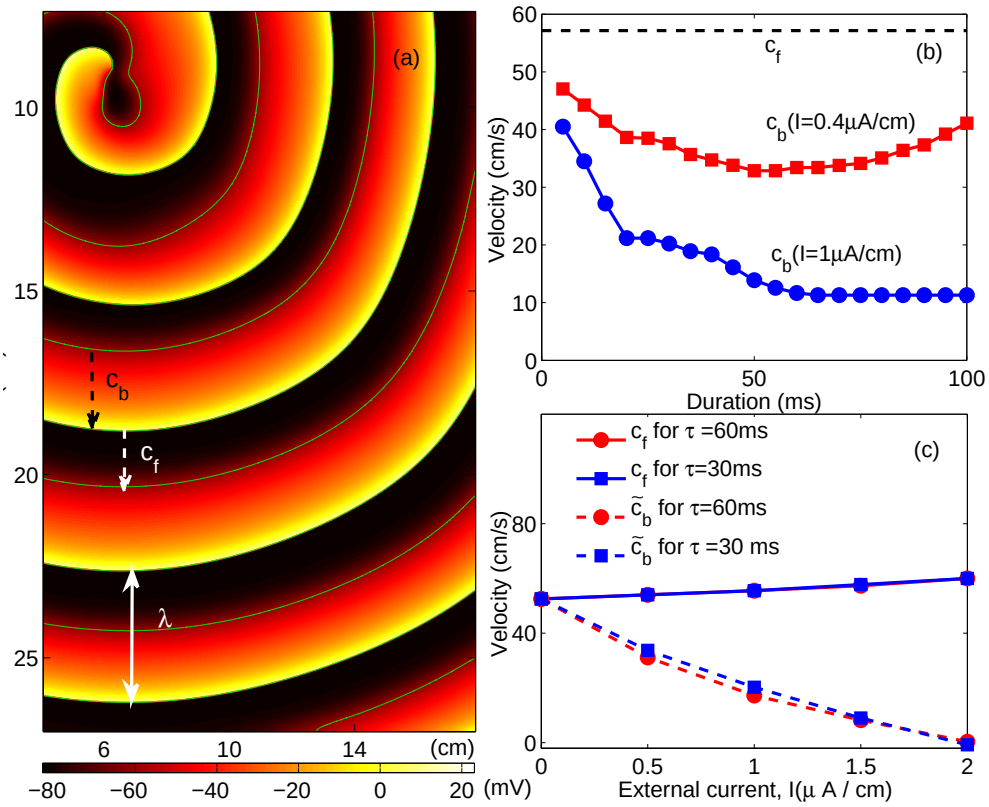

Figure 6.3: (a) Pseudocolor plot of a spiral wave indicating the wavelength λ, the wavefront velocity c_f and the instantaneous waveback velocity $c_b(= c_f)$ in the absence of external stimulation. (b) Time-evolution of c_b during external stimulation of duration $\tau = 100$ ms using two different I corresponding to failed (squares) and successful termination(circles) of activity in the medium. During the course of stimulation, c_f is unchanged. (c) The average waveback velocity $\tilde{c_b}$ (broken lines) reduces with I in contrast to c_f (solid lines)

two successive waves propagate along the cable, globally applying the sub-threshold stimulus reduces the excitable gap between the recovery front of the leading wave (whose velocity c_b has decreased) and the excitation front of the following wave (whose velocity c_f is unchanged). For a high sub-threshold I applied for a long enough duration, the waveback of the first wave slows down sufficiently to collide with the succeeding wavefront. This collision results in termination of the excitation front for the second wave which subsequently disappears from the medium. The above physical picture is fundamentally unchanged for a rotating spiral wave with multiple turns as shown in Fig. 6.3 (a). We now use this to propose a simple semi-analytical theory for the mechanism by which the sub-threshold stimulus suppresses spatially heterogeneous activity.

Theory of sub-threshold suppression

In the absence of any external stimulus, the width of the excited region of a wave lying between its excitation and recovery fronts is $l = c_f \tau_r$, where τ_r is the period for which the active cells remain excited. This time period is operationally measured as the duration for which the transmembrane potential of a cell (V) remains above its excitation threshold. On applying a sub-threshold external current I, c_f is almost unchanged but the resultant waveback velocity, $c_b(I,t)$, which varies with time over the duration of the stimulus τ, is seen to decrease with increasing I. If I is large or τ is small, the time-variation of c_b can be neglected and it is reasonably well-approximated by the time-independent average value $\tilde{c_b}(I)$ over the stimulus duration. Thus, the width of the excited region of the wave increases to

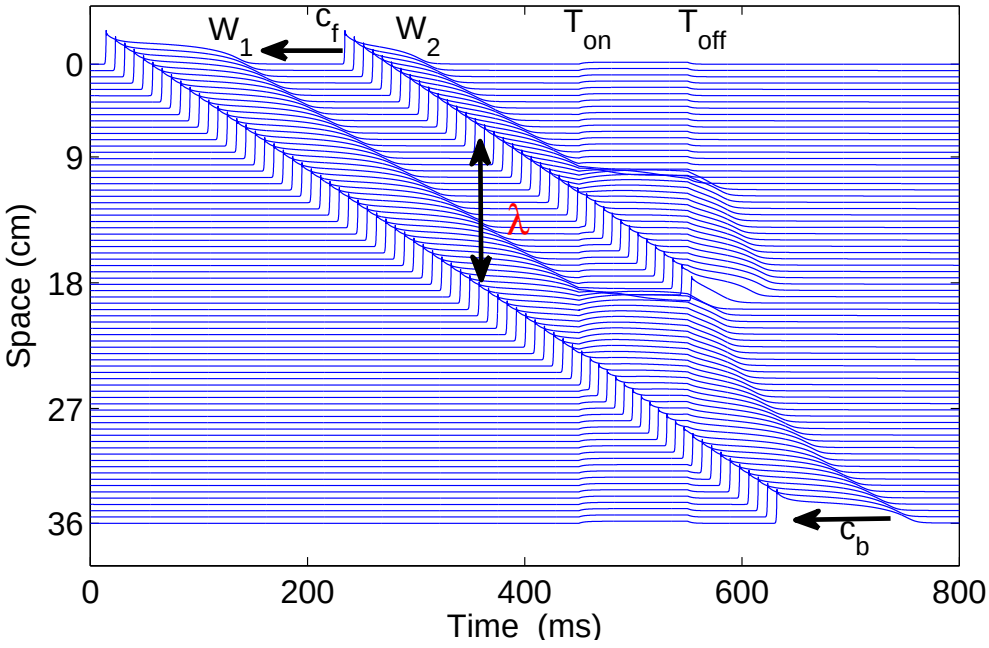

Figure 6.4: Spatiotemporal evolution of two successive waves propagating along a 1-dimensional cable of excitable cells when a sub-threshold stimulus is applied over the time interval $[T_{on}, T_{off}]$. The propagation of the wave W_2 is blocked by the recovery front of W_1 due to reduction of its velocity, c_b. The wavefront velocities c_f of both waves are almost unchanged. The spatial interval between the two successive waves at a time instant is indicated by λ.

$l(I) = l + [c_f - \tilde{c_b}(I)]\tau$. If λ is the distance between excitation fronts of two successive waves in the medium, then collision between the recovery front of the leading wave and the excitation front of the following wave takes place when $l(I) \geq \lambda$. Thus, for a sub-threshold stimulus I, the shortest stimulus duration τ_{min} necessary to eliminate a source of recurrent activity such as a spiral wave is,

$$\tau_{min} = \frac{\lambda - c_f \tau_r}{c_f - \tilde{c_b}(I)}. \tag{6.2}$$

Eq. (6.2) provides us with an analytical relation between the stimulus magnitude and its minimum duration necessary for terminating activity in the medium in terms of measurable dynamical characteristics of the system. Fig. 6.5 shows that this theoretical strength-duration curve for the external stimulation necessary to terminate activity matches very well with the empirical data obtained from numerical simulations for both single spiral wave as well as spatiotemporal chaos. In general, the weaker the sub-threshold current, the longer it has to be applied in order to alter the dynamical behavior of the system. However, there is a lower bound for I below which there is no discernible effect of the sub-threshold stimulation regardless of its duration. Note that, for values of I just above this lower bound, the required τ_{min} is extremely long and the temporal variation of c_b over the duration of the stimulation can no longer be neglected. By explicitly considering the time-dependence of c_b in Eq. (6.2), one can theoretically estimate the value of I where the strength-duration curve becomes independent of τ.

6.4 Discussion

The mechanism of the sub-threshold response of excitable media proposed here depends only on the recovery dynamics of the system. In detailed ionic models of biological excitable cells, this dependence is manifested as a decrease in the ion channel conductance responsible for the slow, outward K^+ current during the sub-threshold stimulation [2]. Thus, simplistic models of excitable media which do not incorporate the effect of external current stimulation on the recovery dynamics are inadequate to reproduce this enhanced sub-threshold response reported here. Our results provide a framework for explaining earlier experimental observations that, in the human heart, sub-threshold stimulation can prevent subsequent activation [133].

The results reported here may have potential significance for understanding the spatiotemporal dynamics of excitable media in several practical situations such as, during clinical treatment of life-threatening arrhythmias. Current methods are primarily aimed towards synchronizing the activity of all regions by using supra-threshold stimuli having relatively larger amplitudes [3].

[2]The decrease in waveback velocity compared to the wavefront velocity under certain conditions has been associated with the existence of a steep slope in the APD restitution curve for the excitable medium, which relates the APD to the time-interval between the recovery and subsequent re-excitation of a local region [132].

[3]Proposed methods for controlling spatiotemporal chaos in simple models of excitable media have occasionally applied stimuli to an aggregated *recovery* variable [44] which has no direct correspondence in biologically realistic models such as LRI. However, such methods rely on driving the medium to a bistable regime which requires the application of a supra-threshold external current in a realistic model of biological excitable media. Hence, such control schemes are also supra-threshold as per the definition used here.

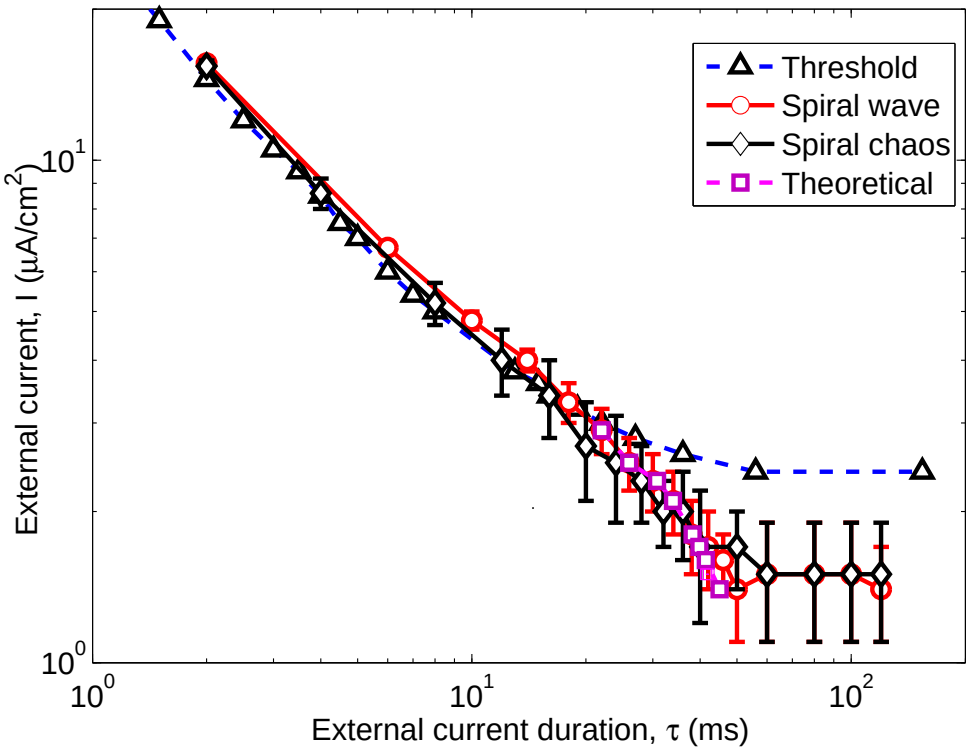

Figure 6.5: Strength-duration curves for a two-dimensional medium with the external current applied at all points of a quiescent medium (triangles) or a medium with existing excitation activity, either a single spiral (circles) or spatiotemporal chaos (diamond). The theoretical prediction given in Eq. (6.2) is also shown (square). Each (τ,I) point is averaged over 10 initial conditions.

However, in such an approach, regions that have been rendered temporarily inexcitable due to prior activity remain unaffected. Thus, these regions can subsequently be re-activated by any remaining excitation after the stimulus is removed, leading to failure of control. By contrast, a sub-threshold stimulus slows the recovery of excited regions, thereby reducing the pool of cells available for excitation by existing activity in the medium. This suggests an alternative mechanism for the efficient termination of spatially extended chaos in excitable systems. It may provide a key towards understanding how spatially irregular activity in biological systems (e.g., fibrillation) are significantly affected by signals that have been strongly attenuated during passage through the intervening medium [134, 135].

Chapter 7

Conclusion

> He that will not apply New Remedies must expect
> New Evils, for Time is the greatest Innovator.
> — *Francis Bacon*

While the mathematical study of pattern formation in excitable media has tended to focus on homogeneous systems, we observe that many excitable systems occurring in nature are inhomogeneous. Heterogeneities in an excitable medium can be of several different types, such as, inexcitable obstacles, regions of slow conduction comprising partially excitable units, gradients in the coupling or in excitability, etc. Biological excitable organs like the heart are especially likely to develop various kinds of heterogeneities with time as a result of aging, often with serious implications for the normal functioning of the entire system. In this thesis, we have performed computational and theoretical studies using a number of mathematical models for excitation dynamics in order to investigate the effects of different kinds of heterogeneities on wave propagation and pattern formation in active media.

As discussed earlier in the thesis, heterogeneities can significantly affect the spatiotemporal evolution of excitation patterns giving rise to a diverse range of phenomena: from anomalous drift of spiral waves to the pinning of vortices and obstacle-induced transitions from pinned reentry to spatiotemporal chaos. The results of our study have a special relevance for the dynamics of excitation in cardiac tissue, where the different types of patterns we observe have been correlated with the occurrence of several forms of arrhythmia. In view of this connection, we have also explored methods to control these patterns in heterogeneous excitable media using low-amplitude stimuli. The inhomogeneous nature of real excitable systems need to be especially taken into account when designing such control methods, as heterogeneities can have a significant impact on the success of these techniques. For instance, while the generation of a series of waves by high-frequency periodic stimulation of localized region has been previously proposed as an efficient method for terminating chaos in homogeneous medium, it is not always likely to be successful in the presence of inexcitable obstacles. Such heterogeneities can result in wavebreaks on the excitation fronts generated by the control stimulation, thereby creating new sources of incoherent activity in a medium. The possibility of failure of control in the presence of heterogeneities underlines the need to consider the effect of different types of inhomogeneities on wave propagation dynamics when devising techniques for terminating chaos in real excitable media.

In the following section, the important results and conclusions reported in the thesis are summarized. We conclude with a brief discussion of the possible future extensions and implications of our results.

7.1 Summary of Main Results

Anomalous drift of spiral waves

In Chapter 2 of the thesis, we investigate the effect of different types of heterogeneity gradients on the drift dynamics of spiral waves. Drift in excitable media has special relevance in connection with the heart, as it has been suggested to be linked with the genesis of rapidly rotating "mother rotors". These high-frequency sources of excitation are considered to be the progenitors of chaotic activity during instances of ventricular fibrillation. In this thesis we describe the phenomenon of drift that results in the translational motion of spirals towards regions of faster rotation, increasing the likelihood of breakup away from the spiral core. This is a novel and important observation, as all previous studies of excitable media had reported drift towards regions where the spiral rotation is slower. The *anomalous drift* reported by us occurs over a range of parameters for gradients in either intercellular coupling or in excitability. The description of this kind of drift to regions with faster spiral rotation periods or having higher excitability, hints at a possible mechanism for the origin of mother rotors. Further, we have discussed the possibility of a connection between the existence of anomalous drift in two-dimensional media and scroll ring expansion in three-dimensional media. As the observation of the former for a given parameter regime in 2-D appears to suggest the existence of the latter in 3-D and vice versa, this provides a method for identifying the appropriate conditions in different systems for which anomalous drift may be possible.

Removing pinned spiral waves by pacing

Spiral waves of excitation are often observed to attach themselves to inexcitable obstacles in a heterogeneous active medium. In the heart, such pinned rotating waves have been associated with tachycardia, a class of arrhythmia characterized by abnormally rapid activity. While freely rotating spiral waves can, in principle, be terminated by forcing them to drift towards the inexcitable system boundaries (where such waves are absorbed) through the application of higher frequency periodic stimuli (pacing), these methods are unsuccessful when the spiral is pinned to an obstacle and cannot be dislodged through pacing. Indeed, a classical result of Wiener and Rosenblueth suggests that pacing will always fail in terminating such pinned reentrant excitation sources. Given the high success rate of pacing in terminating tachycardia in the heart, which often possess significant numbers of inexcitable obstacles, this result appears to be paradoxical. In Chapter 3 of the thesis, we show that there are specific conditions under which a spiral wave pinned to an inexcitable obstacle can be removed by waves from a localised source of high frequency excitation. In particular, unpinning by a pacing source that uses a frequency higher than that of the spiral wave is possible if the size of the obstacle is smaller than that of the spiral core. We also report an analytically derived relation between the size of the obstacle and the maximum pacing period that can result in successful unpinning. Our results suggest that lowering the excitability of the medium (possibly by using pharmaceutical agents) can make it easier to remove pinned spirals through pacing, a phenomenon that has been recently observed in experiments with monolayers of cultured myocytes.

Obstacle-induced breakup of scroll waves

Inexcitable obstacles, such as scar tissue resulting from myocardial infarction, can occur deep inside cardiac tissue and hence may not be observed on imaging the epicardial surface. Nevertheless, they can play a significant role in the evolution of reentrant waves. As such an obstacle does not span the entire thickness of the heart wall, a scroll wave that is adjacent to the obstacle will be only partially attached to it, causing the scroll to deform as a result of the differential periods of rotation in different sections of the wave. In Chapter 4 we explore the possible eventual consequences of the resulting winding of the wave around the obstacle, as a function of the model parameters determining excitability of the medium and the dimensions of the obstacle. Previous studies of wave breakup resulting in spatiotemporal chaos in three-dimensional systems have typically focused on the deformation dynamics of the scroll filament. Here we show an alternative mechanism of scroll breakup where the filament does not directly take part, with the principal events occurring far from the existing singularities. The geometry considered prevents the original filament from breaking while at the same time promoting a break on the wavefront at an edge of the obstacle where a transition from a quasi 2-dimensional to fully 3-dimensional propagation occurs with an associated change in the curvature of the front. As the increased convex curvature of the wave, which develops as it crosses the obstacle edge, reduces the propagation speed, the possibility of its waveback interacting with the front of the following wave increases. This can result in partial conduction block at the edge of the obstacle, which is further enhanced by fluctuations in the time interval between successive waves as a result of dispersion and

restitution properties of the medium as well as Doppler effects resulting from meander of the scroll filament. The break subsequently evolves into fully developed spatiotemporal chaos. We have explicitly verified that the scroll wave is stable in the absence of the obstacle and also when the obstacle spans the entire thickness of the medium (effectively approximating a two-dimensional system). Therefore, the breakup mechanism described in this chapter is an exclusively three-dimensional phenomenon that points out the possibly critical role that heterogeneities play in the evolution of arrhythmia, and specifically, the onset of fibrillation.

Terminating spatiotemporal chaos using an array of control points

In the preceding chapter, we have seen how spatiotemporal chaos in excitable media arises through interaction between waves and heterogeneities. In Chapter 5 of the thesis, we explore how such chaos can be eliminated by using low-amplitude stimuli. In the context of the heart, the spatially incoherent states that result from the chaotic dynamics have been implicated in several life-threatening arrhythmia such as Ventricular Fibrillation. Thus, controlling chaos using small external perturbations is a problem of great practical interest and has been a challenge in view of the heterogeneous nature of cardiac muscles. In this chapter we have proposed a spatially extended but non-global control method involving an array of control points. The points are stimulated in a specific sequence so as to simulate a wave of control moving across the medium with a pre-defined velocity. The applied signal at each site stimulates all potentially excitable cells in the local region

so that as the control wave travels through the medium there is no excitable region left behind its wake. When a part of the induced wave collides with a chaotic fragment, they mutually annihilate each other. However, the stimulation of points further along the medium regenerates the complete control wave once again, so that it can continue to successfully engage and eliminate all chaotic activity until the boundary of the medium is reached. The process results in complete elimination of all chaotic activity after a single application of the control signal. The efficiency of the method is underlined by the fact that the magnitude of applied current used is comparable to that of the ionic currents in cardiac cells. We have explicitly verified that the presence of large heterogeneities do not affect the efficacy of the proposed technique, which is an important criterion for implementing control methods in real biological systems.

Response of spatially extended incoherent activity to sub-threshold stimuli

Almost all methods of controlling spatiotemporal chaos in excitable media that are available in the literature requires using stimuli that are supra-threshold, i.e., which can elicit action potentials in resting medium. In Chapter 6 of the thesis, we describe a novel technique for suppressing incoherent activity that involves the application of sub-threshold signals. The physical principle involved in this control method differs from the usual paradigm of chaos suppression in that, instead of trying to activate all potentially excitable regions by applying a sufficiently strong stimulus, our method prevents already excited regions from becoming excitable as long as the chaotic

activity persists in the medium. Although the signals that we use are insufficient to excite resting medium, they do prolong the recovery period resulting in a significant decrease in the waveback velocity (keeping the wavefront velocity unchanged). In a medium undergoing spatiotemporal chaos, this results in enhanced interaction between the multiple wavefronts and wavebacks existing in the different patches of activity leading to rapid termination of all excitation. The sub-threshold nature of the stimulus is significant, as using a supra-threshold but otherwise low-amplitude signal may result in very different outcome, for example, in an extended excitable medium with a single propagating wave. Applying the sub-threshold signal leaves the situation unchanged when the signal is withdrawn; however, applying a low-amplitude but suprathreshold signal can result in cessation of the wave. Thus, the effect that these two types of signals can have on activity in a medium may be quite different. Our proposed method, in addition to suggesting a different physical mechanism for chaos control, may also provide a key to understand how spatially irregular activity like fibrillation are significantly affected by signals that are strongly attenuated during their passage through biological tissue.

7.2 Outlook

In this thesis we have used both simple phenomenological models of generic excitable media as well as realistic models for ventricular tissue involving detailed descriptions of ionic currents for cardiac myocytes, to explore the role of heterogeneities in dynamical pattern formation. We have also proposed

multiple methods for controlling spatiotemporal activity in such systems. While our studies have helped in establishing several new insights on the excitation dynamics and its control in heterogeneous active media that are model-independent, it is also possible to take these results further in several directions. For example, from a clinical perspective it is important to consider how some of our observations extend to the case where the complicated geometry of the hearts of different animals are incorporated in the spatially extended models. Conduction in heart tissue is anisotropic with the direction of fast conduction along the principal direction of muscle fibre orientation; in addition, the fibre orientation itself rotates along the thickness of the heart wall as one progresses from the epi- to the endo-cardial surface. Such complexity can result in effects such as twist in the filament of the scroll wave, that can have significant repercussions on the propagation of excitation fronts along the heart. Incorporating these features into our models may lead to additional insights on the genesis and evolution of arrhythmias.

Our results may have immediate consequences for current methods of treating several types of cardiac arrhythmias. For example, the observation in Chapter 3 that removing reentrant excitation that is pinned to an obstacle by rapid pacing is critically dependent on the size of the inexcitable obstacle should be considered when efficient strategies for pacing termination of ventricular tachycardia by implantable devices are being designed. The discovery of anomalous drift in cardiac tissue models reported in Chapter 2 opens up the possibility that in the future one can connect measurable characteristics of a heart that governs its excitation properties to the likelihood that it will be subjected to instances of mother-rotor fibrillation. The possibility of using

these results as diagnostic tools for detecting patients at serious risk may be worth exploring. In addition, the interaction between anomalous drift and reentrant activity occurring around an obstacle may give rise to new phenomena in both two and three-dimensional media. An intriguing possibility is that obstacle-induced breakup of scroll waves reported in Chapter 4 may be enhanced in the presence of anomalous drift. It will be also of interest to explore the effect of rapid pacing on such partially pinned scroll waves.

The control methods proposed in Chapters 5 and 6 can, in principle, be developed to serve as efficient and safer methods for treating cardiac fibrillation. At present, both methods require applying low-amplitude control signals over a spatially extended region. Given that the current technology of implantable devices for treating arrhythmia allows applying electrical stimuli only at a few sites, the next step would be to explore the possibility of reducing the number of control points in our proposed methods. Additional complexities of the real heart can also be incorporated, such as the motion of the heart surface during its mechanical action, to observe how the control methods function in such circumstances. In view of the gradually increasing instances of cardiac arrhythmia related fatalities around the world, it is necessary to explore such physics-inspired methods for devising improved therapies that can terminate life-threatening dynamical disorders in the heart.

Bibliography

[1] E. Meron, *Physics Reports* **218**, 1 (1992).

[2] J. Keener, J. Sneyd, *Mathematical Physiology*. Springer-Verlag, New York (1998).

[3] F. Siegert, C. Weijer, *Curr. Biol* **5**, 937 (1995).

[4] J. Lechleiter, S. Girard, E. Peralta, D. Clapham, *Science* **252**, 123 (1991).

[5] W. J. E. P. Lammers, *Pflügers Arch.* **433**, 287 (1997).

[6] M. E. Harris-White, S. A. Zanotti, S. A. Frautschy, A. Charles, *J. Neurophysiol* **79**, 1045 (1998).

[7] X. Huang, W. C. Troy, Q. C. Yang, H. Ma, C. R. Laing, S. J. Schiff, J.-Y. Wu, *J. Neurosci* **24**, 9897 (2004).

[8] A. N. Zaikin, A. M. Zhabotinsky, *Nature (Lond.)* **225**, 535 (1970).

[9] S. Jakubith, H. H. Rotermund, W. Engel, A. von Oertzen, G. Ertl, *Phys. Rev. Lett.* **65**, 3013 (1990).

[10] R. FitzHugh, *Bull. Math. Biophysics* **17**, 257 (1955).

[11] J. Nagumo, S. Arimoto, S. Yoshizawa, *Proc. I.R.E.* **50**, 2061 (1962).

[12] D. Barkley, M. Kness, L. Tuckerman, *Phys. Rev. A* **42**, 2489 (1990).

[13] A. Panfilov, P. Hogeweg, *Phys. Lett. A* **176**, 295 (1993).

[14] A. Panfilov, *Chaos* **8**, 57 (1998).

[15] J. Jalife, J. M. Anumonwo, M. Delmar, J. M. Davidenko, *Basic Cardiac Electrophysiology for the Clinician*. Futura Publishing, Armonk (1999).

[16] M. Bär, M. Falcke, M. Or-Guil, *Lecture Notes in Physics 532*. Springer, New York (1999).

[17] F. Fenton, E. M. Cherry, H. M. Hastings, S. J. Evans, *Chaos* **12**, 852 (2002).

[18] R. Pandit, A. Pande, S. Sinha, A. Sen, *Physica A* **306**, 211 (2002).

[19] S. Alonso, F. Sagués, A. Mikhailov, *Science* **299**, 1722 (2003).

[20] M. Bär, M. Eiswirth, *Phys. Rev. E* **48**, R1635 (1993).

[21] M. Woltering, M. Markus, *ScienceAsia* **28**, 43 (2002).

[22] R. Aliev, A. Panfilov, *Chaos, Solitons and Fractals* **7**, 293 (1996).

[23] H. Sakaguchi, T. Fujimoto, *Phys. Rev. E* **67**, 067202 (2003).

[24] H. Sakaguchi, Y. Kido, *Phys. Rev. E* **71**, 052901 (2005).

[25] C. Luo, Y. Rudy, *Circ. Res* **68**, 1501 (1991).

[26] A. S. Mikhailov, A. V. Panfilov, A. N. Rudenko, *Phys. Lett. A* **109**, 246 (1985).

[27] V. G. Fast, A. M. Pertsov, *Biophysics* **35**, 478 (1990).

[28] A. V. Panfilov, J. P. Keener, *Int. J. Bif. Chaos.* **3**, 445 (1993).

[29] J. M. Davidenko, A. V. Pertsov, R. Salomonsz, W. Baxter, J. Jalife, *Nature* **355**, 349 (1992).

[30] A. Panfilov, J. Keener, *J. Theor. Biol* **163**, 439 (1993).

[31] F. Xie, Z. Qu, A. Garfinkel, *Phys. Rev. E* **58**, 6355 (1998).

[32] M. Valderrabano, Y.-H. Kim, M. Yashima, T.-J. Wu, *Journal of the American College of Cardiology* **36**, 2000 (2000).

[33] T. Shajahan, S. Sinha, R. Pandit, *Phys. Rev. E* **75**, 011929 (2007).

[34] Z. A. Jimenez, B. Marts, O. Steinbock, *Phys. Rev. Lett.* **102**, 244101 (2009).

[35] M. Vinson, A. Pertsov, J. Jalife, *Physica D* **72**, 119 (1993).

[36] A. Pertsov, M. Vinson, *Phil. Trans. R. Soc. Lond. A* **347**, 687 (1994).

[37] A. T. Winfree, *Journal of Cardiovascular Electrophsyiology* **1**, 393 (1990).

[38] D. J. Gauthier, G. M. Hall, R. A. Oliver, E. G. Dixon-Tulloch, P. D. Wolf, S. Bahar, *Chaos* **12**, 952 (2002).

[39] I. Aranson, L. Kramer, *Rev. Mod. Phys.* **74**, 99 (2002).

[40] A. Garfinkel, M. Spano, W. Ditto, J. Weiss, *Science* **257**, 1230 (1992).

[41] E. Ott, C. Grebogi, J. A. Yorke, *Phys. Rev. Lett.* **64**, 1196 (1990).

[42] D. Christini, J. Collins, *Phys. Rev. E* **52**, 5806 (1995).

[43] W. Ditto, M. Spano, V. In, J. Neff, B. Meadows, J. Langberg, A. Bolmann, K. McTeague, *Int. J. Bif. Chaos.* **52**, 593 (2000).

[44] G. Osipov, J. Collins, *Phys. Rev. E* **60**, 54 (1999).

[45] R. Gray, *Chaos* **12**, 941 (2002).

[46] S. Alonso, F. Sagués, A. Mikhailov, *Chaos* **16**, 023124 (2006).

[47] S. Alonso, J. Sancho, F. Sagués, *Phys. Rev. E* **70**, 067201 (2004).

[48] K. Lee, R. Goldstein, E. Cox, *Phys. Rev. Lett.* **87**, 068101 (2001).

[49] A. Muñuzuri, V. Pérez-Villar, M. Markus, *Phys. Rev. Lett.* **79**, 1941 (1997).

[50] R. Gray, N. Chattipakorn, *Proc. Natl. Acad. Sci. U.S.A.* **102**, 4672 (2005).

[51] S. Sinha, A. Pande, R. Pandit, *Phys. Rev. Lett.* **86**, 3678 (2001).

[52] A. Winfree, *When Time Breaks Down.* Princeton University Press, Princeton (1987).

[53] Y.-H. Kim, A. Garfinkel, T. Ikeda, T.-J. Wu, C. Athill, J. Weiss, H. Karagueuzian, P.-S. Chen, *J. Clin. Invest* **100**, 2486 (1997).

[54] W.-J. Rappel, F. Fenton, A. Karma, *Phys. Rev. Lett.* **83**, 456 (1999).

[55] A. Stamp, G. Osipov, J. Collins, *Chaos* **12**, 931 (2002).

[56] H. Zhang, B. Hu, G. Hu, *Phys. Rev. E* **68**, 026134 (2003).

[57] G. Yuan, G. Wang, S. Chen, *Europhys. Lett.* **72**, 908 (2005).

[58] J. Breuer, S. Sinha, *arxiv:nlin.CD/0406047* (2004).

[59] H. Zhang, Z. Cao, N.-J. Wu, H.-P. Ying, G. Hu, *Phys. Rev. Lett.* **94**, 188301 (2005).

[60] N. Wiener, A. Rosenblueth, *Arch. Inst. Cardiol. Mexico* **16**, 205 (1946).

[61] S. Sinha, D. J. Christini, *Phys. Rev. E* **66**, 061903 (2002).

[62] J. Brueur, S. Sinha, *Pramana* **64**, 553 (2005).

[63] A. Garfinkel, Z. Qu, in D. P. Zipes, J. Jalife (eds.), *Cardiac Eletrophysiology: From Cell to Bedside*, chap. 36. Saunders, Philadelphia (2004).

[64] R. A. Gray, J. Jalife, A. V. Panfilov, W. T. Baxter, C. Cabo, J. M. Davidenko, A. M. Pertsov, *Circulation* **91**, 2454 (1995).

[65] S. M. Cobbe, A. C. Rankin, in D. A. Warrell, T. M. Cox, J. D. Firth, E. J. Benz (eds.), *Oxford Textbook of Medicine*, chap. 15. Oxford University Press, USA (2005).

[66] V. Krinsky, *Problemy Kibernetiki* **2**, 59 (1968).

[67] M. Markus, Z. Nagy-Ungavarai, B. Hess, *Science* **257**, 225 (1992).

[68] A. N. Rudenko, A. V. Panfilov, *Studia Biophysica* **98**, 183 (1983).

[69] A. V. Panfilov, B. N. Vasiev, *Physica D* **49**, 107 (1991).

[70] K. H. W. J. ten Tusscher, A. V. Panfilov, *Am. J. Physiol. Heart Circ. Physiol* **284**, H542 (2003).

[71] G. R. Ivanitsky, V. I. Krinsky, A. V. Panfilov, M. A. Tsiganov, *Biofizika* **34**, 297 (1989).

[72] A. S. Mikhailov, V. A. Davydov, V. S. Zykov, *Physica D* **70**, 1 (1994).

[73] R. A. Gray, A. M. Pertsov, J. Jalife, *Circulation* **94**, 2649 (1996).

[74] J. Jalife, O. Berenfeld, M. Mansour, *Cardiovasc. Res* **54**, 204 (2002).

[75] R. H. Keldermann, K. H. W. J. ten Tusscher, M. P. Nash, C. P. Bradley, R. Hren, P. Taggart, A. V. Panfilov, *Am. J. Physiol. Heart Circ. Physiol* **296**, H370 (2009).

[76] F. G. Akar, D. S. Rosenbaum, *Circ. Res.* **93**, 638 (2003).

[77] G. Bub, A. Shrier, L. Glass, *Phys. Rev. Lett.* **88**, 058101 (2002).

[78] A. Pumir, S. Sinha, S. Sridhar, M. Argentina, M. Hrning, S. Filippi, C. Cherubini, S. Luther, V. Krinsky, *Phys. Rev. E* **81**, 010901(R) (2010).

[79] F. H. Fenton, A. Karma, *Chaos* **8**, 20 (1998).

[80] V. Hakim, A. Karma, *Phys. Rev. E* **60**, 5073 (1999).

[81] V. I. Krinsky, E. Hamm, V. Voignier, *Phys. Rev. Lett.* **76**, 3854 (1996).

[82] A. V. Panfilov, A. N. Rudenko, *Physica* **28D**, 215 (1987).

[83] S. A. Alonso, A. V. Panfilov, *Phys. Rev. Lett.* **100**, 218101 (2008).

[84] H. Henry, V. Hakim, *Phys. Rev. E* **65**, 046235 (2002).

[85] H. Henry, *Phys. Rev. E* **70**, 026204 (2004).

[86] K. H. W. J. ten Tusscher, D. Noble, P. J. Noble, A. V. Panfilov, *Am. J. Physiol. Heart Circ. Physiol* **286**, H1573 (2004).

[87] G. Schram, M. Pourrier, P. Melnyk, S. Nattel, *Circ. Res.* **90**, 939 (2002).

[88] M. C. Boerlijst, P. Hogeweg, *Physica D* **88**, 29 (1995).

[89] A. Pumir, A. Arutunyan, V. Krinsky, N. Sarvazyan, *Biophys. J* **89**, 2332 (2005).

[90] V. N. Biktashev, A. Arutunyan, N. A. Sarvazyan, *Biophys. J* **94**, 3726 (2008).

[91] S. Takagi, A. Pumir, D. Pazo, I. Efimov, V. Nikolski, V. Krinsky, *Phys. Rev. Lett.* **93**, 058101 (2004).

[92] H. Zhang, Z. Cao, N. J. Wu, H. P. Ying, G. Hu, *Phys. Rev. Lett.* **94**, 188301 (2005).

[93] S. Sinha, S. Sridhar, in E. Schöll, H.-G. Schuster (eds.), *Handbook of Chaos Control*, chap. 32, p. 703. Wiley-VCH Verlag, Weinheim, 2 edn. (2007).

[94] S. Sridhar, S. Sinha, *Europhys. Lett* **81**, 50002 (2008).

[95] A. Isomura, M. Horning, K. Agladze, K. Yoshikawa, *Phys. Rev. E* **78**, 066216 (2008).

[96] M. Hörning, A. Isomura, K. Agladze, K. Yoshikawa, *Phys. Rev. E* **79**, 026218 (2009).

[97] F. H. Fenton, S. Luther, E. M. Cherry, N. F. Otani, V. Krinsky, A. Pumir, E. Bodenschatz, R. F. Gilmour.Jr, *Circulation* **120**, 467 (2009).

[98] D. P. Zipes, J. Jalife, *Cardiac Electrophysiology: From Cell to Bedside.* Saunders, Philadelphia (2004).

[99] V. Krinsky, K. Agladze, *Physica D* **8**, 50 (1983).

[100] K. Agladze, M. W. Kay, V. Krinsky, N. Sarvazyan, *Am. J. Physiol. Heart Circ. Physiol* **293**, H503 (2007).

[101] G. Gottwald, A. Pumir, V. Krinsky, *Chaos* **11**, 487 (2001).

[102] G. Blatter, M. V. Feigel'man, V. B. Geshkenbein, A. I. Larkin, V. M. Vinokur, *Rev. Mod. Phys.* **66**, 1125 (1994).

[103] D. Pazo, L. Kramer, A. Pumir, S. Kanani, I. Efimov, V. Krinsky, *Phys. Rev. Lett.* **93**, 168303 (2004).

[104] A. M. Pertsov, E. Ermakova, A. Panfilov, *Physica D* **14**, 117 (1984).

[105] B. T. Ginn, O. Steinbock, *Phys. Rev. Lett.* **93**, 158301 (2004).

[106] Z. Y. Lim, B. Maskara, F. Aguel, R. Emokpae, L. Tung, *Circulation* **114**, 2113 (2006).

[107] L. Glass, M. E. Josephson, *Phys. Rev. Lett.* **75**, 2059 (1995).

[108] L. Glass, *Science* **198**, 321 (1977).

[109] For illustration of wave-train induced termination with the Luo-Rudy model, see supplementary material at http://link.aps.org/supplemental/10.1103/PhysRevE.81.01.0901.

[110] S. Sinha, K. M. Stein, D. J. Christini, *Chaos* **12**, 893 (2002).

[111] A. Winfree, *Science* **181**, 937 (1973).

[112] B. Welsh, J. Gomatam, A. Burgess, *Nature (Lond.)* **304**, 611 (1983).

[113] O. Steinbock, F. Siegert, S. Muller, C. Weijer, *Proc. Natl. Acad. Sci. USA* **90**, 7332 (1993).

[114] C. Weijer, *Seminars in Cell and Developmental Biology* **10**, 609 (1999).

[115] T. Shajahan, S. Sinha, R. Pandit, *Int. J. Mod. Phys. B* **17**, 5645 (2003).

[116] T. K. Shajahan, A. R. Nayak, R. Pandit, *PLoS One* **4**, e4738 (2009).

[117] N. Peters, J. Coromilas, N. Severs, A. Wit, *Circulation* **95**, 988 (1997).

[118] N. Peters, J. Coromilas, M. Hanna, M. Josephson, C. Costeas, A. Wit, *Circ. Res.* **82**, 279 (1998).

[119] R. A. Gray, A. M. Pertsov, J. Jalife, *Nature (Lond.)* **392**, 75 (1998).

[120] F. X. Witkowski, L. J. Leon, P. A. Penkoske, W. R. Giles, M. L. Spano, W. L. Ditto, A. T. Winfree, *Nature (Lond.)* **392**, 78 (1998).

[121] D. Christini, K. Stein, S. Markowitz, S. Mittal, D. Slotwiner, M. Scheiner, S. Iwai, B. Lerman, *Proc. Natl. Acad. Sci. U.S.A.* **98**, 5827 (2001).

[122] A. Pumir, V. Nikolski, M. Hörning, A. Isomura, K. Agladze K., Yoshikawa, R. Gilmour, E. Bodenschatz, V. Krinsky, *Phys. Rev. Lett.* **99**, 208101 (2007).

[123] L. Geddes, W. Tacker, J. Mcfarlane, J. Bourland, *Circ. Res.* **27**, 551 (1970).

[124] M. Gold, S. Shorofsky, *Circulation* **96**, 3517 (1997).

[125] P. Jung, G. Mayer-Kress, *Phys. Rev. Lett.* **74**, 2130 (1995).

[126] A. S. Pikovsky, J. Kurths, *Phys. Rev. Lett.* **78**, 775 (1997).

[127] S. Alonso, I. Sendiña Nadal, V. Pérez-Muñuzuri, J. M. Sancho, F. Sagués, *Phys. Rev. Lett.* **87**, 078302 (2001).

[128] C. B. Muratov, E. Vanden-Eijnden, E. Weinan, *Proc. Natl. Acad. Sci. U.S.A.* **104**, 702 (2007).

[129] S. Sinha, B. K. Chakrabarti, *Phys. Rev. E* **58**, 8009 (1998).

[130] S. Sinha, *Physica A* **270**, 204 (1999).

[131] S. Sridhar, S. Sinha, A. V. Panfilov, *Phys. Rev. E* **82**, 051908 (2010).

[132] M. Courtmanche, *Chaos* **6**, 579 (1996).

[133] E. N. Prystowsky, D. P. Zipes, *Circulation* **68**, 707 (1983).

[134] J. P. Keener, A. V. Panfilov, *Biophys. J* **71**, 1335 (1996).

[135] V. Krinsky, A. Pumir, *Chaos* **8**, 188 (1999).